Sagar Dipak Silva Pratapsi

Effects of Strong Magnetic Fields on the Crust and Entrainment in Neutron Stars

Dissertation presented to the Physics Department at the
University of Coimbra to obtain the Master's Degree in Physics

September 2017

UNIVERSIDADE DE COIMBRA

Holy Roman Emperor Henry III witnessing the birth of a new star near Tivoli, Italy, in the 11^{th} century. The star is possibly the Crab Nebula, which hosts a pulsar in its center. The phenomenon happened in 1054 and was visible for two days. It was observed and recorded in different parts of the world.

Illustration from the story "Seven wise masters", *circa* 1450, Haguenau, Germany
Original in German. Cod. Pal. germ. 149, University Library of Heidelberg
Facsimile obtained from http://digi.ub.uni-heidelberg.de/diglit/cpg149

Effects of Strong Magnetic Fields on the Crust and Entrainment in Neutron Stars

Author: Sagar Pratapsi

Supervisor: Prof. Dr. Constança Providência

A thesis submitted in fulfillment of the requirements for the Master's Degree in Physics at the

Department of Physics of the
Faculty of Sciences and Technology
University of Coimbra

September 2017

Resumo

Os pulsares são estrelas de neutrões magnetizadas que rodam a taxas excecionalmente estáveis. No entanto, pulsares mais jovens sofrem eventos esporádicos, conhecidos por *glitches*, em que a frequência de rotação aumenta de forma súbita, para de seguida decrescer gradualmente. Acredita-se que os *glitches* resultam de uma transferência de momento angular entre a crosta e superfluidos no interior da estrela. No entanto, a crosta poderá não ser capaz de armazenar a quantidade do momento de inércia necessária para validar este modelo.

Campos magnéticos fortes afectam significativamente as propriedades das estrelas de neutrões, o que pode indicar terem um papel relevante no mecanismo dos *glitches*. Contudo, são necessários campos excecionalmente elevados, da ordem de 10^{18} G, para se observarem alterações na equação de estado da matéria estelar. Como consequência, estes efeitos não são tidos em conta em cálculos da magnetohidrodinâmica das estrelas. No entanto, verificou-se recentemente que poderá existir um efeito na equação de estado da crosta que, na presença de um campo magnético forte, se traduz num aumento da extensão da mesma.

O objetivo deste projeto é estudar os efeitos do campo magnético na equação de estado da matéria estelar, em particular aqueles que afetem diretamente os *glitches* de pulsares. São analisados dois problemas:

- Quão forte deve ser o campo magnético para que tenha um efeito significativo nas dimensões da crosta?
- Como é que o campo magnético afeta o entrainment entre os neutrões superfluidos e a crosta?

Para a primeira questão, usamos o método da spinodal dinâmica para determinar o tamanho da crosta sob campos magnéticos fortes. Para a segunda questão, estudamos o efeito do campo magnético na matriz de entrainment relativístico, para uma mistura de protões e neutrões, no contexto da teoria de Landau-Fermi para líquidos relativistas, generalizada de modo a incluir superfluidez.

Abstract

Pulsars are magnetized neutron stars that rotate at exceptionally stable rates. Nevertheless, younger pulsars exhibit sporadic events called *glitches*, in which the rotation frequency suddenly increases and then steadily decreases. It is believed that the glitches are a consequence of angular momentum transfer between the crust and superfluids in the star's interior. The crust, however, may not be able to store enough momentum of inertia to validate this model.

Magnetic fields of high intensity significantly affect the properties of neutron stars, which may indicate they play a role in the glitch mechanism. However, their intensity must be of the order of 10^{18} G to significantly alter the equation of state of stellar matter. As a result, such effects are not usually considered when performing magnetohydrodynamic calculations in stars. Recently, however, a possible effect on the crust's equation of state has been discovered which, under a strong magnetic field, results in the increase of the crust's extension.

The goal of this thesis is to study the effects of magnetic fields on the stellar matter's equation of state, particularly those that are most directly related to pulsar glitches. We analyze two problems:

- How strong must a magnetic field be to significantly alter the crust's dimensions?
- How does the magnetic field affect the entrainment between superfluid neutrons and the crust?

For the first problem, we use the dynamical spinodal method in order to determine the crust's size under strong magnetic fields. For the second, we study the effect of the magnetic field on the relativistic entrainment matrix for a mixture of protons and neutrons, using a relativistic Landau Fermi liquid theory, generalized to include superfluidity.

Agradecimentos

Deixo, em primeiro lugar, os meus agradecimentos à Prof.ª Doutora Constança Providência por todo o acompanhamento durante este ano, desde a atenção inicial dada aos meus interesses na escolha do tema da tese à constante disponibilidade mostradas para resolver os problemas que foram surgindo.

Não posso deixar de agradecer aos professores Fernando Nogueira e António Paixão por, há vários anos, me terem introduzido à área da Física, na escola Quark!, e pela atenção e paciência em me ouvir antes de ter tomado a decisão de seguir este caminho.

Por fim, agradeço à minha família e amigos, que me apoiaram de diferentes maneiras, todas elas complementares, e que me permitiram chegar mais longe.

Contents

List of Figures

1. Introduction

In this thesis, we will study properties of the matter inside neutron stars, one of the most extreme places in the universe, which, alongside white dwarfs and black holes, are an end-point in the life of stars. Before presenting our motivation and goals, we will briefly introduce these astrophysical objects.

1.1 Neutron stars

The existence of neutron stars was originally proposed by Baade and Zwicky in 1934, a year after the discovery of the neutron itself. They were seeking an explanation for the formation of supernovæ, and proposed that they were the result of stars collapsing and releasing their gravitational binding energy, leaving in their place a condensed object made of neutrons.

An ordinary, luminous star is in a state of constant collapse, due to its high gravitational mass. The fusion reactions in its interior, facilitated by the high densities, pressures and temperatures of the core, release an immense amount of energy, enough to create a counter-balancing force to gravity; the star is then said to be in a state of suspended collapse. The first reaction to occur is the fusion of hydrogen to helium. As hydrogen runs out, helium accumulates in the center of the star, and there comes a point when helium itself starts to fuse together to produce carbon. All the reactions that take place inside a star are more complicated than this simplified picture, but the overall trend is for lighter nuclei to produce heavier elements, all the while releasing energy. If the star is massive enough, there comes a point when nuclear fusion stops being exothermic. This point is reached when the nucleus with the least binding energy per nucleon, iron, starts to form.

When the center of the star starts accumulating iron, the core begins to lose its ability to support the outer layers. Through a complex interplay between the infalling material, the still-burning outer regions of the core and the dense center of the star, a strong ejection of material happens – a supernova –, releasing a significant part of the gravitational binding energy of the star. What is left of this explosion is the solid core, of a few solar masses. If it is not too massive, the core avoids becoming a black hole, becoming a neutron star instead.

A neutron star is a very compact object, being typically at least as massive as the sun, all the while having a radius of around 10 km. It has a very thin atmosphere of hot plasma, with a thickness of micrometers. Below the atmosphere there is the crust, divided in outer and inner parts. The outer crust is composed of a lattice of nuclei in a sea of electrons. The inner crust has nuclei with a higher neutron content, and there comes a density, called the *neutron*

drip point, in which free neutrons start to appear rapidly. It is possible to find superfluid neutrons in the inner crust. Below the crust, one finds the core, whose composition is still being heavily investigated. For our purposes, it is important to know that the outer core contains superfluid neutrons and superconducting protons. The composition of the inner core is still uncertain.

In this work, we will study properties of the neutron star matter that contribute for an interaction between the solid crust and the superfluid neutrons and superconducting protons . In particular, these interactions may explain why some rotating neutron stars, called pulsars, suddenly increase their angular velocity, in events called *glitches*. One mechanism for explaining this phenomenon involves vortices of superfluid neutrons. These are *quanta* of angular momentum of the superfluid, and it is believed that they are pinned to the crust by fixing themselves inside the solid lattice of nuclei. To contribute to the understanding of this phenomenon, we will study how the superfluids in the outer core interact. This may help in performing more realistic magnetohydrodynamic simulations of neutrons stars, and eventually help to understand the glitch mechanism.

1.2 Motivation

Recent results show that some astrophysical objects, such as soft γ-ray repeaters (SGR) and some anomalous X-ray pulsars, are neutron stars with magnetic fields of up to 10^{14} G—10^{15} G on the surface [1] – the so-called magnetars. The strongest magnetic field was detected in a specially young star, SGR 1806-20, and was estimated as $B = 2 \times 10^{15}$ G. The magnetic field strength inside a magnetar is unknown but, using the virial theorem, it is estimated to reach up to 10^{18} G. In general, the magnetic field on the surface of a neutron star may vary between 10^{9} and 10^{15} G.

A strong magnetic field affects neutron stars in different ways: by changing the equations of state (EoS); by quantizing the charged particles' orbits in the so-called Landau levels [2], and by breaking the spherical symmetry of the star. As such, strong magnetic fields may affect observable quantities, such as the star's maximum mass. Only fields above 10^{18} G affect the EoS in a significant way [3]. Nevertheless, it is expected that fields weaker than 10^{18} G still have non-negligible effects on low-density regions and, as a result, these effects must be felt on the star's crust [4]. Recently, it has been shown that strong magnetic fields, of the order of 10^{15} G—10^{17} G, have a non-negligible effect on the extension of the crust of magnetized neutron stars [5]. The extension of the crust was determined by calculating the region of dynamic instability of neutron-proton-electron (npe) matter, which occurs at densities below the nuclear saturation. Furthermore, finding the mode with the highest growth rate has allowed the estimation of the size of the aggregates and their electric charge content. It was possible to conclude that a strong magnetic field increases the extension of the crust and the charge content of the aggregates, but these effects seem to be highly sensitive to the density dependence of the symmetry energy. These results must be confirmed using realistic nuclear models.

Pulsars are considered to be magnetized neutron stars that rotate at exceptionally stable rates. There are, however, exceptions to this regularity, such as the *glitch* events in younger pulsars. Glitches are sudden increases of the frequency of rotation, followed by a period of steady decline called the spin-down.

It is believed that glitches are a manifestation of the superfluids that exist on the inside of neutron stars. In particular, the relaxation of the rotation and the rate of the spin-down that occur after a glitch seem to indicate the lowering of viscosity, associated with the superfluidity, weakens the coupling between superfluid neutrons and the crust. It is believed that these events are sudden releases of tensions built up in the crust, in which there is a transfer of angular momentum between the superfluid neutrons and the rest of the star. According to Link [6], glitches in the Vela star can be well-reproduced if the crust is able to account for 1.4% of the star's moment of inertia. However, it was recently shown that the non-dissipative entrainment between the different superfluids inside neutron stars reduced the coupling between superfluid neutrons and the network of aggregates that constitutes the crust. The amount of moment of inertia needed to store to explain the measured glitches would be greater than what the crust can support [7, 8].

1.3 Goals

The main object of study of this thesis are the effects of magnetic fields on the equation of state of the stellar matter, in particular those that can directly affect pulsar glitches. We will analyze two problems:

- How strong must a magnetic field be to significantly alter the crust's dimensions?
- How does the magnetic field affect the entrainment between superfluid neutrons and the crust?

Answering these questions may have implications to the glitch mechanism, in particular if the inner crust is increased [9].

Determining the crust size

Several different methods may be used to determine the transition density between the crust and the core of a neutron star. In Avancini et al. [10], the dynamical spinodal method proposed by Providência et al. [11], i.e. finding the region in isospin space where nuclear matter is unstable to small perturbations of nuclear density, predicts values which are in close agreement with a Thomas-Fermi description of the inner crust. As such, we apply this method to determine the size of a neutron's star crust under a strong magnetic field. We will use a nuclear model that satisfies the constraints imposed by laboratory experiences and astrophysical observations (see [12]); we will also discuss uncertainties that may affect the main conclusions. The dynamical spinodal method was recently applied to magnetized nuclear matter [5], but there are still several problems that warrant discussion. In particular, it is essential to consider realistic models, given that the results obtained may be highly sensitive to the density dependence of the symmetry energy. It is also necessary to understand the relevance of including the protons' and neutrons' anomalous magnetic moment. This method also allows us to predict the clusters' size and the trend defined by the instabilities with respect to the isospin asymmetry of the clusters. The magnetic field induces the appearance of Landau levels for protons and electrons. The opening

of new Landau levels in neutron-rich matter may originate instabilities that would induce the appearance of clusterized matter at densities above the ones predicted for a zero magnetic field, to which neutron superfluid vortices may pin.

Calculating the entrainment

Inside neutron stars, densities are such that the pairing nuclear force gives rise to superfluid neutrons in the crust and superfluid neutrons and superconducting protons in the core. The neutron superfluidity is essential to explain the vortex-mediated glitches, since they constitute a component that can move independently from the rest of the star. Is is, however, necessary to understand the mechanism that allows for the transfer of angular momentum between the rotation-decoupled components.

Since the neutron star is composed by a mixture of fluids, namely normal and superfluid protons and neutrons, relativistic hydrodynamics of superfluid mixtures including entrainment must be considered [13]. This formalism is both applied to the description of the glitch mechanism and the pulsations of cold neutron matter. The possible detection of gravitational waves from neutron stars opens a completely new opportunity of constraining dense, neutron-rich nuclear matter.

A relativistic formalism is essential to probe the regions deep inside the neutron star. As such, we will study the effect of the magnetic field on the relativistic entrainment matrix for a proton-neutron mixture, in the framework of the relativistic Landau–Fermi liquid theory, generalized to include superfluidity [14, 15]. It turns out that the superfluidity of neutrons not only contributes to the neutron mass current density, but also to that of the proton, and vice-versa. At finite temperature, three independent motions will occur inside a mixture of two superfluids: the two superfluid motions and the motion of the thermal excitations. In a zero temperature calculation, as the one that will be carried out in this project, the last component does not exist. The sensitivity of the entrainment matrix to the nuclear model within which it is evaluated will be discussed.

1.4 Units and dimensions

In this work, we use a system of units that is convenient in nuclear physics. The preferred unit of length is the the femtometer, or fermi, $\mathrm{fm} = 1 \times 10^{-15}\mathrm{m}$, and energies will be measured in MeV. In our equations, we will set $\hbar = c = 1$, which amounts to saying we measure our quantities as multiples of $\hbar$ and c. We used the value $\hbar c = 197.32\,\mathrm{MeV\,fm}$ in our computations.

We will also use magnetic fields B of very high intensity, so we will write them usually as B^*, a multiple of a critical field,

$$B^* = \frac{B}{B_{\mathrm{crit}}} \quad \text{with} \quad B_{\mathrm{crit}} = \frac{m_e^2 c}{e\hbar} \approx 4.4 \times 10^{13}\,\mathrm{G}. \tag{1.1}$$

2. Modelling the stellar matter

In order to study the properties of matter inside a neutron star, we will use an effective relativistic quantum field model, originally proposed by Teller [16], Duerr [17] and Walecka [18], an introduction to which may be found in Glendenning [19]. Our model is an extended version, called NL3$\omega\rho$, and was constructed to better fit experimental data of atomic nuclei, in particular those properties that are determined by the density dependence of the symmetry energy [20, 21, 22]. The meaning of this statement will be better understood in the Results section, when we study some properties of NL3$\omega\rho$. The fundamental features of this field theory is that it includes neutrons, protons and electrons interacting via the scalar σ meson, the vector ω meson and the isovector $\vec{\rho} = (\rho_1, \rho_2, \rho_3)$ mesons. Additionally, we will include a static magnetic field via the electromagnetic potential A.

2.1 The NL3$\omega\rho$ model Lagrangian

We begin by introducing the Lagrangian of the NL3$\omega\rho$ model in its compact, component form:

$$\mathcal{L} = \mathcal{L}_b + \mathcal{L}_e + \mathcal{L}_\sigma + \mathcal{L}_\omega + \mathcal{L}_\rho + \mathcal{L}_{\omega\rho}. \tag{2.1}$$

The baryonic part of the Lagrangian, $\mathcal{L}_b$, accounts for the motions of protons and neutrons, as well as their interactions with the force fields. Using

$$\Psi = \begin{pmatrix} \Psi_p \\ \Psi_n \end{pmatrix} \tag{2.2}$$

as the baryon field, with Ψ_p and Ψ_n respectively standing for the proton and neutron fields, this Lagrangian has the form

$$\mathcal{L}_b = \overline{\Psi}[\gamma_\mu i\mathcal{D}^\mu - m^*]\Psi. \tag{2.3}$$

The symbol $i\mathcal{D}^\mu$ is the covariant derivative

$$i\mathcal{D}^\mu = i\partial^\mu - g_\omega\omega^\mu - \frac{g_\rho}{2}\vec{\tau}\cdot\vec{\rho}^\mu - eA^\mu\frac{1+\tau_3}{2}, \tag{2.4}$$

As usual, e stands for the elementary charge (the coupling constant of the electromagnetic potential field), and g_ω and g_ρ are the coupling constants for the ω and $\vec{\rho}$ fields, respectively. The symbol $\vec{\tau} = (\tau_1, \tau_2, \tau_3)$ stands for the Pauli matrices

$$\tau_1 = \begin{pmatrix} 0 & 1 \\ 1 & 0 \end{pmatrix} \quad \tau_2 = \begin{pmatrix} 0 & -i \\ i & 0 \end{pmatrix} \quad \tau_3 = \begin{pmatrix} 1 & 0 \\ 0 & -1 \end{pmatrix}.$$

Finally, m^* should be read as

$$m^* = m - g_\sigma \sigma = \begin{pmatrix} m_p & 0 \\ 0 & m_n \end{pmatrix} - g_\sigma \sigma, \tag{2.5}$$

with m_p and m_n being the proton and neutron masses.

The electron part of the Lagrangian is given by

$$\mathcal{L}_e = \overline{\Psi}_e [\gamma_\mu (i\partial^\mu + eA^\mu) - m_e] \Psi_e. \tag{2.6}$$

The Lagrangians for the interaction fields are given by

$$\begin{aligned}
\mathcal{L}_\sigma &= \frac{1}{2}\left(\partial_\mu \sigma \partial^\mu \sigma - m_\sigma^2 \sigma^2\right) - \frac{\kappa}{3!}\sigma^3 - \frac{\lambda}{4!}\sigma^4 \\
\mathcal{L}_\omega &= -\frac{1}{4}\Omega_{\mu\nu}\Omega^{\mu\nu} + \frac{1}{2}m_\omega^2 \omega_\mu \omega^\mu + \frac{\xi}{4!}g_\omega^4 (\omega_\mu \omega^\mu)^2 \\
\mathcal{L}_\rho &= -\frac{1}{4}\vec{B}_{\mu\nu} \cdot \vec{B}^{\mu\nu} + \frac{1}{2}m_\rho^2 \vec{\rho}_\mu \cdot \vec{\rho}^\mu
\end{aligned}$$

where we define the tensors

$$\begin{cases}
\Omega^{\mu\nu} = \partial^\mu \omega^\nu - \partial^\nu \omega^\mu \\
\vec{B}^{\mu\nu} = \partial^\mu \vec{\rho}^\nu - \partial^\nu \vec{\rho}^\mu - g_\rho (\vec{\rho}^\mu \times \vec{\rho}^\nu).
\end{cases}$$

The masses of the σ, ω and $\vec{\rho}$ fields are, respectively, m_σ, m_ω and m_ρ, and the constants κ, λ and ξ determine the strengths of the self-interactions. It should be noted that we do not include the Lagrangian $-\frac{1}{4}F^{\mu\nu}F_{\mu\nu}$ which accounts for the dynamics of the electromagnetic field A. In the following sections, we will impose a constant magnetic field, so we will have no need for the respective equations of motion. The electromagnetic field thus appears only by interacting with the proton and electron fields. By ignoring this contribution to the Lagrangian, we also avoid adding the electromagnetic energy to the total energy, which would have the effect of shifting the latter by a constant amount.

Finally, there is an additional term coupling the ω and the $\vec{\rho}$ fields,

$$\mathcal{L}_{\omega\rho} = \Lambda_{\omega\rho}\ g_\omega^2\ g_\rho^2\ \left(\vec{\rho}_\lambda \cdot \vec{\rho}^\lambda\right)(\omega_\mu \omega^\mu),$$

with $\Lambda_{\omega\rho}$ defining the intensity of this coupling. The existence of this coupling is reflected in the name NL3$\omega\rho$.

2.1.1 Parameterizations

Our model would not be complete without specifying the masses of the particles and the coupling constants. We present these values in the following tables. We will be using different parameterizations of the NL3$\omega\rho$ model. They mainly differ on the way the symmetry energy varies with density. In fact, we will name these models after a number, L, which is the slope of the symmetry energy at the nuclear saturation density. We will see precisely how to calculate this value in the results; its meaning can be seen in Figure 4.4. We also use the experimental masses of the protons, neutrons and electrons.

Table 2.1: Masses of the particles

m_p (MeV)	m_n (MeV)	m_e (MeV)
938.272	939.565	0.511

Table 2.2: Common parameters of the NL3$\omega\rho$ models

m_σ (MeV)	m_ω (MeV)	m_ρ (MeV)	g_σ	g_ω	κ (fm^{-1})	λ	ξ
508.194	782.501	763	10.217	12.868	8.948	$2 \cdot 10.431$	$-6 \cdot 28.885$

Table 2.3: Coupling constants for the different NL3$\omega\rho$ models

L (MeV)	118	88	68	61	55
g_ω	12.868	9.9536	10.297	10.753	11.276
$\Lambda_{\omega\rho}$	0	0.01	0.02	0.025	0.03

2.2 Equations of motion

To obtain the equations of motion for the fields, we apply the Euler–Lagrange equations

$$\frac{\partial \mathcal{L}}{\partial \phi} = \frac{\partial}{\partial x^\mu}\left(\frac{\partial \mathcal{L}}{\partial(\partial_\mu \phi)}\right)$$

to each of the fields defined before.

Applying the Euler–Lagrange equations to Ψ gives us the equations of motion for the nucleons

$$\left[\gamma_\mu\left(i\partial^\mu - g_\omega\omega^\mu - \frac{g_\rho}{2}\vec{\tau}\cdot\vec{\rho}^\mu - eA^\mu\frac{1+\tau_3}{2}\right) - m^*\right]\Psi = 0. \tag{2.7}$$

Similarly, the equations of motion for electrons obey a Dirac equation of the form

$$\Big[\gamma_\mu(i\partial^\mu + eA^\mu) - m_e\Big]\Psi_e = 0. \tag{2.8}$$

The remaining equations for the fields are

$$\big(\Box\,\sigma + m_\sigma^2\sigma\big) + \frac{\kappa\sigma^2}{2} + \frac{\lambda\sigma^3}{6} = g_\sigma\overline{\Psi}\Psi \tag{2.9}$$

$$\big(\Box\,\omega^\mu + m_\omega^2\omega^\mu\big) - \partial^\mu\big(\partial_\lambda\omega^\lambda\big) + \frac{\xi}{3!}\big(\omega_\lambda\omega^\lambda\big)\omega^\mu + 2\Lambda_{\omega\rho}\; g_\omega^2\; g_\rho^2\; \big(\vec{\rho}_\lambda\cdot\vec{\rho}^\lambda\big)\omega^\mu = g_\omega\overline{\Psi}\gamma^\mu\Psi \tag{2.10}$$

$$\Big(\partial_\lambda\vec{B}^{\lambda\mu} + m_\rho^2\vec{\rho}^\mu\Big) + g_\rho\vec{\rho}_\lambda\times\vec{B}^{\mu\lambda} + g_\rho^2\big((\vec{\rho}_\lambda\cdot\vec{\rho}^\mu)\vec{\rho}^\lambda - \big(\vec{\rho}_\lambda\cdot\vec{\rho}^\lambda\big)\vec{\rho}^\mu\big) + 2\Lambda_{\omega\rho}\; g_\omega^2\; g_\rho^2\; \big(\omega_\lambda\omega^\lambda\big)\vec{\rho}^\mu = \frac{g_\rho}{2}\big(\overline{\Psi}\gamma^\mu\vec{\tau}\Psi\big) \tag{2.11}$$

Solving these equations is, in general, a difficult problem, so in the next sections we are going to explain how they are usually evaluated, using a technique called *relativistic mean-field approximation*.

2.3 Mean-field approximation

The starting point for the mean-field approximation are the assumptions that our system 1) extends indefinitely; 2) is composed of stationary, uniform matter; and that 3) matter is in its ground state. The second point means that any observable quantity, such as densities and currents, take the same value everywhere and do not change with time. However, it is worthwhile to emphasize that only the *observable* quantities are assumed to be stationary; other quantities, such as wavefunctions, may be time-dependent. An example is the plane wave $\Psi_0 e^{-i\boldsymbol{k}\cdot\boldsymbol{r}}$, which has a time-independent density $\left(\Psi_0^* e^{i\boldsymbol{k}\cdot\boldsymbol{r}}\right)\left(\Psi_0 e^{-i\boldsymbol{k}\cdot\boldsymbol{r}}\right) = |\Psi_0|^2$.

The second part of our approximation consists of setting the meson fields σ, ω, $\vec{\rho}$ to their expectation values in the ground state,

$$\sigma \to \langle\sigma\rangle \qquad \omega \to \langle\omega\rangle \qquad \vec{\rho} \to \langle\vec{\rho}\rangle\,.$$

We do this by taking the mean values of equations 2.9, 2.10 and 2.11, and evaluating the mean source densities and currents (the right-hand sides) at the ground-state of matter. The fields σ, ω and $\vec{\rho}$ become classical, and the protons, neutrons and electrons move in an environment defined by them. We will also keep using the symbols σ, ω, $\vec{\rho}$, while remembering that they stand for mean values.

2.3.1 Force field equations

Since we assume that matter is uniform, the mean values of the densities and currents are independent of the position. This, in turn, implies that the meson fields are constant. As such, derivatives of the meson fields vanish, and the previous equations become

$$m_\sigma^2\sigma + \frac{\kappa\sigma^2}{2} + \frac{\lambda\sigma^3}{6} = g_\sigma \left\langle\overline{\Psi}\Psi\right\rangle \tag{2.12}$$

$$m_\omega^2\omega^\mu + \frac{\xi}{3!}\big(\omega_\lambda\omega^\lambda\big)\omega^\mu + 2\Lambda_{\omega\rho}\, g_\omega^2\, g_\rho^2\, \big(\vec{\rho}_\lambda\cdot\vec{\rho}^{\,\lambda}\big)\omega^\mu = g_\omega \left\langle\overline{\Psi}\gamma^\mu\Psi\right\rangle \tag{2.13}$$

$$m_\rho^2\vec{\rho}^{\,\mu} + g_\rho^2\big((\vec{\rho}_\lambda\cdot\vec{\rho}^{\,\mu})\vec{\rho}^{\,\lambda} - \big(\vec{\rho}_\lambda\cdot\vec{\rho}^{\,\lambda}\big)\vec{\rho}^{\,\mu}\big) + 2\Lambda_{\omega\rho}\, g_\omega^2\, g_\rho^2\, \big(\omega_\lambda\omega^\lambda\big)\vec{\rho}^{\,\mu} = \frac{g_\rho}{2}\left\langle\overline{\Psi}\gamma^\mu\vec{\tau}\Psi\right\rangle. \tag{2.14}$$

Let us now focus on the term $\overline{\Psi}\gamma^\mu\vec{\tau}\Psi$ of the third equation, which acts as the source of the $\vec{\rho}^{\,\mu}$ fields. Explicitly, its components are

$$\begin{aligned}
\overline{\Psi}\gamma^\mu\tau_1\Psi &= \overline{\Psi}_p\gamma^\mu\Psi_n + \overline{\Psi}_n\gamma^\mu\Psi_p \\
\overline{\Psi}\gamma^\mu\tau_2\Psi &= -i\big(\overline{\Psi}_p\gamma^\mu\Psi_n - \overline{\Psi}_n\gamma^\mu\Psi_p\big) \\
\overline{\Psi}\gamma^\mu\tau_3\Psi &= \overline{\Psi}_p\gamma^\mu\Psi_p - \overline{\Psi}_n\gamma^\mu\Psi_n.
\end{aligned}$$

The first and second components have cross terms mixing the proton and neutron fields, which means that the ρ_1 and ρ_2 fields mediate an exchange of isospin. We

are going to assume that the ground-state is composed of particles with definite isospin (we want to know exactly how many protons and neutrons there are), so these two fields become unnecessary. However, even unnecessary fields come at the cost of increasing the total energy, so we will set the values of ρ_1 and ρ_2 to zero. By removing their contribution from the previous equations, we are left with

$$m_\sigma^2\sigma + \frac{\kappa\sigma^2}{2} + \frac{\lambda\sigma^3}{6} = g_\sigma \left\langle \overline{\Psi}\Psi \right\rangle \tag{2.15}$$

$$m_\omega^2\omega^\mu + \frac{\xi}{3!}\big(\omega_\lambda\omega^\lambda\big)\omega^\mu + 2\Lambda_{\omega\rho}\, g_\omega^2\, g_\rho^2\, \big(\rho_{3\lambda}\rho_3^\lambda\big)\omega^\mu = g_\omega \left\langle \overline{\Psi}\gamma^\mu\Psi \right\rangle \tag{2.16}$$

$$m_\rho^2\rho_3^\mu + 2\Lambda_{\omega\rho}\, g_\omega^2\, g_\rho^2\, \big(\omega_\lambda\omega^\lambda\big)\rho_3^\mu = \frac{g_\rho}{2} \left\langle \overline{\Psi}\gamma^\mu\tau_3\Psi \right\rangle . \tag{2.17}$$

Notice that we can factor σ, ω^μ and ρ_3^μ from the left-hand sides of these equations. We are then lead to define the effective masses

$$m_\sigma^{*\,2} = m_\sigma^2 + \frac{\kappa\sigma}{2} + \frac{\lambda\sigma^2}{6} \tag{2.18}$$

$$m_\omega^{*\,2} = m_\omega^2 + \frac{\xi}{3!}g_\omega^4(\omega^\lambda\omega_\lambda) + 2\Lambda_{\omega\rho}\, g_\omega^2\, g_\rho^2(\rho_3^\lambda\rho_{3\lambda}) \tag{2.19}$$

$$m_\rho^{*2} = m_\rho^2 + 2\Lambda_{\omega\rho}\, g_\omega^2\, g_\rho^2\, (\omega^\lambda\omega_\lambda), \tag{2.20}$$

which leads us to the simplified form of the previous equations:

$$m_\sigma^{*\,2}\sigma \;\; = g_\sigma \left\langle \overline{\Psi}\Psi \right\rangle \tag{2.21}$$

$$m_\omega^{*\,2}\omega^\mu = g_\omega \left\langle \overline{\Psi}\gamma^\mu\Psi \right\rangle \tag{2.22}$$

$$m_\rho^{*2}\rho_3^\mu = \frac{g_\rho}{2} \left\langle \overline{\Psi}\gamma^\mu\tau_3\Psi \right\rangle . \tag{2.23}$$

We still need to evaluate the currents on the right-hand sides. In order to do so, we need to solve equations of motion for the protons, neutrons and electrons.

2.3.2 Matter field equations

In the relativistic mean-field approximation, the nucleons and electron equations maintain the form of Equations 2.7 and 2.8, the difference being that the fields σ, ω and ρ_3 now take their mean-values and can thus be treated as classical fields. We can separate the proton and neutron equations, which leaves us with the three equations

$$\Big[\gamma_\mu\Big(i\partial^\mu - g_\omega\omega^\mu - \frac{g_\rho}{2}\rho_3^\mu - eA^\mu\Big) - m_p^*\Big]\Psi_p = 0 \tag{2.24}$$

$$\Big[\gamma_\mu\Big(i\partial^\mu - g_\omega\omega^\mu + \frac{g_\rho}{2}\rho_3^\mu\Big) - m_n^*\Big]\Psi_n = 0 \tag{2.25}$$

$$\Big[\gamma_\mu(i\partial^\mu + eA^\mu) - m_e\Big]\Psi_e = 0. \tag{2.26}$$

Since the force fields are classical, these equations describe particles moving through external, imposed potentials, without changing them (although the actual values of the potentials will be found later to depend on the solutions of these equations, when we impose self-consistency). We can then define single-particle states, which will be the basic building blocks of our system.

We will begin by finding the single-particle states of the neutrons. Being a modified version of the free Dirac equation, it is the easiest equation to solve. For convenience, we leave the actual calculations for Appendix A. The main results we are interested in is that the solutions are plane waves of definite four-momentum $p^\mu = (E_n, \boldsymbol{p})$ obeying

$$E_n(\boldsymbol{p}) = g_\omega \omega^0 - \frac{g_\rho}{2}\rho_3^0 + \sqrt{\left(\boldsymbol{p} - g_\omega \boldsymbol{\omega} + \frac{g_\rho}{2}\boldsymbol{\rho_3}\right)^2 + (m_n - g_\sigma \sigma)^2}. \tag{2.27}$$

It is convenient to define effective energies and momenta by subtracting the constant potentials

$$\bar{p}^\mu = p^\mu - \left(g_\omega \omega^\mu - \frac{g_\rho}{2}\rho_3^\mu\right) \Leftrightarrow \begin{cases} \bar{E}_n = E_n - \left(g_\omega \omega^0 - \frac{g_\rho}{2}\rho_3^0\right) \\ \bar{\boldsymbol{p}} = \boldsymbol{p} - \left(g_\omega \boldsymbol{\omega} - \frac{g_\rho}{2}\boldsymbol{\rho_3}\right), \end{cases} \tag{2.28}$$

so we can write the previous relationship more compactly as

$$\bar{E}_n(\bar{\boldsymbol{p}}) = \sqrt{\bar{\boldsymbol{p}}^2 + m_n^{*\,2}}. \tag{2.29}$$

The equations for protons and electrons have more involved calculations because, unlike the neutrons, they are subject to the position-dependent electromagnetic potential. The details of these calculations can also be found in Appendix A. The main results are that, under a constant magnetic field, these charged particles behave like quantum harmonic oscillators and their energy levels are quantized in the so-called *Landau levels*. For the proton, the total energy is given by

$$\begin{aligned} E_p(p_z, \nu) = {} & g_\omega \omega^0 + \frac{g_\rho}{2}\rho_3^0 \\ & + \sqrt{\left(p_z - g_\omega \omega - \frac{g_\rho}{2}\rho_3\right)^2 + (m_p - g_\sigma \sigma)^2 + 2\nu e B}. \end{aligned} \tag{2.30}$$

The variable ν is a natural number that can be $0, 1, 2, \dots$, which labels the Landau levels. The momentum in the z direction, p_z, has no restriction and can take any value. For $\nu \neq 0$, the Landau levels are doubly degenerate, accounting for both spin projections. The $\nu = 0$ level occurs only for the spin-up projection. Defining the effective energy and momentum as before

$$\begin{cases} \bar{E}_p = E_p - \left(g_\omega \omega^0 + \frac{g_\rho}{2}\rho^0\right) \\ \bar{p}_z = p_z - \left(g_\omega \omega^z + \frac{g_\rho}{2}\rho^z\right) \end{cases} \tag{2.31}$$

simplifies the energy expression to

$$\bar{E}_p(\bar{p}_z, \nu) = \sqrt{\bar{p}_z^2 + m_p^{*\,2} + 2\nu e B}. \tag{2.32}$$

Finally, the electron energy levels are similar to that of the protons, and are given by

$$E_e(p_z, \nu) = \sqrt{p_z^2 + m_e^2 + 2\nu e B}, \tag{2.33}$$

again for $\nu = 0, 1, 2, \dots$, with every level except $\nu = 0$ being doubly degenerate.

2.3.3 Evaluating the source currents

We now turn to the question of calculating the source currents

$$\rho_s = \left\langle \overline{\Psi}\Psi \right\rangle, \quad j^\mu = \left\langle \overline{\Psi}\gamma^\mu\Psi \right\rangle \quad \text{and} \quad j_3^\mu = \left\langle \overline{\Psi}\gamma^\mu\tau_3\Psi \right\rangle,$$

which are, respectively, the scalar density, baryon current and isospin current. Since we are going to consider single-particle states with definite numbers of protons and neutrons, we can expand this in the Ψ_p and Ψ_n components

$$\begin{cases} \rho_s = \left\langle \overline{\Psi}_p\Psi_p \right\rangle + \left\langle \overline{\Psi}_n\Psi_n \right\rangle = \rho_{s,p} + \rho_{s,n} \\ j^\mu = \left\langle \overline{\Psi}_p\gamma^\mu\Psi_p \right\rangle + \left\langle \overline{\Psi}_n\gamma^\mu\Psi_n \right\rangle = j_p^\mu + j_n^\mu \\ j_3^\mu = \left\langle \overline{\Psi}_p\gamma^\mu\Psi_p \right\rangle - \left\langle \overline{\Psi}_n\gamma^\mu\Psi_n \right\rangle = j_p^\mu - j_n^\mu. \end{cases} \tag{2.34}$$

Our general goal is then to calculate quantities of the form $\left\langle \overline{\Psi}_i\Gamma\Psi_i \right\rangle$ (the index i standing for n and p) in the ground-state. We write $(\overline{\Psi}_i\Gamma\Psi_i)_S$ as the expectation value of Γ for the single-particle state with quantum numbers $S = (s_1, s_2, \ldots)$. It is clear that $\left\langle \overline{\Psi}_i\Gamma\Psi_i \right\rangle$ is a sum of all these contributions, that is,

$$\left\langle \overline{\Psi}_i\Gamma\Psi_i \right\rangle = \sum_{\{S\}} (\overline{\Psi}_i\Gamma\Psi_i)_S. \tag{2.35}$$

We use S to label a state instead of the explicit quantum numbers because the neutrons and protons are characterized by very different numbers. A neutron state may be completely identified by the pair $(\boldsymbol{p}, s)$ of its momentum and spin projection, while a proton may be characterized by the triple (p_z, ν, s) of its z-momentum, Landau level and spin projection. The sum itself is just a convenient notation: it may partly be an integral, since both $\boldsymbol{p}$ and p_z are continuous variables.

We could calculate the expectation values $(\overline{\Psi}_i\Gamma\Psi_i)_S$ by performing the actual multiplication of the spinor solutions we have obtained for protons and neutrons. Instead, we will follow a simple strategy, which will allow us to do these calculations faster (see Glendenning [19]).

Neutron currents

The method is more easily illustrated in the neutron case. The first step is to calculate the Hamiltonian operator from the Lagrangian part of our model that describes the motion of neutrons:

$$\mathcal{L}_\mathrm{n} = \overline{\Psi}_n \Big[\gamma^\mu (i\partial_\mu - V_\mu) - m_n^* \Big] \Psi_n. \tag{2.36}$$

The potential with which the neutrons interact is

$$V^\mu = g_\omega \omega^\mu - \frac{g_\rho}{2}\rho_3^\mu. \tag{2.37}$$

We find the Hamiltonian density via the Legendre transformation

$$\mathcal{H} = \frac{\partial\mathcal{L}}{\partial(\partial_0\Psi_n)}\partial_0\Psi_n - \mathcal{L} \tag{2.38}$$

$$= \overline{\Psi}_n\gamma_0 \Big[-i\boldsymbol{\gamma}\cdot\boldsymbol{\nabla} + \gamma^\mu V_\mu + m_n^* \Big] \Psi_n. \tag{2.39}$$

Now, we will let Ψ_n be a state of definite momentum $\boldsymbol{p}$ and spin s, that is, a plane wave. We can then partially evaluate the Hamiltonian density:

$$\mathcal{H} = \overline{\Psi}_n \gamma_0 \Big[\boldsymbol{\gamma} \cdot \boldsymbol{p} + \gamma^\mu V_\mu + m_n^* \Big] \Psi_n. \tag{2.40}$$

From this we can extract the (partially evaluated) Hamiltonian operator:

$$H = \gamma_0 \Big[\boldsymbol{\gamma} \cdot \boldsymbol{p} + \gamma^\mu V_\mu + m_n^* \Big]. \tag{2.41}$$

It is obvious that the expectation value $(\Psi_n^\dagger H \Psi_n)_{(\boldsymbol{p},s)}$ is the energy of this state, which we obtained in Equation 2.27, that is

$$(\Psi_n^\dagger H \Psi_n)_{(\boldsymbol{p},s)} = E_n(\boldsymbol{p}). \tag{2.42}$$

Let us now take the derivative of this quantity with respect to some variable ξ that appears in H (which could be, for instance, p_z or m_n). Applying the product rule, we obtain

$$\frac{\partial}{\partial \xi} \big(\Psi_n^\dagger H \Psi_n \big)_{(\boldsymbol{p},s)} = \left(\frac{\partial \Psi_n^\dagger}{\partial \xi} H \Psi_n \right)_{(\boldsymbol{p},s)} + \left(\Psi_n^\dagger \frac{\partial H}{\partial \xi} \Psi_n \right)_{(\boldsymbol{p},s)} + \left(\Psi_n^\dagger H \frac{\partial \Psi_n}{\partial \xi} \right)_{(\boldsymbol{p},s)} \tag{2.43}$$

By using $H\Psi_n = E_n \Psi_n$, the first and last terms on the right-hand side can be brought together again with the product rule

$$\frac{\partial}{\partial \xi} \big(\Psi_n^\dagger H \Psi_n \big)_{(\boldsymbol{p},s)} = E_n \frac{\partial}{\partial \xi} \big(\Psi_n^\dagger \Psi_n \big)_{(\boldsymbol{p},s)} + \left(\Psi_n^\dagger \frac{\partial H}{\partial \xi} \Psi_n \right)_{(\boldsymbol{p},s)}$$

Of course, $\big(\Psi_n^\dagger \Psi_n \big)_{(\boldsymbol{p},s)} = 1$, so its derivative vanishes and we are left with

$$\frac{\partial}{\partial \xi} \big(\Psi_n^\dagger H \Psi_n \big)_{(\boldsymbol{p},s)} = \left(\Psi_n^\dagger \frac{\partial H}{\partial \xi} \Psi_n \right)_{(\boldsymbol{p},s)} \tag{2.44}$$

or, in a more expressive way,

$$\left(\Psi_n^\dagger \frac{\partial H}{\partial \xi} \Psi_n \right)_{(\boldsymbol{p},s)} = \frac{\partial E_n}{\partial \xi}. \tag{2.45}$$

Calculating the expectation value can then be achieved by simply taking a derivative of the energy. Remember that we want to evaluate quantities of the form $(\overline{\Psi}_n \Gamma \Psi_n) = (\Psi_n^\dagger \gamma^0 \Gamma \Psi_n)$, so we only need to find a variable ξ in Equation 2.41 such that

$$\frac{\partial H}{\partial \xi} = \gamma^0 \Gamma.$$

Our choices for the variables ξ are presented in the following table.

Quantity	**Exp. value**	$\gamma^0\Gamma$	ξ
$\rho_{s,n}$	$\langle \overline{\Psi}_n \Psi_n \rangle$	γ^0	m_n
n_n	$\langle \Psi_n^\dagger \Psi_n \rangle$	$1 = \gamma^0\gamma^0$	V_0
$\boldsymbol{j}_n$	$\langle \Psi_n^\dagger \boldsymbol{\gamma} \Psi_n \rangle$	$\gamma^0 \boldsymbol{\gamma}$	$\boldsymbol{p}$

Notice, for instance, that for n_n we obtain the normalization condition

$$(\Psi_n^\dagger \Psi_n) = \frac{\partial E_n}{\partial V_0} = 1. \tag{2.46}$$

All we have left to do, after finding out how to calculate the expectation values, is to sum over all states. In the neutron case, we perform an integral over the momenta $\boldsymbol{p}$ and a sum over the spins s. Since the energy does not depend on the spin projection, we only need to multiply by two. We then have

$$\rho_{s,n} = 2\int \frac{\mathrm{d}^3 p}{(2\pi)^3}\frac{\partial E_n}{\partial m_n} \tag{2.47}$$

$$n_n = 2\int \frac{\mathrm{d}^3 p}{(2\pi)^3} \tag{2.48}$$

$$\boldsymbol{j}_n = 2\int \frac{\mathrm{d}^3 p}{(2\pi)^3}\boldsymbol{\nabla}_{\boldsymbol{p}} E_n. \tag{2.49}$$

The actual computation of the integrals will depend on the distribution of momenta, which we will present later.

Proton currents

The proton part of the Lagrangian is similar in form to that of the neutrons (Equation 2.36). However, the potential V^μ now includes the electromagnetic field:

$$V^\mu = g_\omega \omega^\mu + \frac{g_\rho}{2}\rho_3^\mu + eA^\mu = V_0^\mu + eA^\mu, \tag{2.50}$$

with V_0^μ standing for the constant part.

The Hamiltonian density is still given by Equation 2.40. The most involved part is the calculation of the term $-i\boldsymbol{\gamma}\cdot\boldsymbol{\nabla}$, which we will skip, and leave only the resulting Hamiltonian operator

$$H = \gamma_0\Big[\gamma^1\Big(i\big((p_y - V_0^2) - eBx\big) - V_0^1\Big) + \gamma^2 p_y + \gamma^3 p_z + \gamma_\mu V_0^\mu + \gamma_\mu A^\mu + m_p^*\Big] \tag{2.51}$$

The strategy is still to choose the appropriate ξ, which we do in table below

Quantity	**Exp. value**	$\gamma^0\Gamma$	ξ
$\rho_{s,p}$	$\langle\overline{\Psi}_p\Psi_p\rangle$	γ^0	m_n
n_p	$\langle\Psi_p^\dagger\Psi_p\rangle$	$1 = \gamma^0\gamma^0$	V_0^0
$j_p^3 = j_p$	$\langle\Psi_p^\dagger\gamma^3\Psi_p\rangle$	$\gamma^0\gamma^3$	p_z

Notice that we left out the x and y components of the proton current in this table. The reason for this is that they vanish. By letting $\xi = \rho_3^1$, for instance, we can calculate the expectation of the operator $\gamma^0\gamma^1$ (ρ_3^1 is hidden in V_0^1, in the last equation). However, the proton energy does not depend on ρ_3^1 (Equation 2.30), so this current must be zero:

$$\frac{\partial E_p}{\partial \rho_3^1} = 0 \Rightarrow \big(\overline{\Psi}_p\gamma^1\Psi_p\big) = 0 \Rightarrow j_p^1 = 0. \tag{2.52}$$

If we choose $\xi = \rho_3^2$, we actually obtain the expectation value of the operator $\Gamma = (\gamma^2 + i\gamma^1)$, and not just γ^2. But, again, the energy does not depend on ρ_3^2. We then conclude that

$$\frac{\partial E_p}{\partial \rho_3^2} = 0 \Rightarrow \left(\overline{\Psi}_p \gamma^2 \Psi_p\right) + i\left(\overline{\Psi}_p \gamma^1 \Psi_p\right) = 0. \tag{2.53}$$

Since $\left(\overline{\Psi}_p \gamma^1 \Psi_p\right)$ was already found to be zero, it must be that $\left(\overline{\Psi}_p \gamma^2 \Psi_p\right)$ is also zero. Therefore, j_3^2 vanishes as well.

Finally, we find the quantities we want by summing over all states. In the proton case, this is achieved by integrating over all momenta p_z, and summing over the Landau levels ν and spins s:

$$\rho_{s,p} = \frac{eB}{2\pi} \sum_{\nu=0}^{\nu_{\max}^p} g_\nu \int \frac{\mathrm{d}p_z}{2\pi} \frac{\partial E_p}{\partial m_p} \tag{2.54}$$

$$n_p = \frac{eB}{2\pi} \sum_{\nu=0}^{\nu_{\max}^p} g_\nu \int \frac{\mathrm{d}p_z}{2\pi} \tag{2.55}$$

$$j_p = \frac{eB}{2\pi} \sum_{\nu=0}^{\nu_{\max}^p} g_\nu \int \frac{\mathrm{d}p_z}{2\pi} \frac{\partial E_p}{\partial p_z}. \tag{2.56}$$

The coefficient $(eB/2\pi)$ is the density of states of a Landau level. The factor g_ν is the spin degeneracy

$$g_\nu = \begin{cases} 1, & \nu = 0 \\ 2, & \nu > 0. \end{cases} \tag{2.57}$$

To evaluate these currents, we need only define what the ground state actually is, which is what we will do next.

2.4 Ground-state at zero temperature

2.4.1 The ground state

In neutron stars, it is a good approximation to set the temperature to $T = 0$ (see Glendenning [19]). In this limit, the protons, neutrons and electrons occupy the lowest energy states up to a maximum energy, called the Fermi energy. We will denote the Fermi energies by μ_n, μ_p and μ_e.

The occupied neutron states are those with momenta $\boldsymbol{p}$ such that the energy

$$E_n(\boldsymbol{p}) = g_\omega \omega^0 - \frac{g_\rho}{2}\rho_3^0 + \sqrt{\left(\boldsymbol{p} - g_\omega \boldsymbol{\omega} + \frac{g_\rho}{2}\boldsymbol{\rho_3}\right)^2 + m_n^{*\,2}}$$

is at most μ_n. These states are occupied twice, once for each spin projection $\pm 1/2$. If we define the effective Fermi energy

$$\bar{\mu}_n = \mu_n - \left(g_\omega \omega^0 - \frac{g_\rho}{2}\rho_3^0\right), \tag{2.58}$$

then the previous condition is equivalent to saying that the neutron states are those for which $\bar{\boldsymbol{p}} = \boldsymbol{p} - \left(g_\omega \boldsymbol{\omega} - \frac{g_\rho}{2}\boldsymbol{\rho_3}\right)$ is such that

$$\bar{\boldsymbol{p}}^2 \leq \bar{\mu}_n^2 - m_n^{*\,2} = \bar{p}_{Fn}^2, \tag{2.59}$$

which makes it evident that the Fermi surface is, in essence, a translated sphere whose radius is the effective Fermi momentum $\bar{p}_{Fn}$.

Proceeding still with effective quantities, the condition for protons is that

$$\begin{aligned}\sqrt{\bar{p}_z^2 + m_p^{*2} + 2\nu eB} &\leq \bar{\mu}_p \\ &= \mu_p - \left(g_\omega \omega^0 + \frac{g_\rho}{2}\rho_3^0\right)\end{aligned} \tag{2.60}$$

and $\bar{p}_z$ is defined as before, in Equation 2.31. We can see that there is a maximum possible value for ν. We will call this level $\nu^p_{\max}$ and we can calculate it from the previous condition by setting $\bar{p}_z$ to zero:

$$\nu^p_{\max} = \left\lfloor \frac{\bar{\mu}_p^2 - m_p^{*2}}{2eB} \right\rfloor. \tag{2.61}$$

The function $\lfloor x \rfloor$, called the floor function, returns the greatest integer that is at most x. For each ν between 0 and $\nu^p_{\max}$, there is a maximum $\bar{p}_z$ that can be achieved. We will call this momentum $\bar{p}_{Fp}$, for proton Fermi momentum, and its value depends on ν:

$$\bar{p}_{Fp}(\nu) = \sqrt{\bar{\mu}_p^2 - m_p^{*2} - 2\nu eB}. \tag{2.62}$$

The distribution of electrons is similar to that of the protons. The occupied states are those with momentum p_z and Landau level ν such that

$$\sqrt{p_z^2 + m_e^2 + 2\nu eB} \leq \mu_e. \tag{2.63}$$

The highest Landau level and Fermi momenta are, respectively,

$$\nu^e_{\max} = \left\lfloor \frac{\mu_e^2 - m_e^2}{2eB} \right\rfloor \quad \text{and} \quad p_{Fe}(\nu) = \sqrt{\mu_p^2 - m_e^2 - 2\nu eB}. \tag{2.64}$$

2.4.2 Source currents

We are now able to evaluate the source currents with the method we presented before.

Proton and neutron currents

We are going to calculate the neutron current (Equation 2.49) by evaluating its i-th component. We change variables to the reduced momentum, giving us

$$j_n^i = \frac{2}{(2\pi)^3}\int \mathrm{d}\bar{p}_i\,\mathrm{d}\bar{p}_j\,\mathrm{d}\bar{p}_k\,\frac{\partial \bar{E}_n}{\partial \bar{p}_i} = \frac{2}{(2\pi)^3}\int \mathrm{d}\bar{p}_j\,\mathrm{d}\bar{p}_k\left[\int \mathrm{d}E_n\right]. \tag{2.65}$$

Notice that the endpoints of the integral are $\bar{\mu}_p$, because the limits of the momentum $\bar{p}_i$ lie on the Fermi surface. Therefore the integral over the energy evaluates to $\bar{\mu}_n - \bar{\mu}_n = 0$, telling us that

$$\boldsymbol{j}_n = 0. \tag{2.66}$$

We write the proton current using the effective momenta and energy:

$$j_p = \frac{eB}{2\pi}\sum_\nu g_\nu \int \frac{\mathrm{d}\bar{p}_z}{2\pi}\frac{\partial \bar{E}_p}{\partial \bar{p}_z} = \frac{eB}{4\pi^2}\sum_\nu g_\nu \int \mathrm{d}\bar{E}_p. \tag{2.67}$$

As for the neutron currents, the endpoints of the integral over $\mathrm{d}\bar{E}_p$ are equal, they are the Fermi energy $\bar{\mu}_p$. As such, this current is also zero:

$$j_p = 0. \tag{2.68}$$

Notice now that, since both currents are zero, according to Equations 2.22 and 2.23, $\boldsymbol{\omega}$ and $\boldsymbol{\rho}$ must also be zero. This means that the effective momenta coincide with the normal momenta.

Neutron density or zero-field density

As we have seen, the neutron number density is

$$n_n = 2\int \frac{\mathrm{d}p^3}{(2\pi^2)}, \tag{2.69}$$

Since this relationship must be valid for any particle at zero field, including protons (the Dirac equation loses the eA^μ term), we will write n_i instead of n_n for generality. The integral must be the volume of the momentum sphere. Since we have concluded that $\boldsymbol{\omega} = \boldsymbol{\rho} = 0$, we do not need to use the effective momentum. The density is then

$$\begin{aligned} n_i &= \frac{1}{4\pi^3}\int \sin^2(\theta)\ p^2\ \mathrm{d}p\ \mathrm{d}\theta\ \mathrm{d}\phi \\ &= \frac{1}{4\pi^3} 4\pi \int p^2\,\mathrm{d}p. \end{aligned} \tag{2.70}$$

Since the momentum magnitude ranges from 0 to p_{Fi}, integrating yields

$$n_i = \frac{p_{Fi}^3}{3\pi^2}. \tag{2.71}$$

Proton and electron densities

We can rewrite the proton density equation to use the effective momentum:

$$n_p = \frac{eB}{2\pi}\sum_\nu g_\nu \int_{-p_{Fp}(\nu)}^{p_{Fp}(\nu)} \frac{\mathrm{d}p}{2\pi} = \frac{eB}{2\pi^2}\sum_\nu g_\nu p_{Fe}(\nu) \tag{2.72}$$

Even though we did not derive the electron density explicitly, its value is given by an expression similar to that of the protons. As such, it is given by

$$n_e = \frac{eB}{2\pi^2}\sum_\nu g_\nu p_{Fe}(\nu) \tag{2.73}$$

Neutron scalar density

We now evaluate the neutron scalar density. Notice that, when $B = 0$, the same expression will give us the proton scalar density.

$$\rho_{s,n} = 2\int \frac{\mathrm{d}^3p}{(2\pi)^3}\frac{\partial E_n}{\partial m_n} = \\ = \frac{2}{(2\pi)^3}\int \mathrm{d}^3p\left[\frac{m_n - g_\sigma\sigma}{\sqrt{\left(\boldsymbol{p} - g_\omega\boldsymbol{\omega} + -\frac{g_\rho}{2}\boldsymbol{\rho}_3\right)^2 + (m_n - g_\sigma\sigma)^2}}\right] \tag{2.74}$$

The integral must now be performed over the ground-state we presented before. Since $\boldsymbol{\omega} = \boldsymbol{\rho} = 0$, our integral simplifies to

$$\rho_{s,n} = \frac{2m_n^*}{(2\pi)^3}\int \frac{\mathrm{d}^3p}{\sqrt{p^2 + m_n^{*\,2}}} \tag{2.75}$$

and the integral is over the sphere of momenta with magnitude smaller than p_{Fn}. Switching to spherical coordinates and integrating over the angular variables, we obtain

$$\rho_{s,n} = \frac{m_n^*}{\pi^2}\int \frac{p^2\ \mathrm{d}p}{\sqrt{p^2 + m_n^{*\,2}}} \tag{2.76}$$

This integral is an instance of

$$\int \frac{x^2\ \mathrm{d}x}{\sqrt{x^2 + a^2}} = \frac{1}{2}\Big(x\sqrt{a^2 + x^2} - a^2\ln\Big(\sqrt{a^2 + x^2} + x\Big)\Big) + C, \tag{2.77}$$

with C being some constant. We are integrating from 0 to p_{Fn}, so we obtain

$$\rho_{s,n} = \frac{m_n^*}{2\pi^2}\left[p_{Fn}\sqrt{p_{Fn}^2 + m_n^{*\,2}} - m_n^{*\,2}\ln\left(\frac{\sqrt{p_{Fn}^2 + m_n^{*\,2}} + p_{Fn}}{m_n^*}\right)\right] = \\ = \frac{m_n^*}{2\pi^2}\left[p_{Fn}\bar{\mu}_n - m_n^{*\,2}\ln\left(\frac{\bar{\mu}_n + p_{Fn}}{m_n^*}\right)\right]. \tag{2.78}$$

Proton scalar density

When we have a finite magnetic field, we must calculate the proton scalar current by summing over the Landau levels, instead of using an expression similar to that of the neutrons. As such, we have

$$\rho_{s,p} = \frac{eB}{2\pi}\sum_{\nu=0}^{\nu_{\max}^p} g_\nu \int \frac{\mathrm{d}p_z}{2\pi}\frac{\partial E_p}{\partial p_z} \\ = \frac{eB}{2\pi}\sum_{\nu=0}^{\nu_{\max}^p} g_\nu \int \frac{\mathrm{d}p_z}{2\pi}\frac{m_p - g_\sigma\sigma}{\sqrt{\left(p_z - g_\omega\omega^z - \frac{g_\rho}{2}\rho_3^z\right)^2 + (m_p - g_\sigma\sigma)^2 + 2\nu eB}} \tag{2.79}$$

Again, $\omega^z = \rho^z = 0$, giving us

$$\rho_{s,p} = \frac{eB}{(4\pi)^2}\sum_{\nu=0}^{\nu_{\max}^p} g_\nu m_p^* \int \frac{\mathrm{d}p_z}{\sqrt{p_z^2 + m_p^{*\,2} + 2\nu eB}}. \tag{2.80}$$

This integral is an instance of

$$\int \frac{\mathrm{d}x}{\sqrt{x^2+a^2}} = \ln\left(\sqrt{x^2+a^2}+x\right)+C, \tag{2.81}$$

with C being an arbitrary constant. In this case, a^2 would be $m_p^{*2}+2\nu eB$. The proton momentum for each Landau level ranges between $-p_{Fn}(\nu)$ and $+p_{Fn}(\nu)$, so we can evaluate the integral to give the proton current

$$\rho_{s,p} = \frac{eBm_p^*}{(4\pi)^2}\sum_{\nu=0}^{\nu_{\max}^p} g_\nu \ln\left(\frac{\bar{\mu}_p + p_{Fp}(\nu)}{\bar{\mu}_p - p_{Fp}(\nu)}\right). \tag{2.82}$$

2.4.3 Energy and pressure relations

Two quantities we want to extract from our model are the energy density and the pressure, which allow us to compute the equation of state. We do this by evaluating the stress-energy tensor

$$T^{\mu\nu} = \sum_i \frac{\partial\mathcal{L}}{\partial(\partial_\mu\phi_i)}\partial^\nu\phi_i - \mathcal{L}\eta^{\mu\nu}, \tag{2.83}$$

where ϕ_i are all the fields that appear in our Lagrangian. In the mean-field approximation, we are interested in the expectation value of $T^{\mu\nu}$. The energy density will correspond to the T^{00} component, and the pressure will be the average of the three diagonal space components:

$$\varepsilon = \quad \langle T^{00}\rangle = \left\langle \sum_i \frac{\partial\mathcal{L}}{\partial(\partial_0\phi_i)}\partial^0\phi_i \right\rangle - \langle\mathcal{L}\rangle \tag{2.84}$$

$$p = \frac{1}{3}\langle T^{jj}\rangle = \left\langle \sum_i \frac{\partial\mathcal{L}}{\partial(\partial_j\phi_i)}\partial^j\phi_i \right\rangle + \langle\mathcal{L}\rangle \tag{2.85}$$

We will skip the routine calculations and give the final expressions, starting with the energy density

$$\begin{aligned}\varepsilon = {} & \frac{1}{2}\left[m_\sigma^2\sigma^2 + \frac{\kappa\sigma^3}{3!} + \frac{\lambda\sigma^4}{4!}\right] - \left[\frac{m_\omega^2\omega^2}{2} + \xi\frac{g_\omega^4}{4!}(\omega^2)^2\right] \\ & - \frac{m_\rho^2\rho_3^2}{2} - \Lambda_{\omega\rho}(g_\omega g_\rho)^2\omega^2\rho_3^2 \\ & + g_\omega(n_p+n_n)\omega^0 + \frac{g_\rho}{2}(n_p-n_n)\rho_3^0 + \bar{\varepsilon}_n + \bar{\varepsilon}_p + \varepsilon_e.\end{aligned} \tag{2.86}$$

Note that we use $\omega^2 = \omega^\mu\omega_\mu$ and $\rho_3^2 = \rho_3^\mu\rho_{3\mu}$. With a finite magnetic field, the effective energies $\bar{\varepsilon}_n, \bar{\varepsilon}_p, \varepsilon_e$ are given by

$$\bar{\varepsilon}_n = \frac{1}{8}\left[6\bar{\mu}_n n_n + \left(\bar{\mu}_n p_{Fn} - \frac{m_n^{*2}}{2}\ln\left(\frac{\bar{\mu}_n + p_{Fn}}{\bar{\mu}_n - p_{Fn}}\right)\right)\right] \tag{2.87}$$

$$\bar{\varepsilon}_p = \frac{\bar{\mu}_p n_p}{2} + \frac{eB}{4\pi^2}\left[\sum_{\nu=0}^{\nu_{\max}^p} g_\nu\left(m_p^{*2}+2\nu eB\right)\ln\left(\frac{\bar{\mu}_p + p_{Fp}}{\bar{\mu}_p - p_{Fp}}\right)\right] \tag{2.88}$$

$$\varepsilon_e = \frac{\mu_e n_e}{2} + \frac{eB}{4\pi^2}\left[\sum_{\nu=0}^{\nu_{\max}^e} g_\nu\left(m_e^2+2\nu eB\right)\ln\left(\frac{\mu_e + p_{Fe}}{\mu_e - p_{Fe}}\right)\right] \tag{2.89}$$

with p_{Fp}, p_{Fe}, $\nu^p_{\max}$ and $\nu^e_{\max}$ defined as in the preceding section. When the magnetic field is zero, the proton and electron effective energy densities are similar to that of the neutrons:

$$\bar{\varepsilon}_p = \frac{1}{8}\left[6\bar{\mu}_p n_p + \left(\bar{\mu}_p p_{Fp} - \frac{m_p^{*2}}{2}\ln\left(\frac{\bar{\mu}_p + p_{Fp}}{\bar{\mu}_p - p_{Fp}}\right)\right)\right] \tag{2.90}$$

$$\varepsilon_e = \frac{1}{8}\left[6\mu_e n_e + \left(\mu_e p_{Fe} - \frac{m_e^2}{2}\ln\left(\frac{\mu_e + p_{Fe}}{\mu_e - p_{Fe}}\right)\right)\right]. \tag{2.91}$$

Not surprisingly, after computing the stress-energy tensor components, we find the pressure is given by a Legendre transformation of the energy density:

$$p = -\varepsilon + \mu_n\, n_n + \mu_p\, n_p + \mu_e\, n_e \tag{2.92}$$

or, using the effective Fermi momenta,

$$\begin{aligned} p = -\varepsilon + \bar{\mu}_n\, n_n + \bar{\mu}_p\, n_p + \mu_e\, n_e \\ + g_\omega(n_p + n_n)\omega^0 + \frac{g_\rho}{2}(n_p - n_n)\rho_3^0. \end{aligned} \tag{2.93}$$

2.5 Charge neutrality and beta-equilibrium

The equations we have obtained so far are not restrictive enough to uniquely determine our system. We must answer the question: how do we set the values of the Fermi energies μ_n, μ_p and μ_e? We will not prescribe these values directly, but will instead impose physical conditions that our system must obey, and which will define the Fermi energies implicitly.

The first restriction we impose is that matter must be locally neutral, so naturally the number of protons and neutrons must be the same

$$n_p = n_e. \tag{2.94}$$

The second restriction comes from considering the evolution of the neutron star. Neutrons and protons can be converted between themselves through beta decay:

$$n \longleftrightarrow p + e + \bar{\nu}_e. \tag{2.95}$$

Reading from left to right, the process is the usual beta-decay. The inverse process, protons transforming to neutrons, is usually called *inverse* beta decay. Through this reaction, the number of particles of each species may change, so the thermodynamic energy of the system must take this effect into account. The first law of thermodynamics in this case reads

$$\mathrm{d}\left(\frac{\varepsilon}{n_b}\right) = -p\,\mathrm{d}\left(\frac{1}{n_b}\right) + T\,\mathrm{d}s + \mu_n \mathrm{d}\,Y_n + \mu_p \mathrm{d}\,Y_p + \mu_e \mathrm{d}\,Y_e, \tag{2.96}$$

where n_b is the baryon number density (our natural variable), and we have written the law in terms of the energy per nucleon. The values Y_n and Y_p are the neutron and proton fractions (compared to the total number of baryons), and Y_e has a similar interpretation. The values μ_e, μ_p and μ_n are the chemical potentials of each species and, since we have matter at zero temperature, they

coincide with the respective Fermi energies, hence why we have chosen the same symbols. We now assert that the matter we are considering is in equilibrium: its volume does not change ($\mathrm{d}(1/n_b) = 0$) and there is no work done upon the system ($\mathrm{d}(\varepsilon/n_b) = 0$). We also consider it to be thermally isolated, so there is no net exchange of heat: $\delta Q = T\,\mathrm{d}s = 0$. Therefore, the first law reduces to

$$0 = \mu_n \mathrm{d}\,Y_n + \mu_p \mathrm{d}\,Y_p + \mu_e \mathrm{d}\,Y_e. \tag{2.97}$$

If we consider the changes in the numbers of protons, neutrons, electrons and neutrinos in the beta decay reaction, we see that, if our system reached its ground state while respecting this reaction, then

$$\mathrm{d}\,Y_n = -\mathrm{d}\,Y_p = -\mathrm{d}\,Y_e = -\mathrm{d}\,Y_{\bar{\nu}_e}. \tag{2.98}$$

By replacing in the previous equation, we are left with

$$\mu_n = \mu_p + \mu_e. \tag{2.99}$$

This is the β-equilibrium condition we will be using. Note that we did not consider the contribution of neutrinos in our model, because we assume that they have largely been lost during the cooling period of the star.

With these two equations, there is only one variable to be determined among μ_n, μ_p and μ_e. Since we are going to choose the baryonic density n_b as our free variable, the last Fermi energy will be obtained as function of this value.

2.6 Summary of the system of equations

For the sake of summarizing everything in a single place, we list here the system of equations we are trying to solve. We have considered a mean-field model based on the NL3$\omega\rho$ Lagrangian. The equations for the averaged force fields σ, ω and ρ are

$$m_\sigma^{*\,2}\sigma = g_\sigma(\rho_{s,p} + \rho_{s,n}) \tag{2.100}$$

$$m_\omega^{*\,2}\omega^0 = g_\omega(n_p + n_n) \tag{2.101}$$

$$m_\rho^{*\,2}\rho_3^0 = \frac{g_\rho}{2}(n_p - n_n), \tag{2.102}$$

with the effective masses defined as in Equations 2.18:

$$m_\sigma^{*\,2} = m_\sigma^2 + \frac{\kappa\sigma}{2} + \frac{\lambda\sigma^2}{6} \tag{2.103}$$

$$m_\omega^{*\,2} = m_\omega^2 + \frac{\xi}{3!}g_\omega^4\left(\omega^0\right)^2 + 2\Lambda_{\omega\rho}\, g_\omega^2\, g_\rho^2\left(\rho_3^0\right)^2 \tag{2.104}$$

$$m_\rho^{*\,2} = m_\rho^2 + 2\Lambda_{\omega\rho}\, g_\omega^2\, g_\rho^2\left(\omega^0\right)^2. \tag{2.105}$$

The source currents must be computed in different ways, depending on whether we impose a magnetic field.

Without a magnetic field, the densities are given by

$$\begin{cases} n_n = \dfrac{p_{Fn}^2}{3\pi^2} \\ n_p = \dfrac{p_{Fp}^2}{3\pi^2} \\ n_e = \dfrac{p_{Fe}^2}{3\pi^2} \end{cases} \quad \text{with} \quad \begin{cases} p_{Fn} = \sqrt{\bar{\mu}_n^2 - m_n^{*\,2}} \\ p_{Fp} = \sqrt{\bar{\mu}_p^2 - m_p^{*\,2}} \\ p_{Fe} = \sqrt{\mu_e^2 - m_e^2}. \end{cases} \tag{2.106}$$

Notice that we use the the effective Fermi energies for convenience. The scalar currents are given by

$$\rho_{s,n} = \frac{m_n^*}{2\pi^2}\left[p_{Fn}\bar{\mu}_n - m_n^{*\,2}\ln\left(\frac{\bar{\mu}_n + p_{Fn}}{m_n^*}\right)\right] \tag{2.107}$$

$$\rho_{s,p} = \frac{m_p^*}{2\pi^2}\left[p_{Fp}\bar{\mu}_p - m_p^{*\,2}\ln\left(\frac{\bar{\mu}_p + p_{Fp}}{m_p^*}\right)\right]. \tag{2.108}$$

With a magnetic field, the densities are instead given by

$$\begin{cases} n_n = \dfrac{p_{Fn}^2}{3\pi^2} \\ n_p = \dfrac{eB}{2\pi^2}\displaystyle\sum_{\nu=0}^{\nu_{\max}^p} g_\nu p_{Fp}(\nu) \\ n_e = \dfrac{eB}{2\pi^2}\displaystyle\sum_{\nu=0}^{\nu_{\max}^e} g_\nu p_{Fe}(\nu) \end{cases} \quad \text{with} \quad \begin{cases} p_{Fn} &= \sqrt{\bar{\mu}_n^2 - m_n^{*\,2}} \\ p_{Fp}(\nu) &= \sqrt{\bar{\mu}_p^2 - m_p^{*\,2} - 2\nu eB} \\ p_{Fe}(\nu) &= \sqrt{\mu_e^2 - m_e^2 - 2\nu eB} \end{cases} \tag{2.109}$$

The maximum Landau levels are given by

$$\nu_{\max}^p = \left\lfloor \frac{\bar{\mu}_p^2 - m_p^{*\,2}}{2eB} \right\rfloor \quad \text{and} \quad \nu_{\max}^e = \left\lfloor \frac{\mu_e^2 - m_e^2}{2eB} \right\rfloor. \tag{2.110}$$

The scalar currents are computed from

$$\rho_{s,n} = \frac{m_n^*}{2\pi^2}\left[p_{Fn}\bar{\mu}_n - m_n^{*\,2}\ln\left(\frac{\bar{\mu}_n + p_{Fn}}{m_n^*}\right)\right] \tag{2.111}$$

$$\rho_{s,p} = \frac{eBm_p^*}{(4\pi)^2}\sum_{\nu=0}^{\nu_{\max}^p} g_\nu \ln\left(\frac{\bar{\mu}_p + p_{Fp}(\nu)}{\bar{\mu}_p - p_{Fp}(\nu)}\right). \tag{2.112}$$

Besides these relationships, we also impose the charge neutrality and beta equilibrium conditions:

$$\begin{cases} n_p = n_e \\ \bar{\mu}_n = \bar{\mu}_p + \mu_e + g_\rho \rho^0. \end{cases} \tag{2.113}$$

By choosing a particular value of n_b, we can solve these equations. They pose a self-consistency problem that is best solved with numerical methods, which is the strategy we will adopt. We explain the method we used in the Results section.

3. Crust size and entrainment

3.1 Crust size

To determine the crust size, we use the spinodal method described in Avancini et al. [23] and Providência et al. [24]. We leave the details of the explanation for the original sources and explain briefly the main idea. Our starting point is to solve the equations of the NL3$\omega\rho$ model by assuming that we are near a solution, and the difference between the actual solution and our state is just a small perturbation. As such the fields are written as $\sigma = \sigma_0 + \delta\sigma$, $\omega^0 = (\omega^0)_0 + \delta\omega^0$ and $\rho_3^0 = (\rho_3^0)_0 + \delta\rho_3^0$. We then replace these solutions in the Euler–Lagrange equations and obtain equations for the perturbations.

As we usually do in oscillation problems, we consider small, periodic perturbations of frequency ω called the *normal modes*. By substituting the *ansatz*, we end up finding equations for ω. We exclude trivial solutions, and we find we end up with equations not in ω, but in ω^2. It turns out that some of the solutions are negative, which implies that ω is imaginary. As such, the corresponding mode is not an oscillation, but an exponential growth of rate $|\omega|$. We then proceed to find the *maximum growth rate* at each density we are interested in. If it is larger than zero, then we can say that the matter is unstable under small perturbations, in which case we conclude that the homogeneous approximation we used was not a good guess. On the other hand, if the maximum growth rate is zero, then matter is stable and homogeneity is a reasonable assumption. If, at low densities, we find that matter is unstable, then the natural interpretation is that it is aggregating to form nuclei. Therefore, this method may correctly predict where the crust is localized and, especially, the region where the crust ends and the core begins – the density above which matter starts being homogeneous. This method predicts a crust-core transition at a density close to that obtained via pasta-phase calculations [10, 25].

3.2 Superfluid entrainment

It is believed that, inside a neutron star, and especially below the crust, there is a superfluid phase of neutrons and another of superconducting protons. Such mixtures of superfluids have been found in the laboratory, in particular in solutions of ^{3}He in superfluid ^{4}He. These solutions are peculiar, in that it may be possible to define several different velocities at the same point in space, in contrast with the single velocity field of classical fluid mechanics. In the case of the Helium mixture, three velocities are defined: the normal (non-superfluid)

velocity, and the ^{3}He and ^{4}He superfluid velocities. Andreev and Bashkin [26] developed in 1975 a formalism to deal with such cases. After appropriately defining the velocity of the superfluids, which we call $\boldsymbol{v}_1$ and $\boldsymbol{v}_2$, they proposed to calculate the momentum of each species by expanding in small powers of the relative velocities:

$$\boldsymbol{p}_1 = \rho_1 \boldsymbol{v}_n + \rho_{11}(\boldsymbol{v}_1 - \boldsymbol{v}_n) + \rho_{12}(\boldsymbol{v}_2 - \boldsymbol{v}_n) \tag{3.1}$$

$$\boldsymbol{p}_2 = \rho_2 \boldsymbol{v}_n + \rho_{21}(\boldsymbol{v}_1 - \boldsymbol{v}_n) + \rho_{22}(\boldsymbol{v}_2 - \boldsymbol{v}_n). \tag{3.2}$$

Here, $\boldsymbol{v}_n$ is the normal fluid velocity, ρ_1 and ρ_2 are each particle's densities, and the coefficients ρ_{ij} are the main dynamical quantities we are interested in; they form the so-called entrainment matrix. If the helium particles were not superfluid, then these coefficients would necessarily be zero. It is important to note that particles of one species transport mass of the other, which is why we include cross-terms ρ_{12} and ρ_{21}. The physical mechanism behind this are the weak interactions that hold the quasi-particles together; in the Helium case, the ^{3}He quasi-particle has an effective mass 2.3 times greater than that of the helium atom by itself, which shows that these effects are indeed important. In practice, the superfluids drag each other, which is why we say they are *entrained*.

In this work, we are interested in a relativistic formulation, so we will employ the relativistic treatment that is used in Gusakov et al. [15]. The previous equations become

$$\boldsymbol{j}_n = n_n \boldsymbol{u} + Y_{nn}(\boldsymbol{Q}_n - \mu_n \boldsymbol{u}) + Y_{np}(\boldsymbol{Q}_p - \mu_p \boldsymbol{u}) \tag{3.3}$$

$$\boldsymbol{j}_p = n_p \boldsymbol{u} + Y_{pn}(\boldsymbol{Q}_n - \mu_n \boldsymbol{u}) + Y_{pp}(\boldsymbol{Q}_p - \mu_p \boldsymbol{u}). \tag{3.4}$$

Notice that we use the number currents instead of the momentum, but the principle is the same. Here, we use $\boldsymbol{u}$ as the normal fluid velocity, and the Y_{ij} are the relativistic analogues of the entrainment coefficients. Also, $\boldsymbol{Q}_n$ and $\boldsymbol{Q}_p$ are the momenta per particle of the Cooper pairs of the superfluids. In the non-relativistic limit, we have

$$\boldsymbol{u} = \boldsymbol{v}_n \quad \text{and} \quad \rho_{ik} = m_i m_k Y_{ik}. \tag{3.5}$$

In the limit $T \to 0$, the normal fluid component ceases to exist, so the coefficients that multiply $\boldsymbol{u}$ must be such that the corresponding contributions vanish. Therefore, the previous equations reduce to

$$\boldsymbol{j}_n = Y_{nn}\boldsymbol{Q}_n + Y_{np}\boldsymbol{Q}_p \tag{3.6}$$

$$\boldsymbol{j}_p = Y_{pn}\boldsymbol{Q}_n + Y_{pp}\boldsymbol{Q}_p. \tag{3.7}$$

3.2.1 Ground-state with superfluid currents

In order to introduce the superfluid currents in our model, we need to change the ground state of matter of Section 2.4, as was done by Gusakov et al. [15]. The neutron ground state will be the same as before, but the momenta will be shifted by a small amount $\boldsymbol{Q}_n$, giving the new condition

$$|\boldsymbol{p} - \boldsymbol{Q}_n| \leq \sqrt{\bar{\mu}_n^2 - m_n^{*\,2}}. \tag{3.8}$$

We will choose to shift only in the z direction, by defining

$$\boldsymbol{Q}_n = Q_n \hat{\boldsymbol{z}}, \tag{3.9}$$

The proton ground-state will also be defined by shifting the momenta by a small, constant amount Q_p,

$$p_z - Q_p = \sqrt{\bar{\mu}_p^2 - m_p^{*2} - 2\nu eB}. \tag{3.10}$$

The electron ground-state will remain unchanged.

It is important to notice that the fields $\boldsymbol{\omega}$ and $\boldsymbol{\rho}$ are not necessarily zero anymore because we apply $\boldsymbol{Q}_n$ and Q_p. As such, we could write them in functional form as $\boldsymbol{\omega}(\boldsymbol{Q}_n, Q_p)$ and $\boldsymbol{\rho}(\boldsymbol{Q}_n, Q_p)$ and note that, since $\boldsymbol{\omega}(0,0) = \boldsymbol{\rho}(0,0) = 0$, these functions must not have a constant term. On the other hand, since Q_p and $\boldsymbol{Q}_n$ are small, we can neglect the higher powers $\boldsymbol{Q}_n^2, Q_p^2, \ldots$, so $\boldsymbol{\omega}$ and $\boldsymbol{\rho}$ are effectively linear combinations of $\boldsymbol{Q}_n$ and Q_p.

Number densities and scalar densities

Having only shifted the ground-state, the integral over the allowed momenta remains the same (it is, for instance, the volume inside the Fermi sphere for the neutrons). As such, the densities of neutrons, protons and electrons remain the same. The corrections to the scalar densities are of the order of $\boldsymbol{Q}_n^2$ and Q_p^2, so they will be considered unchanged.

Neutron current

We will now evaluate the neutron current (Equation 2.49) in the new ground-state, which is given by

$$\boldsymbol{j}_n = 2\int \frac{\mathrm{d}^3 p}{(2\pi)^3} \boldsymbol{\nabla}_{\boldsymbol{p}} \bar{E}_n(\boldsymbol{p} + \boldsymbol{Q}_n), \tag{3.11}$$

with the integral being performed over the old ground-state. The full expression for the energy inside the integral is

$$\bar{E}_n = \sqrt{\left((\boldsymbol{p} + \boldsymbol{Q}_n) - g_\omega \boldsymbol{\omega} + \frac{g_\rho}{2}\boldsymbol{\rho}\right)^2 + m_n^{*\,2}}. \tag{3.12}$$

Notice that the energy is given by a function of the form

$$f(\boldsymbol{x}) = \sqrt{\boldsymbol{x}^2 + a^2}, \tag{3.13}$$

which can be expanded as a power series in $\boldsymbol{x}_0$ around the point $\boldsymbol{x}$ as

$$f(\boldsymbol{x} + \boldsymbol{x}_0) = \sqrt{\boldsymbol{x}^2 + a^2} + \frac{\boldsymbol{x}\cdot\boldsymbol{x}_0}{\sqrt{\boldsymbol{x}^2 + a^2}} + \mathcal{O}(\boldsymbol{x}_0^2). \tag{3.14}$$

In this case, we will let $\boldsymbol{x} = \boldsymbol{p}$ and $\boldsymbol{x}_0 = \left(\boldsymbol{Q}_n - g_\omega\boldsymbol{\omega} + \frac{g_\rho}{2}\boldsymbol{\rho}\right)$. Since the value of the fields $\boldsymbol{\omega}$ and $\boldsymbol{\rho}$ are at most linear in $\boldsymbol{Q}_n$ and Q_p, we take $\boldsymbol{x}_0$ to be small. We can then discard terms of order $\boldsymbol{x}_0^2$ and greater, writing

$$\boldsymbol{j}_n = 2\int \frac{\mathrm{d}^3 p}{(2\pi)^3} \boldsymbol{\nabla}_{\boldsymbol{p}} \left[\sqrt{\boldsymbol{p}^2 + m_n^{*\,2}} + \frac{\boldsymbol{p}\cdot(\boldsymbol{Q}_n - g_\omega\boldsymbol{\omega} + \frac{g_\rho}{2}\boldsymbol{\rho})}{\sqrt{\boldsymbol{p}^2 + m_n^{*\,2}}}\right] \tag{3.15}$$

To simplify the following calculations, we will use an analogue of Gauss's theorem for gradients:

$$\int_V \mathrm{d}^3 x\, \boldsymbol{\nabla} f(\boldsymbol{x}) = \int_S \mathrm{d}\boldsymbol{S}\, f(\boldsymbol{x}). \tag{3.16}$$

Here, S stands for the surface enclosing the volume of integration V. The vector $\mathrm{d}\boldsymbol{S}$ has the magnitude of a surface element $\mathrm{d}S$ and is perpendicular to S at $\boldsymbol{x}$, pointing in the outwards direction. To prove this result, it suffices to project the integral onto a constant unit vector $\hat{\boldsymbol{n}}$

$$\hat{\boldsymbol{n}} \cdot \int_V \mathrm{d}^3x\, \boldsymbol{\nabla} f(\boldsymbol{x}) = \int_V \mathrm{d}^3x\, \hat{\boldsymbol{n}} \cdot \boldsymbol{\nabla} f(\boldsymbol{x}). \tag{3.17}$$

We can replace the term $\hat{\boldsymbol{n}} \cdot \boldsymbol{\nabla} f(\boldsymbol{x})$ using the product rule:

$$\boldsymbol{\nabla} \cdot (\hat{\boldsymbol{n}} f(\boldsymbol{x})) = (\boldsymbol{\nabla} \cdot \hat{\boldsymbol{n}}) f(\boldsymbol{x}) + \hat{\boldsymbol{n}} \cdot \boldsymbol{\nabla} f(\boldsymbol{x}) = \hat{\boldsymbol{n}} \cdot \boldsymbol{\nabla} f(\boldsymbol{x}). \tag{3.18}$$

Now we can use Gauss's theorem to find

$$\int_V \mathrm{d}^3x\, \boldsymbol{\nabla} \cdot (\hat{\boldsymbol{n}} f(\boldsymbol{x})) = \int_S \mathrm{d}\boldsymbol{S} \cdot \hat{\boldsymbol{n}} f(\boldsymbol{x}) = \hat{\boldsymbol{n}} \cdot \int_S \mathrm{d}\boldsymbol{S}\, f(\boldsymbol{x}). \tag{3.19}$$

Since this is valid for any $\hat{\boldsymbol{n}}$, we prove the theorem we wanted.

The current is therefore given by

$$\boldsymbol{j}_n = \frac{2}{(2\pi)^2} \int_S \mathrm{d}\boldsymbol{S} \left[\sqrt{p_{Fn}^2 + m_n^{*\,2}} + \frac{\boldsymbol{p}_{Fn} \cdot (\boldsymbol{Q}_n - g_\omega \boldsymbol{\omega} + \frac{g_\rho}{2} \boldsymbol{\rho})}{\sqrt{p_{Fn}^2 + m_n^{*\,2}}} \right] \tag{3.20}$$

On the surface of integration, there is a symmetrical element $-\mathrm{d}\boldsymbol{S}$ for every $\mathrm{d}\boldsymbol{S}$. Since the first term inside brackets is constant, this means that its contribution to the integral must be zero. The second term can be calculated using spherical coordinates and choosing the axial direction to coincide with $(\boldsymbol{Q}_n - g_\omega \boldsymbol{\omega} + \frac{g_\rho}{2} \boldsymbol{\rho})$. We skip the calculations to give the final result

$$\boldsymbol{j}_n = \frac{p_{Fn}^3/3\pi^2}{\sqrt{p_{Fn}^2 + m_n^{*\,2}}} (\boldsymbol{Q}_n - g_\omega \boldsymbol{\omega} + \frac{g_\rho}{2} \boldsymbol{\rho}) = \frac{n_n}{\bar{\mu}_n} (\boldsymbol{Q}_n - g_\omega \boldsymbol{\omega} + \frac{g_\rho}{2} \boldsymbol{\rho}). \tag{3.21}$$

It should be noted that this result is applicable to protons when the magnetic field is zero:

$$\boldsymbol{j}_p = \frac{n_p}{\bar{\mu}_p} (\boldsymbol{Q}_p - g_\omega \boldsymbol{\omega} - \frac{g_\rho}{2} \boldsymbol{\rho}). \tag{3.22}$$

Proton current at a finite magnetic field

For the new ground-state, the proton current (Equation 2.56) is given by

$$j_p = \frac{eB}{2\pi} \sum_\nu g_\nu \int \frac{\mathrm{d}p_z}{2\pi} \frac{\partial \bar{E}_p}{\partial p_z} = \frac{eB}{(2\pi)^2} \sum_\nu g_\nu \int \mathrm{d}\bar{E}_p$$

Expanding the energy as we did for the neutrons, yields

$$j_p \approx \frac{eB}{(2\pi)^2} \sum_\nu g_\nu \int \mathrm{d} \left[\sqrt{p_z^2 + m_p^{*\,2} + 2\nu eB} + \frac{p_z (Q_p - g_\omega \omega - \frac{g_\rho}{2} \rho_3)}{\sqrt{p_z^2 + m_p^{*\,2} + 2\nu eB}} \right]$$

The first term inside the brackets vanishes, due to being evaluated in $\pm p_{Fp}(\nu)$. Finally, the expression for the current is

$$\begin{aligned} j_p &= \frac{eB}{2\pi^2}\sum_\nu g_\nu \frac{p_{Fp}(\nu)}{\sqrt{p_{Fp}(\nu)^2 + m_p^{*2} + 2\nu eB}}\Big(Q_p - g_\omega\omega - \frac{g_\rho}{2}\rho_3\Big) \\ &= \frac{n_p}{\bar{\mu}_p}\Big(Q_p - g_\omega\omega - \frac{g_\rho}{2}\rho_3\Big). \end{aligned}$$

Notice that we use ω and ρ_3 for the z component of $\boldsymbol{\omega}$ and $\boldsymbol{\rho}$.

3.2.2 Summary of the system of equations

The system of equations we have to solve is similar to the one we presented in the last chapter, but must now include the neutron and proton currents and take into account the z direction of the ω and ρ fields. This section closely mirrors Section 2.6. The equations for the σ, ω and ρ fields become

$$m_\sigma^{*\,2}\sigma = g_\sigma(\rho_{s,p} + \rho_{s,n}) \tag{3.23}$$

$$m_\omega^{*\,2}\omega^0 = g_\omega(n_p + n_n) \tag{3.24}$$

$$m_\omega^{*\,2}\omega = g_\omega(j_p + j_n) \tag{3.25}$$

$$m_\rho^{*2}\rho_3^0 = \frac{g_\rho}{2}(n_p - n_n) \tag{3.26}$$

$$m_\rho^{*2}\rho_3 = \frac{g_\rho}{2}(j_p - j_n), \tag{3.27}$$

with the effective masses defined as in Equations 2.18:

$$m_\sigma^{*\,2} = m_\sigma^2 + \frac{\kappa\sigma}{2} + \frac{\lambda\sigma^2}{6} \tag{3.28}$$

$$m_\omega^{*\,2} = m_\omega^2 + \frac{\xi}{3!}g_\omega^4\left((\omega^0)^2 - \omega^2\right) + 2\Lambda_{\omega\rho}\, g_\omega^2\, g_\rho^2\left((\rho_3^0)^2 - \rho^2\right) \tag{3.29}$$

$$m_\rho^{*2} = m_\rho^2 + 2\Lambda_{\omega\rho}\, g_\omega^2\, g_\rho^2\left((\omega^0)^2 - \omega^2\right). \tag{3.30}$$

Again, the source currents must be computed in different ways, depending on whether $B = 0$ or not.

Without a magnetic field, the densities are given by

$$\begin{cases} n_n = \dfrac{p_{Fn}^2}{3\pi^2} \\ n_p = \dfrac{p_{Fp}^2}{3\pi^2} \\ n_e = \dfrac{p_{Fe}^2}{3\pi^2} \end{cases} \quad \text{with} \quad \begin{cases} p_{Fn} = \sqrt{\bar{\mu}_n^2 - m_n^{*\,2}} \\ p_{Fp} = \sqrt{\bar{\mu}_p^2 - m_p^{*2}} \\ p_{Fe} = \sqrt{\mu_e^2 - m_e^2}. \end{cases} \tag{3.31}$$

Notice that we use the the effective Fermi energies for convenience. The scalar currents are given by

$$\rho_{s,n} = \frac{m_n^*}{2\pi^2}\left[p_{Fn}\bar{\mu}_n - m_n^{*\,2}\ln\left(\frac{\bar{\mu}_n + p_{Fn}}{m_n^*}\right)\right] \tag{3.32}$$

$$\rho_{s,p} = \frac{m_p^*}{2\pi^2}\left[p_{Fp}\bar{\mu}_p - m_p^{*2}\ln\left(\frac{\bar{\mu}_p + p_{Fp}}{m_p^*}\right)\right]. \tag{3.33}$$

Finally, the proton and neutron currents are given by

$$\boldsymbol{j}_n = \frac{n_n}{\bar{\mu}_n}(\boldsymbol{Q}_n - g_\omega \boldsymbol{\omega} + \frac{g_\rho}{2}\boldsymbol{\rho}) \tag{3.34}$$

$$\boldsymbol{j}_p = \frac{n_p}{\bar{\mu}_p}(\boldsymbol{Q}_p - g_\omega \boldsymbol{\omega} - \frac{g_\rho}{2}\boldsymbol{\rho}). \tag{3.35}$$

With a magnetic field, the densities are instead given by

$$\begin{cases} n_n = \dfrac{p_{Fn}^2}{3\pi^2} \\ n_p = \dfrac{eB}{2\pi^2}\displaystyle\sum_{\nu=0}^{\nu_{\max}^p} g_\nu p_{Fp}(\nu) \\ n_e = \dfrac{eB}{2\pi^2}\displaystyle\sum_{\nu=0}^{\nu_{\max}^e} g_\nu p_{Fe}(\nu) \end{cases} \quad \text{with} \quad \begin{cases} p_{Fn} &= \sqrt{\bar{\mu}_n^2 - {m_n^*}^2} \\ p_{Fp}(\nu) &= \sqrt{\bar{\mu}_p^2 - {m_p^*}^2 - 2\nu eB} \\ p_{Fe}(\nu) &= \sqrt{\mu_e^2 - m_e^2 - 2\nu eB} \end{cases} \tag{3.36}$$

The maximum Landau levels are given by

$$\nu_{\max}^p = \left\lfloor \frac{\bar{\mu}_p^2 - {m_p^*}^2}{2eB} \right\rfloor \quad \text{and} \quad \nu_{\max}^e = \left\lfloor \frac{\mu_e^2 - m_e^2}{2eB} \right\rfloor. \tag{3.37}$$

The scalar currents are computed from

$$\rho_{s,n} = \frac{m_n^*}{2\pi^2}\left[p_{Fn}\bar{\mu}_n - {m_n^*}^2 \ln\left(\frac{\bar{\mu}_n + p_{Fn}}{m_n^*}\right)\right] \tag{3.38}$$

$$\rho_{s,p} = \frac{eBm_p^*}{(4\pi)^2}\sum_{\nu=0}^{\nu_{\max}^p} g_\nu \ln\left(\frac{\bar{\mu}_p + p_{Fp}(\nu)}{\bar{\mu}_p - p_{Fp}(\nu)}\right). \tag{3.39}$$

The proton and neutron currents are given by

$$\boldsymbol{j}_n = \frac{n_n}{\bar{\mu}_n}(\boldsymbol{Q}_n - g_\omega \boldsymbol{\omega} + \frac{g_\rho}{2}\boldsymbol{\rho}) \tag{3.40}$$

$$j_p = \frac{n_p}{\bar{\mu}_p}(Q_p - g_\omega \omega - \frac{g_\rho}{2}\rho). \tag{3.41}$$

Besides these relationships, we also impose the charge neutrality and beta equilibrium conditions:

$$\begin{cases} n_p = n_e \\ \bar{\mu}_n = \bar{\mu}_p + \mu_e + g_\rho \rho^0. \end{cases} \tag{3.42}$$

3.2.3 Calculating the entrainment matrix

We can manipulate Equations 3.40 and 3.41 with the aid of the remaining ones to write, as we wanted (see Equations 3.6 and 3.7),

$$\boldsymbol{j}_n = Y_{nn}\boldsymbol{Q}_n + Y_{np}\boldsymbol{Q}_p \tag{3.43}$$

$$\boldsymbol{j}_p = Y_{pn}\boldsymbol{Q}_n + Y_{pp}\boldsymbol{Q}_p, \tag{3.44}$$

where we conclude that the entrainment matrix elements are given by

$$Y_{nn} = \eta_n \frac{1+\eta_p\Sigma}{(1+\eta_p\Sigma)(1+\eta_n\Sigma)-\eta_p\eta_n\Delta} \tag{3.45}$$

$$Y_{pp} = \eta_p \frac{1+\eta_n\Sigma}{(1+\eta_p\Sigma)(1+\eta_n\Sigma)-\eta_p\eta_n\Delta} \tag{3.46}$$

$$Y_{np} = Y_{pn} = -\frac{\eta_p\eta_n\Delta}{(1+\eta_p\Sigma)(1+\eta_n\Sigma)-\eta_p\eta_n\Delta}, \tag{3.47}$$

with $\eta_n = n_n/\bar{\mu}_n$, $\eta_p = n_p/\bar{\mu}_p$ and

$$\Sigma = \left(\frac{g_\omega}{m^*_\omega}\right)^2 + \left(\frac{g_\rho}{2m^*_\rho}\right)^2 \qquad \Delta = \left(\frac{g_\omega}{m^*_\omega}\right)^2 - \left(\frac{g_\rho}{2m^*_\rho}\right)^2. \tag{3.48}$$

It should be noted that the effective masses m^*_ω and m^*_ρ depend on $\boldsymbol{Q}_n$ and $\boldsymbol{Q}_p$. However, these corrections should be small and, if we expanded the coefficients Y_{ik} in powers of these variables, the constant term would dominate. When solving the equations numerically, we will choose small values for $\boldsymbol{Q}_n$ and Q_p, so we can control the error if needed.

4. Results

4.1 Numerical methods

To solve the equations mentioned in the previous sections, we performed numerical computations. We implemented the systems in C++ and used established routines for finding the zeros of functions, in particular the multivariate Newton–Raphson method. To this end, the systems to solve had to be written in the form $\boldsymbol{F}(\boldsymbol{x}) = 0$. To solve the equations, we start by proposing a solution $\boldsymbol{x}_0$. The algorithm then proceeds to find the zero by computing the Jacobian of $\boldsymbol{F}$ at $\boldsymbol{x}_0$ and using it to compute a new step $\boldsymbol{x}_1$, much like how the one-dimensional Newton's method uses derivatives to find the zero of functions. The solution is found when we reach an $\boldsymbol{x}_n$ such that $\boldsymbol{F}(\boldsymbol{x}_n)$ is sufficiently close to zero (a notion that is appropriately defined with a distance function; we used the maximum, or $\|\cdot\|_\infty$, distance).

Some care had to be taken, because such algorithms are very sensitive to the initial guess. First, we used a good initial point $\boldsymbol{x}_0$, so that it did not take long for the method to find a solution. Second, we always computed nearby points by using a previous solution, so we know that the guess was very reasonable. If somehow a nearby point did not converge, we used a small perturbation of the last known solution; if it still did not work, we used the first, original guess. Finally, we "normalized" the equations to solve so that the equation with the largest deviation from 0 did not consistently dominate all other equations in the distance function.

All of the code used was written *de novo*. We chose C++ to make use of modern, efficient linear algebra libraries, in particular the Eigen library [27].

4.2 Characterizing the ground state

In this section we present the results obtained from numerically integrating the NL3$\omega\rho$ equations. A general theme of this section will be to observe either the effect induced by B, the magnetic field, or by L, the slope of the symmetry energy at the saturation density. When varying B, we will set $L = 118\,\mathrm{MeV}$; when varying L, we will impose $B = 0$.

We start by presenting the main thermodynamic quantities of interest. Since we have fixed the baryon densities to solve the NL3$\omega\rho$ equations, it is natural to use its conjugate variable, the energy per nucleon, obtained from dividing the energy density ε by the baryon density n_b. In Figures 4.1 and 4.2 we show how this energy changes with B and L, respectively, as a function of n_b. To help

understand our results, we subtract from from ε/n_b the nucleon mass

$$m_N = \frac{m_p + m_n}{2}. \tag{4.1}$$

We have used fields of intensities $B^* = 10^4$—10^5, or 4.4×10^{17}—4.4×10^{18} G. We see that, for the 118 MeV model, the effect of B is significant, as it lowers the energy consistently throughout the densities considered. For the highest intensity field, the energy is brought close to zero around 0.05 fm^{-3}, and around the saturation density it is approximately 10 MeV lower than the energy at $B = 0$.

Figure 4.2 shows us that, at $B = 0$, the curves for all models coincide near 0.1 fm^{-3}. This is, by design, a feature of the different NL3$\omega\rho$ parameterizations, which we will comment on the following paragraph. Below this density, lower values of L increase the energy, while above it the relationship is inverted.

To understand the differences between the NL3$\omega\rho$ models, we plot the symmetry energy as a function of the density for each parametrization, in Figure 4.3. This energy can be understood as a "penalty" for having nuclear matter that is highly asymmetric, that is, for which the number of neutrons is significantly different from the proton number. This penalty can be seen in the semi-empirical mass formula for atomic nuclei, or Bethe–Weizsäcker formula, in which the binding energy per nucleon has an additive term of the form

$$\varepsilon_{\text{sym}} \left(\frac{N - Z}{A} \right)^2, \tag{4.2}$$

with N being the neutron number, Z the proton number, $A = N + Z$ and ε_{sym} being the constant coefficient we call symmetry energy. This term is minimal when $N = Z$, and positive otherwise. It is clear that by defining

$$\alpha = \frac{n_n - n_p}{n_b}, \tag{4.3}$$

which is equal to $(N - Z)/A$ for nuclei, we can find ε_{sym} by computing

$$\varepsilon_{\text{sym}} = \frac{1}{2} \left[\frac{\partial^2 (\varepsilon/n_b)}{\partial \alpha^2} \right]_{\alpha=0}. \tag{4.4}$$

This was the procedure we followed to find ε_{sym}: we solved the NL3$\omega\rho$ equations imposing $n_n = n_p$ instead of β-equilibrium, and computed the second derivative with the analytical expression

$$\frac{1}{2} \left[\frac{\partial^2 (\varepsilon/n_b)}{\partial \alpha^2} \right]_{\alpha=0} = \frac{p_F^2}{6\varepsilon_F} + \frac{g_\rho^2}{8 m_\rho^{*2}} n_b, \tag{4.5}$$

where the effective mass is defined as before

$$m_\rho^{*2} = m_\rho^2 + 2\Lambda_{\omega\rho}\, g_\omega^2\, g_\rho^2\, (\omega^0)^2, \tag{4.6}$$

following Cavagnoli et al. [28]. The values p_F and ε_F are the Fermi momentum and energy of the nucleons (assuming, here, that the protons and neutrons are different states of the same particle). As we can see from Figure 4.3, the NL3$\omega\rho$ models present different ε_{sym} profiles. The symmetry energy was fixed near

0.1 fm^{-3}, which is the density at the surface of nuclei, the density experiments are sensitive to. In Figure 4.4 we plot L, a normalized derivative of $\varepsilon_{\mathrm{sym}}$ given by

$$L = 3n_0 \frac{\partial \varepsilon_{\mathrm{sym}}}{\partial n_b} \tag{4.7}$$

with n_0 being the nuclear saturation density. The values of L at the nuclear saturation density are what gives the name to the parameterizations. These models were constructed to study how matter behaves when we consider different preferences for asymmetry. At large densities, the smaller the L, the softer the equations of state is, allowing for larger isospin asymmetries.

Another relationship of interest is the equation of state (pressure vs. energy density), which is necessary for integrating the Tolman–Oppenheimer–Volkoff equations and studying the global behaviour of stars. The equation of state allows us to extract the mass-radius relationships for neutron stars. In Figure 4.5, we present the equation of state for different magnetic fields, using the energy and pressure relations obtained before. We also show in detail regions of low and high densities. The low-density region was chosen to cover the densities between 0.05 and 0.15 fm^{-3}. Notice that at high-intensity fields, the changes are relatively small. For higher densities, higher magnetic fields give rise to higher pressures; for low densities, the strongest magnetic field lowers the pressure, but weaker fields may occasionally increase it. It is difficult to establish a relationship between the magnetic field and pressure at low densities, because the appearance of new Landau levels cause sudden jumps in pressure. In some regions, the equation of state changes only slightly with the magnetic field. However, this does not mean that the magnetic field has no effect on stellar matter; some effects will still be seen, especially those that depend on the slope of $p(\varepsilon)$, such as the adiabatic index and the speed of sound.

In Figure 4.6, we plot the equation of state curve for different values of L, setting $B = 0$. The effect of L on the equation of state is moderate. We also present in more detail the curve at lower and higher densities. At low densities, the higher the L, the higher the pressure. This effect, however, is almost completely inverted at higher densities, the exception being for $L = 118\,\mathrm{MeV}$, which gives a higher pressure than all other models.

An interesting effect happens when we start lowering the baryon density towards very low values (when $\varepsilon < 1\,\mathrm{MeV\,fm}^{-3}$) – the pressure crosses zero and becomes negative (Figure 4.7). In fact, it keeps on decreasing its value while the energy density increases, and we end up with two values of p for the same energy density. The negative pressures should be interpreted as the nucleons starting to aggregate to form nuclei, which points to the limitation of using an homogeneous description of matter. Below such densities, we need to use an approach that considers non-homogeneous matter. In this case, the homogeneous NL3$\omega\rho$ equation of state would describe the background environment in which the nuclei move.

The next step in characterizing our ground state of matter is Figure 4.8, in which we plot the neutron and proton Fermi energies as a function of the baryon density, and show how they change with B. It is clear that, at low densities, the Fermi energies approach the mass of the respective nucleon. They then decrease until they reach a minimum around $n_b = 0.4$ fm^{-3}. The magnetic field seems to have a negligible effect on the Fermi energy.

In Figure 4.9 we see that L has a noticeable effect for densities above $\approx 0.2\,\mathrm{fm}^{-3}$: the proton's Fermi energy increases with greater values of L, while the neutron's decreases. This is due to the density dependence of the symmetry energy: the smaller the value of L, the smaller the symmetry energy is above 0.2 fm^{-3}(as we have seen in Figure 4.3). Therefore, larger isospin asymmetries are allowed, i.e., smaller proton fractions and higher neutron content, corresponding to larger μ_p and smaller μ_n.

The effect of the density dependence of the symmetry energy we mentioned is well seen in Figure 4.11, where the proton fraction n_p/n_b is plotted as a function of the baryon density: the higher the L, the more the proton fraction rises with density to reach symmetry. The fractions coincide around $0.1\,\mathrm{fm}^{-3}$. As we mentioned before, this is a property of the nuclear models, that the proton fraction is the same at the nuclear saturation density, which is a region that we can probe experimentally. At very low densities (Figure 4.12), the proton fractions become indistinguishable.

In Figure 4.10a we see the effect that B has on the proton fraction. Starting from high densities to low densities, it decreases monotonically, approaching zero when $n_b \to 0$. If we pay attention to the lower densities (Figure 4.10b), it is true that the proton fraction approaches zero, but it then suddenly starts to rise and reaches 1, which means that the matter is then totally populated by protons, and devoid of neutrons. The reason for this is that the protons' mass is lower than that of the neutrons and, as such, having more protons reduces the overall energy. The effect of the magnetic field is to bring this proton saturation point to higher densities. In Figure 4.10a, especially at densities below $0.15\,\mathrm{fm}^{-3}$, it is possible to see that the curves with $B \neq 0$ seem to follow the $B = 0$ curve, all the while having some discontinuities or "jumps". Each such discontinuity appears when the Fermi energy is high enough for the protons to populate a new Landau level. For densities above $0.1\,\mathrm{fm}^{-3}$, the effect of the magnetic field, with the intensities considered, is negligible.

In Figures 4.13 and 4.14, we show the effects of L and B on (the square of) the speed of sound s, while in Figures 4.15 and 4.16, we do the same for the adiabatic index γ, an important quantity in dynamical effects. The expressions for these quantities are

$$s^2 = \frac{\partial p}{\partial \varepsilon} \quad \text{and} \quad \gamma = \frac{p+\varepsilon}{p}\frac{\partial p}{\partial \varepsilon}. \tag{4.8}$$

The speed of sound is given in units of c. It is always smaller than 1, so we do not encounter a violation of causality for the densities shown. This is to be expected, since we have developed the whole calculations within a relativistic approach. There is some variation due to L up to $n_b \approx 0.3\,\mathrm{fm}^{-3}$. The most noticeable effects, however, appear when we apply a magnetic field, especially of high intensity. When the density increases, new Landau levels become available, and the speed of sound suddenly decreases. It then increases rapidly, and the curves seem to overall follow the values for $B = 0$.

A similar effect of B can be seen in the adiabatic index curves. The effect of L, however, is much more pronounced for γ.

4.3 Crust size

Following the spinodal analysis described before, we calculated normal modes of matter by imposing small perturbations on matter in equilibrium. Some of these modes are unstable and bring the system out of equilibrium at a certain growth rate $|\omega|$. We calculated the maximum of these growth rates, $|\omega|_{\max}$ for every density n_b. If $|\omega|_{\max} = 0$, then we can say that the matter is stable; otherwise, there is a tendency to form aggregates. Some of the results presented here have been published [29, 30].

In Figure 4.20, we calculate these modes for $L = 55\,\mathrm{MeV}$ and different values of B. Instead of imposing β-equilibrium, we fixed the proton fraction at 0.035, and we have included the anomalous magnetic moment. It is clear that, as we lower B, we are approaching a limiting case where there are unstable modes up to some density (slightly above 0.08 fm^{-3}) and, above that point, matter is stable. This situation is more clearly visible with $B^* = 100$. The unstable region corresponds to the crust, while the stable corresponds to the core. At $B = 0$ we would observe a clear crust-core transition. In Figure 4.21 we show the growth rates around this transition zone. What we observe is that, after $|\omega|_{\max}$ reaches zero for the first time, even if it remains zero for some densities, it eventually starts to rise, and some "peaks" begin to form. These peaks always come in pairs, associated with the spin-up and spin-down configurations (for $B = 2.25 \times 10^3$, the last peak looks isolated, but that is because the numerical calculations did not have enough resolution). It is clear that the well-defined crust-core transition is lost when we apply a magnetic field. To characterize the crust-core transition zone, it would be interesting to answer two questions: 1) how large are the individual peaks and how are they distributed?; 2) how large is the crust-core transition zone? To answer these questions, we adapted the growth-rate calculation program to find the densities of the beginning and the end of each peak.

In Figure 4.22 (the top panel) we plot the width (measured in baryon density) of each peak as a function of the density at which it first appears. We performed these calculations for two fields: $B^* = 10^2$ and 10^3. We see that the size of the corresponding clusters decreases exponentially, which happens faster for $B^* = 10^2$. To provide the clusters with realistic information, we considered the particular case of a star with 1.4 solar masses. By integrating the Tolman–Oppenheimer–Volkoff equations, we can translate densities into distances. As such, we determined the thickness Δl of the instability regions (middle panel) and the distance between the instabilities, ΔL (bottom panel). For $B^* = 10^2$, the spacing between the peaks increases with density, ranging between approximately 6 m and 9 m. Below those densities, the homogeneous core is reached. For $B^* = 10^3$, the spacings are one order of magnitude larger. The width of the peaks decreases exponentially with density, ranging between 1 m and 5 mm for $B^* = 10^2$ and being one to two orders of magnitude larger for $B^* = 10^3$. It is interesting to note that the spacings between the clusters lie on two nearly parallel lines.

In Figure 4.23 we present the results obtained for the extension of the transition region, defined as the region between two densities ρ_1 and ρ_2, which are respectively the first time the growth rates reach zero and the last time they differ from zero. We do this for different values of L. In this calculation, we

also included the anomalous magnetic moment of neutrons, and we considered a constant proton fraction up to the density ρ_t^0 (the crust-core transition density at zero field) and β-equilibrium above that point. By fixing a neutron star mass as before, we can integrate the Tolman–Oppenheimer–Volkoff equations to give us a distance $R(n_b)$ for every density n_b: the distance from the center of the star. Of course, $R(0)$ must be the radius of the star. As such, because of the the crust-core transition region at finite B, we calculate two different sizes for the crust: $\Delta R = R(0) - R(\rho_2)$ and $\Delta R^* = R(0) - R(\rho_1)$. Whatever the real size of the crust may be, it must lie between these two values, which we plot for different values of L in the middle panel. Finally, we attribute to the crust two fractional (compared with the size of the star) moment of inertia: one assuming that the crust ends at the density ρ_1 and another at ρ_2. We use the approximation [31]

$$\frac{\Delta I_{\text{crust}}}{I} \approx \frac{28\pi P_t R^3}{3M}\frac{(1-1.67\beta-0.6\beta^2)}{\beta}\left[1+\frac{2P_t(1+5\beta-14\beta^2)}{\rho_t m\beta^2}\right]^{-1}, \quad (4.9)$$

and we will use as ρ_t and P_t the densities and pressures at the two transitions. Here, ΔI_{crust} is the moment of inertia of the crust, while I is that of the whole star, M and R are the mass and radius of the star, $\beta = GM/R$ and m is the nucleon mass.

In Figure 4.23, we only calculated the $B = 10^2$ case for $L = 55\,\text{MeV}$ (blue stars in the graph). It is apparent that, the larger the L, the greater the effect of B, that is, the larger the transition zone is. This is mainly due to the proton fraction of each model (recall Figure 4.10a). If we compare with the $B = 0$ case, the effect of the magnetic field can be as large as 100% for $L = 118\,\text{MeV}$. It should be noted, however, that experimental constraints [32, 33] and microscopic nuclear matter calculations [34] indicate that models with L between 30 and 80 are more realistic. For the $L = 55\,\text{MeV}$ case, the increase is of the order of 20%. The lower limit of the crust-core transition zone is only slightly smaller than the $B = 0$ crust-core transition. The effect of the magnetic field is to create a complex transition region above this density. By taking $L = 55\,\text{MeV}$ and decreasing the magnetic field an order of magnitude from $B^* = 10^3$ to 10^2, quantities such as the transition density, crust thickness and crust fraction of moment of inertia, defined with the density ρ_2, suffer a reduction of around 3—5%, but are still larger than the corresponding quantities at $B = 0$.

From this analysis, it is apparent that properties of magnetized neutron stars that directly depend on the thickness of the crust may give us a way of imposing strict constraints on the values of L.

4.4 Entrainment matrix

In the following results, the numeric values for the entrainment matrix elements will be normalized by the constant $Y = 3.99 \times 10^{-4}\,\text{MeV}^3\,\text{fm}^{-1}$, as was done by Gusakov et al. [15].

In Figure 4.17 we observe the effects of B on the entrainment matrix elements Y_{ik}. It is clear that the element Y_{pp}, measuring the proton-proton entrainment, is the most affected by the magnetic field. The Landau level transitions are clearly visible. The neutron-proton component is also affected, as is the neutron-neutron, although this last effect is much more modest. The reason why Y_{nn}

still changes with the magnetic field, even when B has no effect on the neutron wave functions, could be via the σ field in the effective mass $m_n^* = m_n - g_\sigma \sigma$.

In Figure 4.18, we see the the effect of L on the entrainment matrix elements. It is clear that Y_{pp} increases with greater values of L. This effect is a consequence of the higher proton fraction achieved when L is increased, as we have seen in Figure 4.11. The trend is reversed for Y_{nn} for similar reasons. In the Y_{np} case, the magnitude of the entrainment is greater for higher values of L.

In Figures 4.19a—4.19f we see the effects of B and L on the entrainment matrix elements with more detail, at low densities. In the graphs where we show the effects of B, we indicate with dashed lines the densities for which the proton fraction saturates to 1. The matrix element Y_{nn} (Figure 4.19a), for instance, seems to asymptotically approach zero at these saturations, which is the expected behaviour – at these densities, there are no more neutrons and, therefore, no more neutron fluids for entrainment to occur. At higher densities, the curves are almost indistinguishable. Varying the value of L seems to have a negligible effect on Y_{nn} (Figure 4.19b). This is because the neutron fraction is above 95% (see Figure 4.11), and a small change on the neutron density will not be noticeable, contrary to the effect on the proton fraction, where even small deviations become large in comparison.

Going from higher to lower densities, the proton-proton elements Y_{pp} stabilize at different values depending on B (Figure 4.19c), before reaching proton saturation, when the curves start to decline steadily. When this happens, all the curves start to follow the same line (this can be seen from the explicit form of Y_{pp} given in Equation 3.45: at low densities, $\eta_p \approx n_p/m_p \to 0$ and $\eta_n \approx n_n/m_n \to 0$, which implies $Y_{pp} \approx \eta_p$; but if the proton fraction is 1, then $n_p = n_b$ and Y_{pp} is a line of slope $1/m_p$). In the other direction, when we increase n_b and the first Landau levels start appearing, the curves appear to follow the $B = 0$ behaviour. The value of L has a slight effect on the element Y_{pp} at low densities (Figure 4.19d).

Finally, in Figure 4.19e we see the effect of B on Y_{np}. Since the neutron fraction goes to zero at the dotted lines, the matrix element also vanishes at those densities, just as it did for the Y_{nn}. In Figure 4.19f we see that L has a slight effect on Y_{np}.

It is worth mentioning that the NL3$\omega\rho$ model does not include hyperons. However, if they were present, they would certainly decrease the proton and neutron fractions. As such, they could have a significant effect on the entrainment matrix elements, as was observed by Gusakov et al. [15].

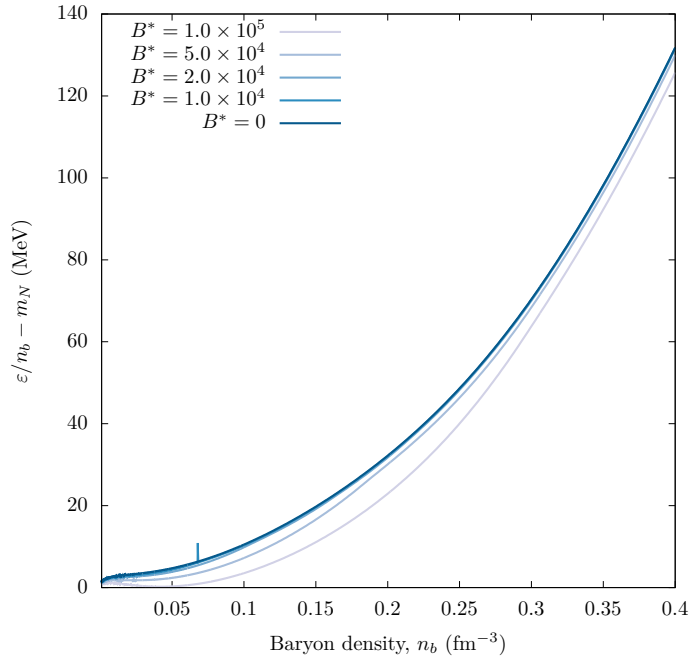

Figure 4.1: Energy per nucleon as a function of density for different magnetic fields and $L = 118\,\text{MeV}$. We have subtracted the nucleon mass.

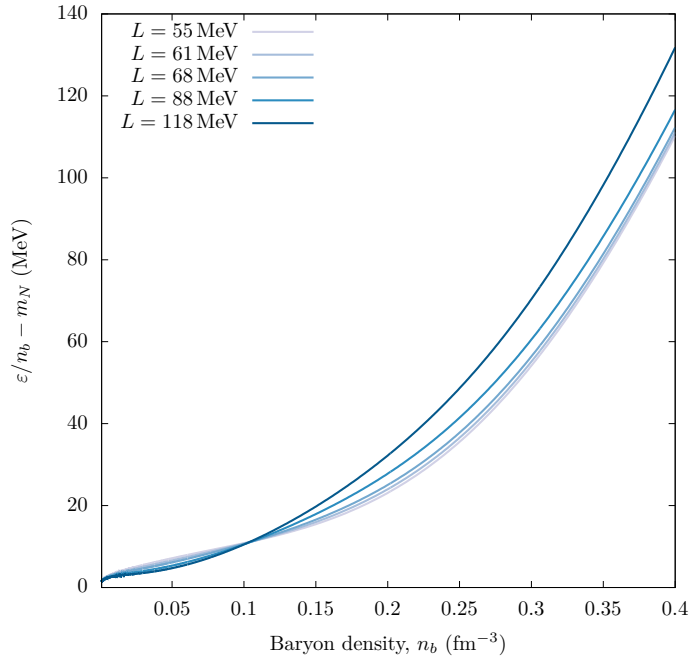

Figure 4.2: Energy per nucleon as a function of density, for different parametrizations of the NL3$\omega\rho$ model, for different values of L and $B = 0$. We have subtracted the nucleon mass.

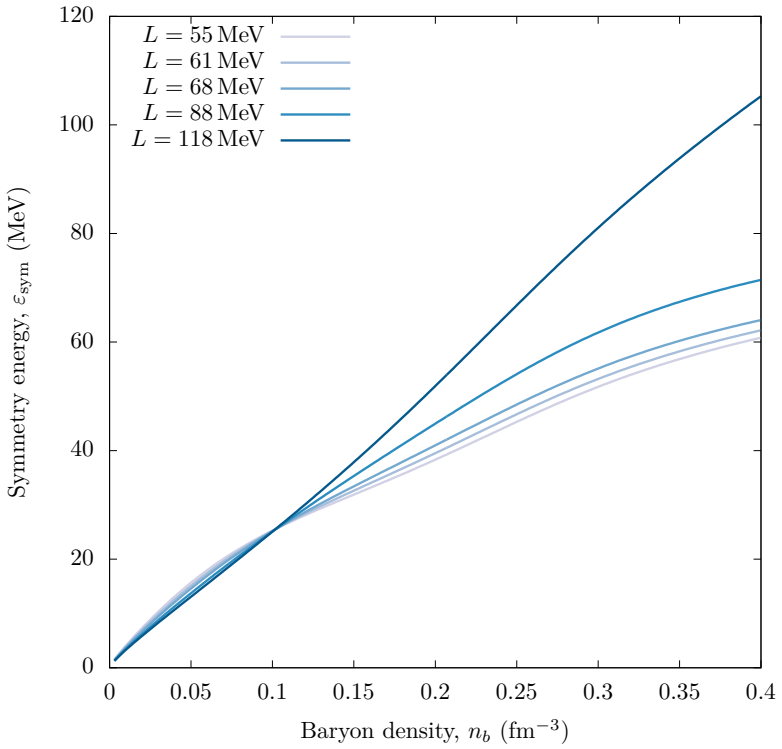

Figure 4.3: Symmetry energy as a function of density, for different parameterizations of the NL3$\omega\rho$ model. The value of the slope of each curve at the nuclear saturation density is L.

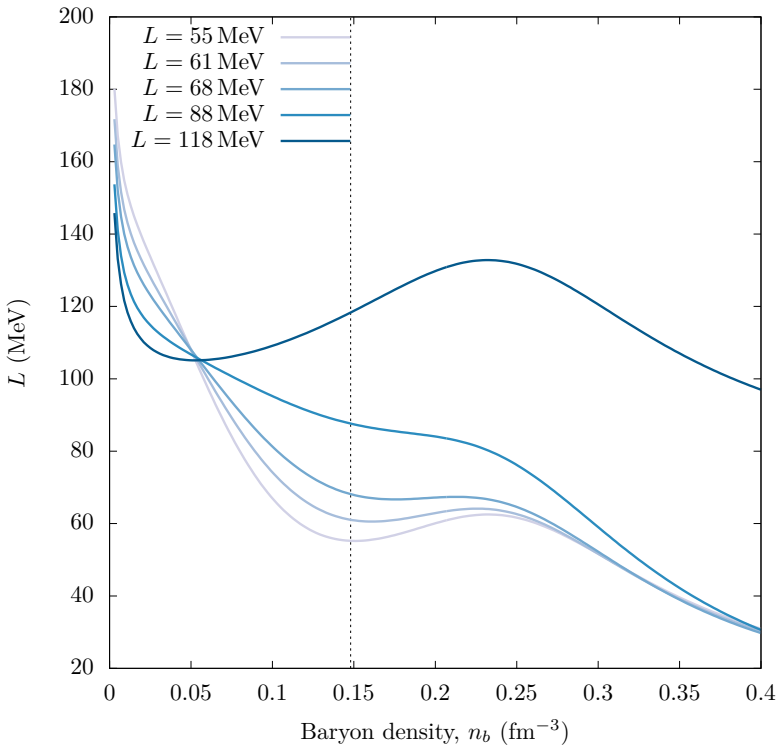

Figure 4.4: Derivative of the symmetry energy as a function of density. The value L is the value of these slopes at the saturation density (dashed line).

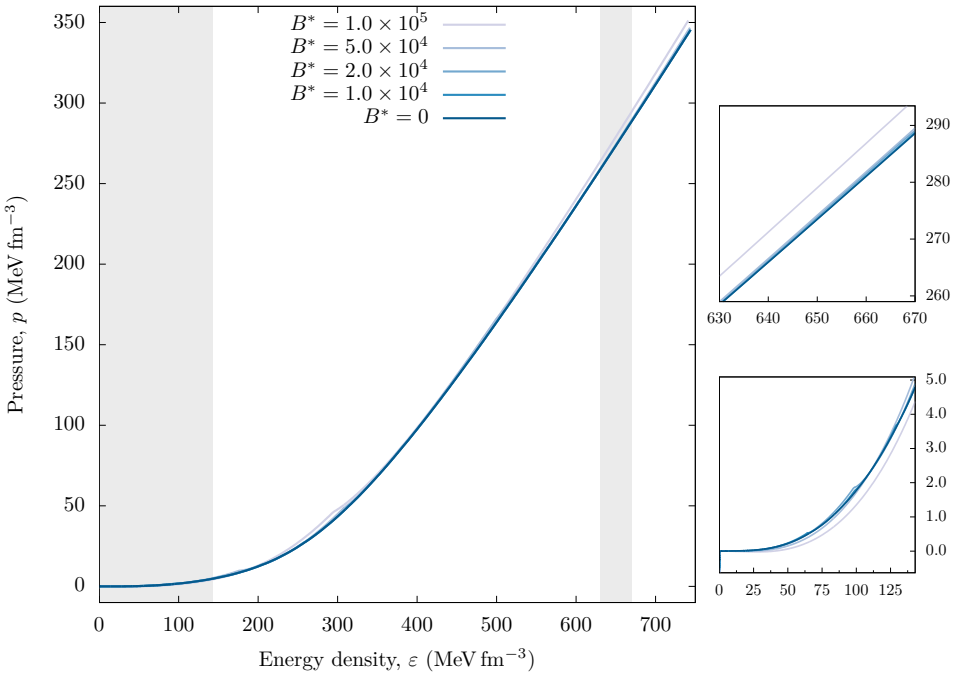

Figure 4.5: Effect of the magnetic field on the equation of state of the NL3$\omega\rho$ model, for $L = 118$ MeV. In gray, the regions zoomed in on the right. The low densities capture the region where $n_b \in [0.05, 0.15]$ fm^{-3}.

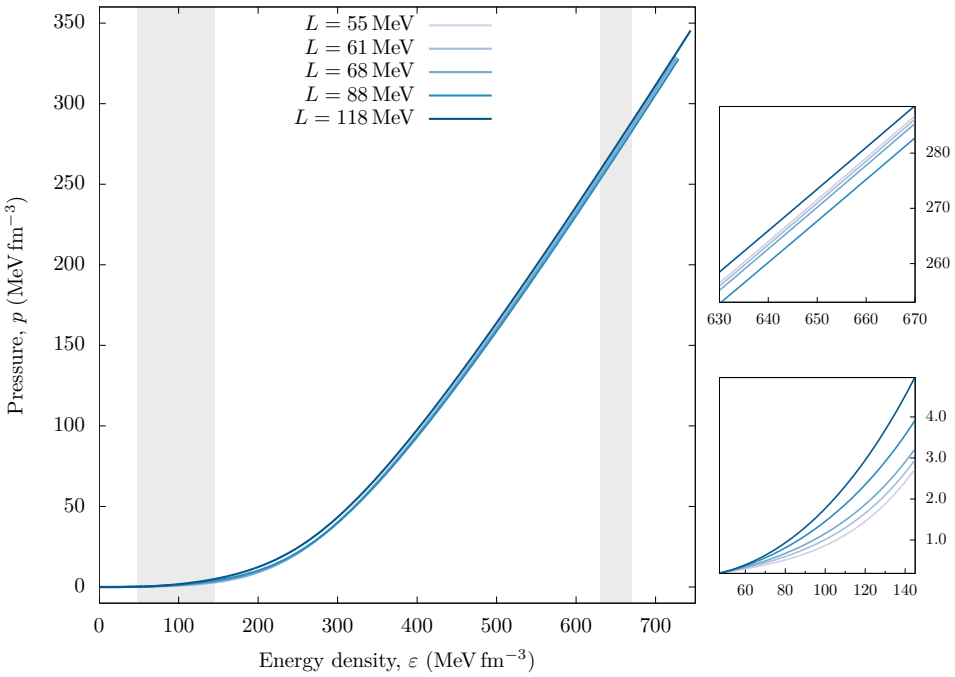

Figure 4.6: Effect of L on the equation of state of the NL3$\omega\rho$ model, for $B = 0$. In gray, the regions zoomed in on the right. The low densities capture the region where $n_b \in [0.05, 0.15]$ fm^{-3}.

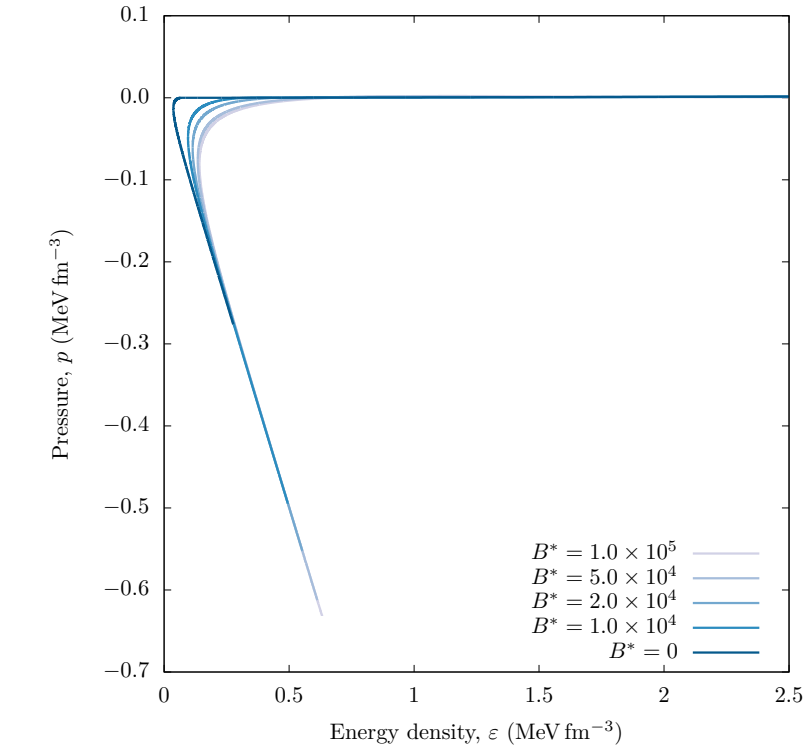

(a)

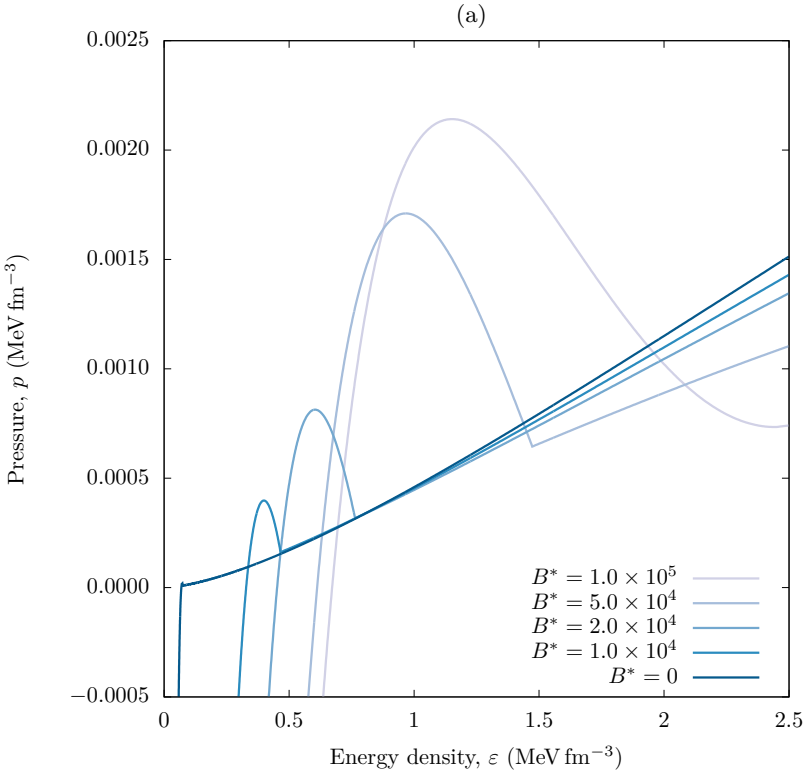

(b)

Figure 4.7: The equation of state for the NL3$\omega\rho$ model at very low densities, for different magnetic fields and $L = 118\,\mathrm{MeV}$, showing negative pressures and non-uniqueness.

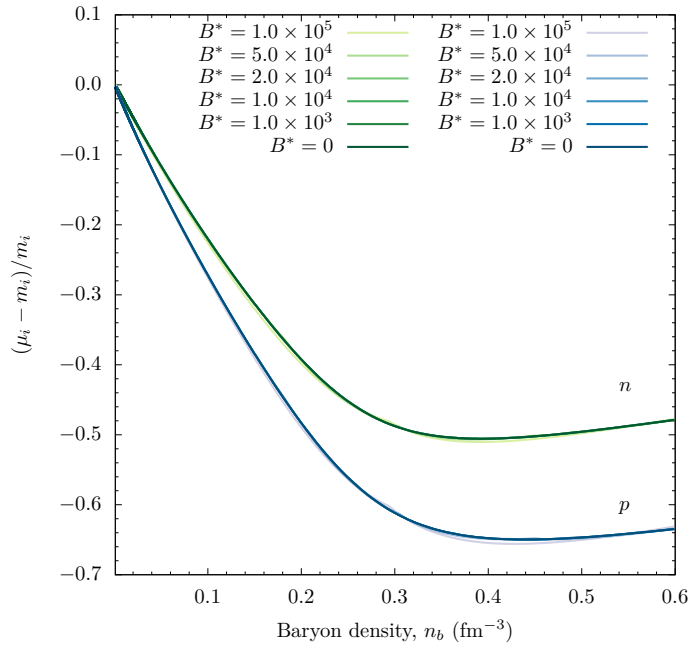

Figure 4.8: Effect of the magnetic field on the Fermi energies of protons and neutrons in the NL3$\omega\rho$ model, for $L = 118$ MeV.

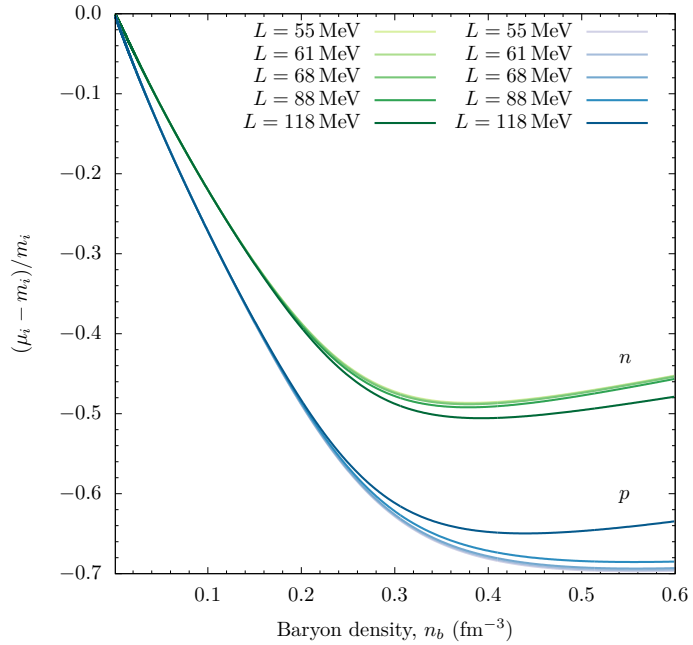

Figure 4.9: Effect of L on the Fermi energies of protons and neutrons in the NL3$\omega\rho$ model, for $B^* = 0$.

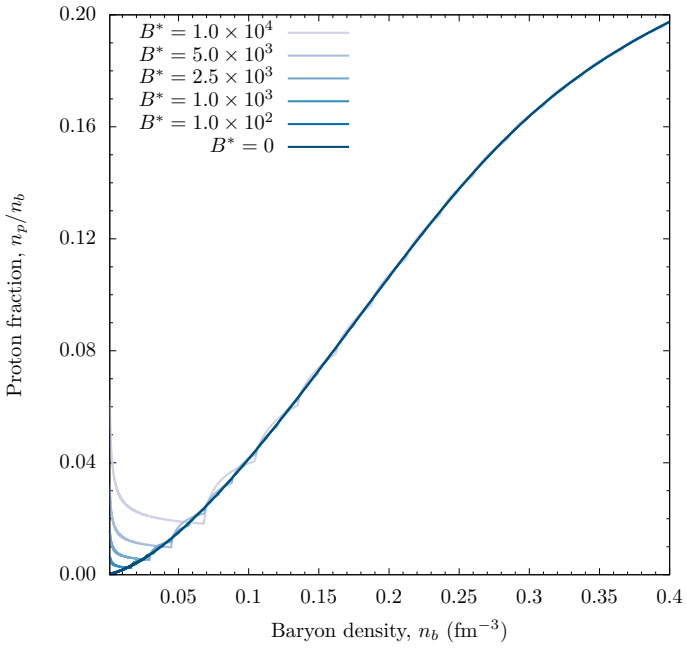

(a)

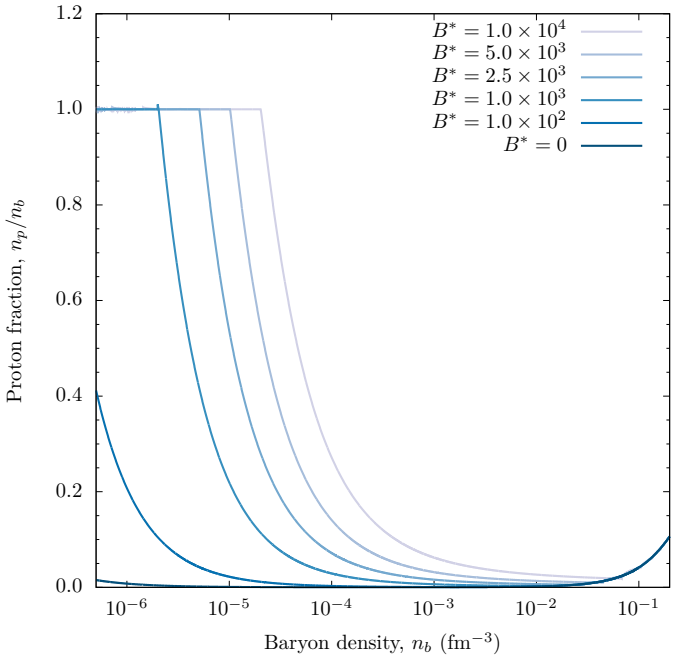

(b)

Figure 4.10: Effect of the magnetic field on the proton fraction in the NL3$\omega\rho$ model, for $L = 118\,\text{MeV}$. Notice that the graphs highlight different regions: (a) goes from 0.001 to 0.4 fm^{-3}; (b) goes from 5×10^{-7} to 0.2 fm^{-3}. Also notice that the scale is different: in (a) the graph reaches $0.2\,\text{fm}^{-3}$, while (b) reaches unity.

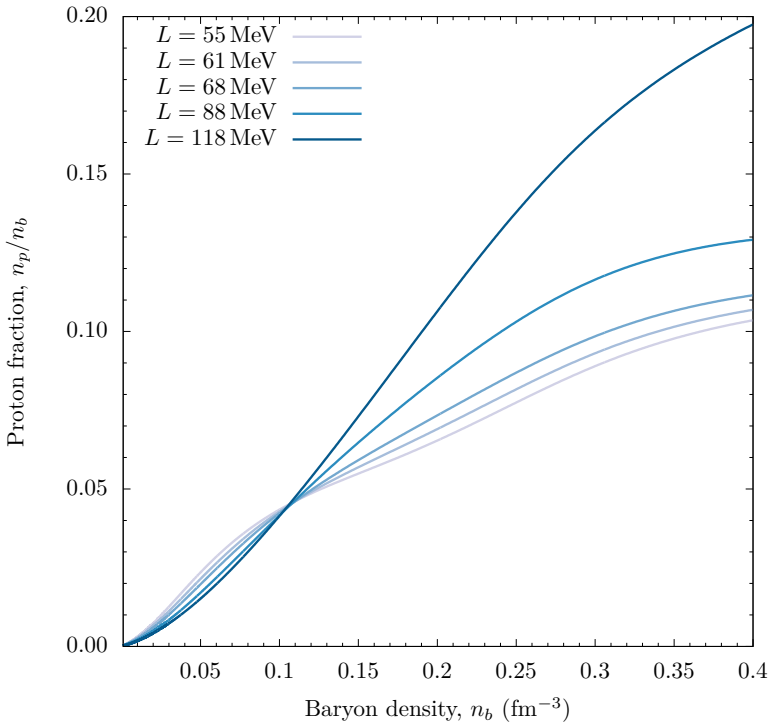

Figure 4.11: Effect of the magnetic field on the proton fraction in the NL3$\omega\rho$ model, for $L = 118\,\mathrm{MeV}$.

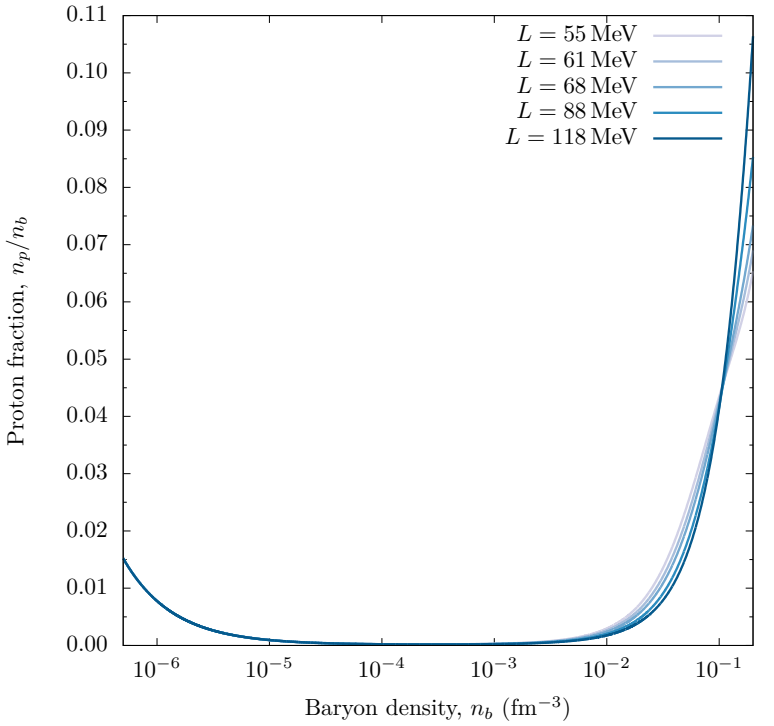

Figure 4.12: Effect of L on the proton fraction in the NL3$\omega\rho$ model at low densities, for $B^* = 0$.

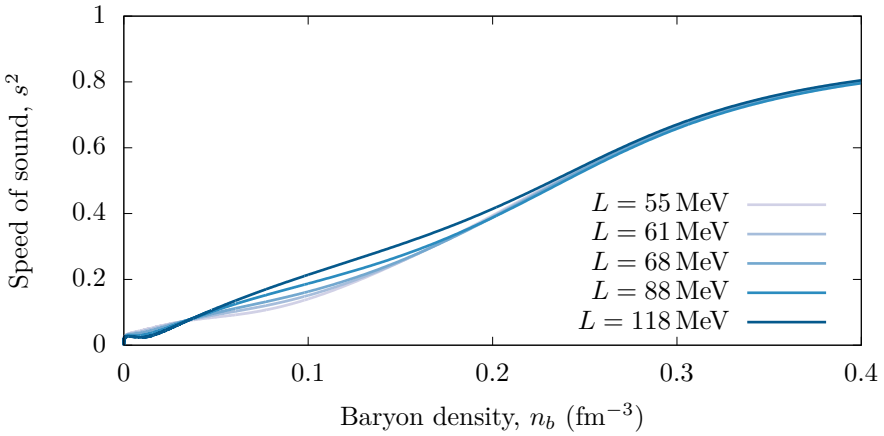

Figure 4.13: Effect of L on the speed of sound in the NL3$\omega\rho$ model, for $B^* = 0$.

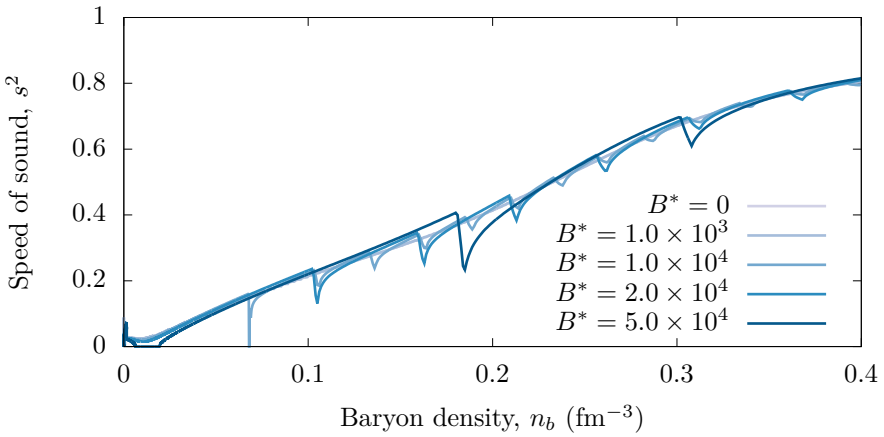

Figure 4.14: Effect of the magnetic field on the speed of sound in the NL3$\omega\rho$ model, for $L = 118$ MeV.

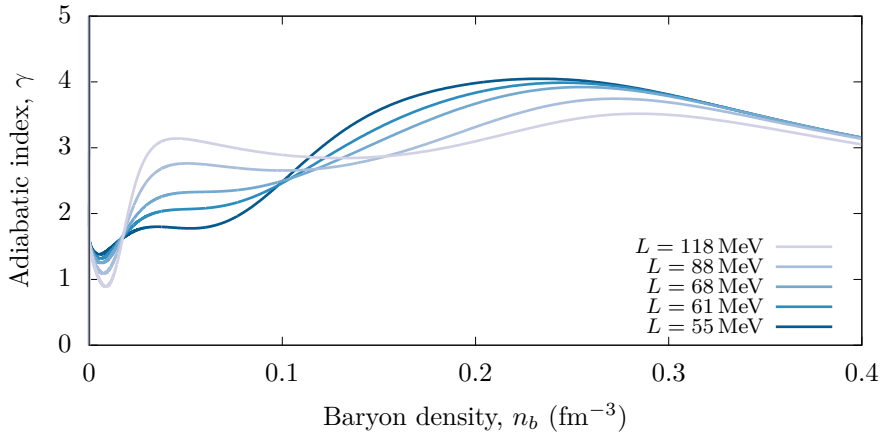

Figure 4.15: Effect of L on the adiabatic index in the NL3$\omega\rho$ model, for $B^* = 0$.

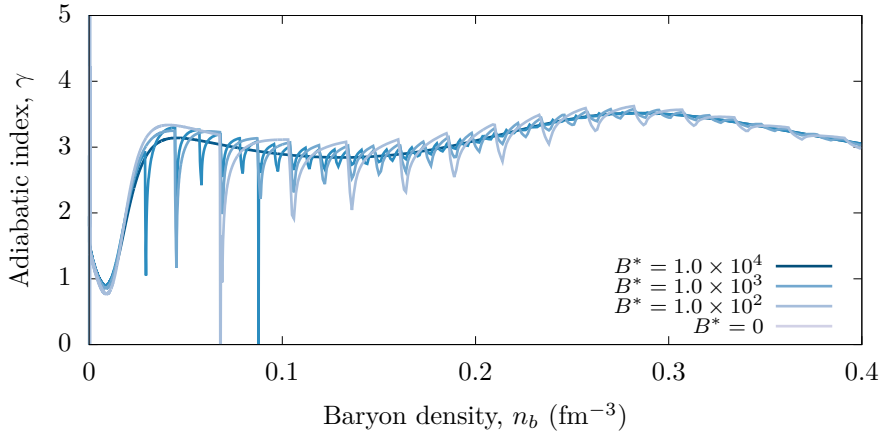

Figure 4.16: Effect of the magnetic field on adiabatic index in the NL3$\omega\rho$ model, for $L = 118$ MeV.

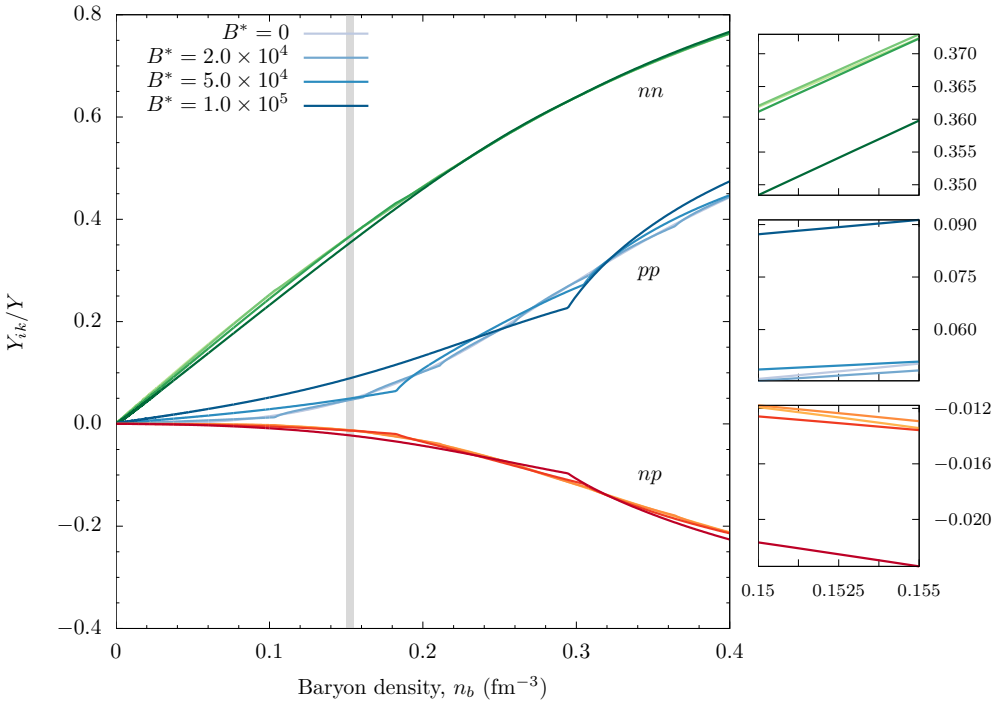

Figure 4.17: Entrainment matrix elements Y_{ik} normalized by $Y = 3.99 \times 10^{-4}\,\mathrm{MeV}^{-1}\,\mathrm{fm}^{-3}$, for different magnetic fields, with $L = 118\,\mathrm{MeV}$. In gray, the region zoomed in on the right.

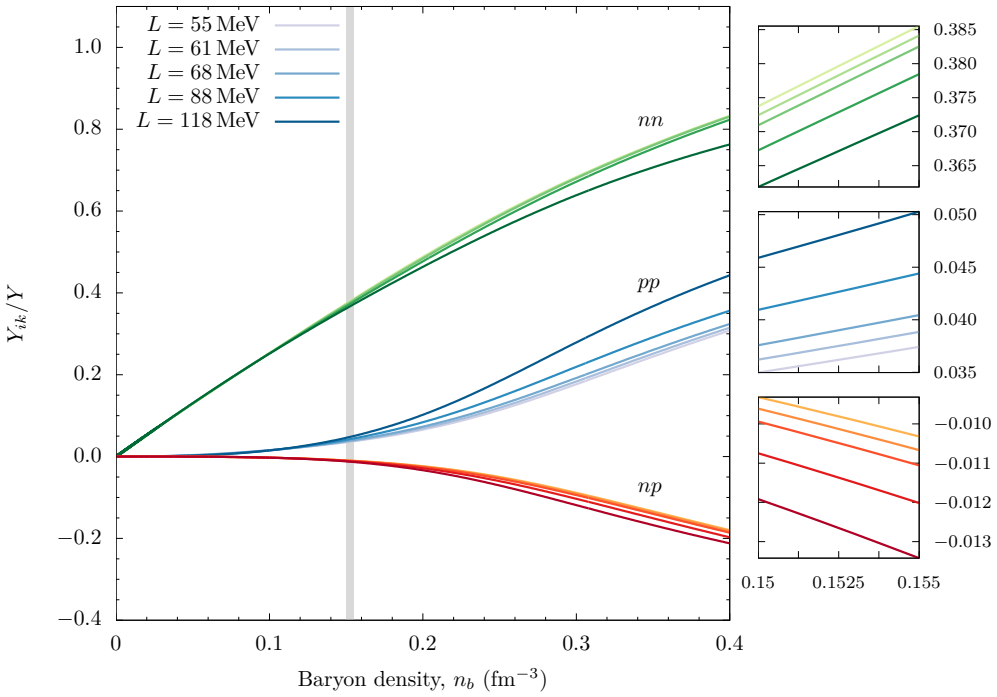

Figure 4.18: Entrainment matrix elements Y_{ik} normalized by $Y = 3.99 \times 10^{-4}\,\mathrm{MeV}^{-1}\,\mathrm{fm}^{-3}$, for different values of L and $B^* = 0$. In gray, the region zoomed in on the right.

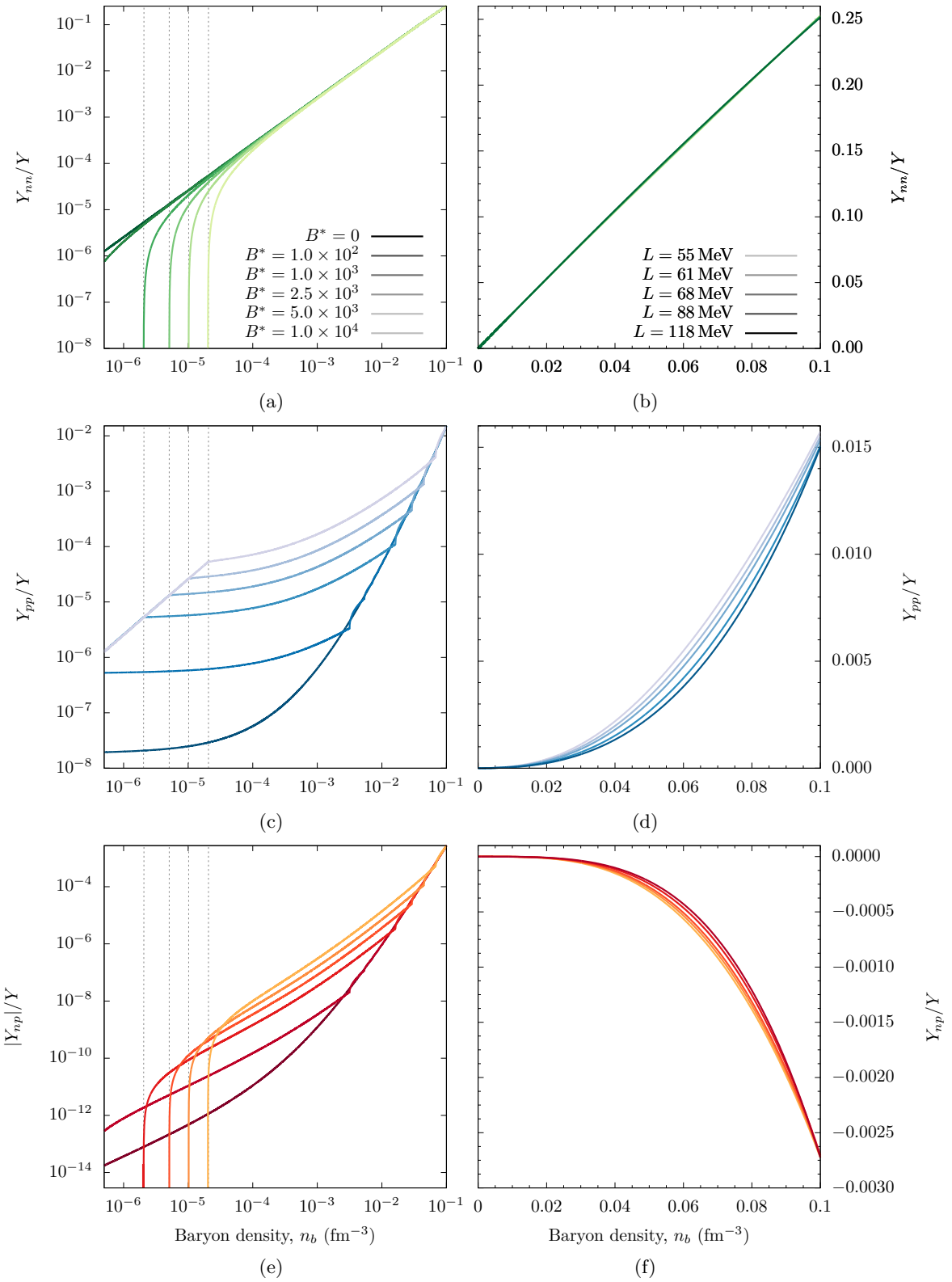

Figure 4.19: Low-density details of the effects of B (on the left) and L (on the right) on the entrainment matrix elements (from top to bottom, respectively in green, blue, red: Y_{nn}, Y_{pp}, Y_{np}). The dashed lines indicate the densities where the proton fraction reaches 1. Normalization with $Y = 3.99 \times 10^{-4}\,\mathrm{MeV}^{-1}\,\mathrm{fm}^{-3}$.

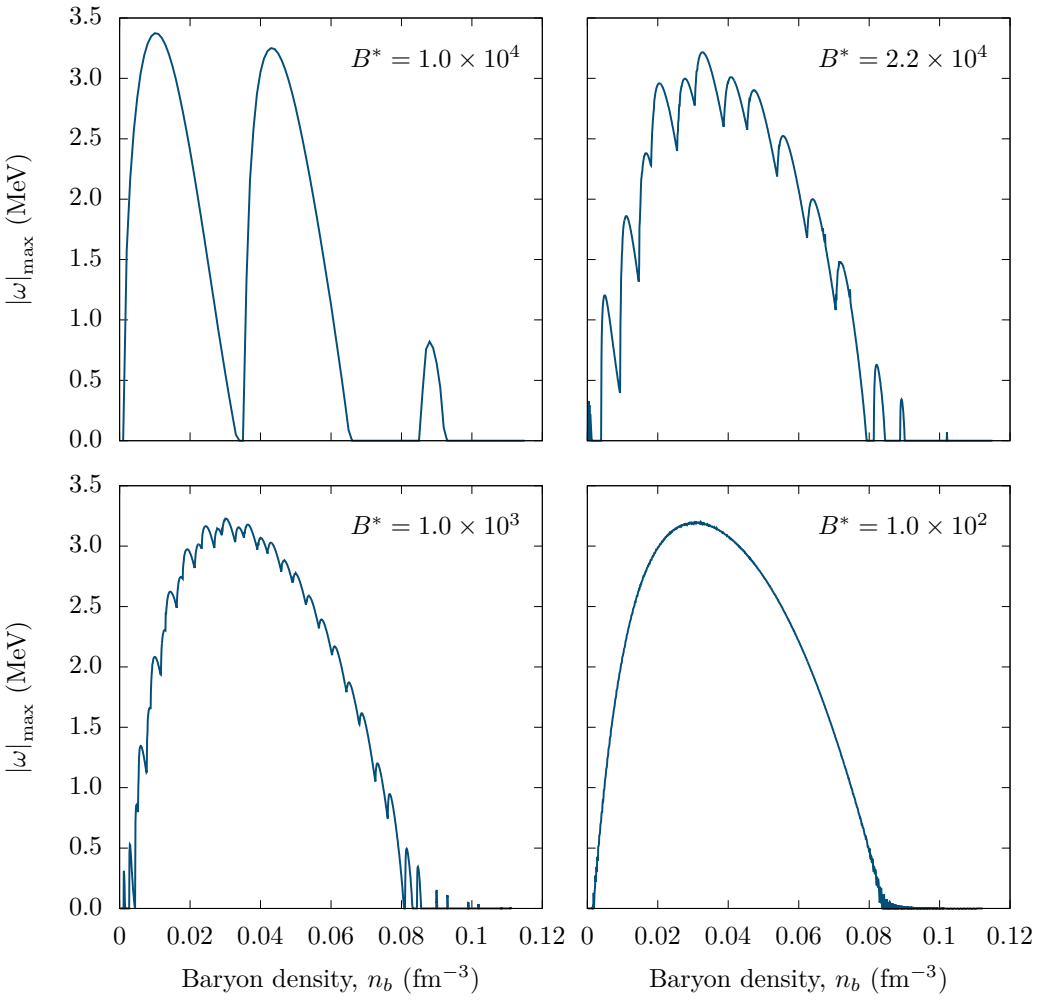

Figure 4.20: Maximum growth rates for different values of B in the NL3$\omega\rho$ model, for $L = 55\,\mathrm{MeV}$.

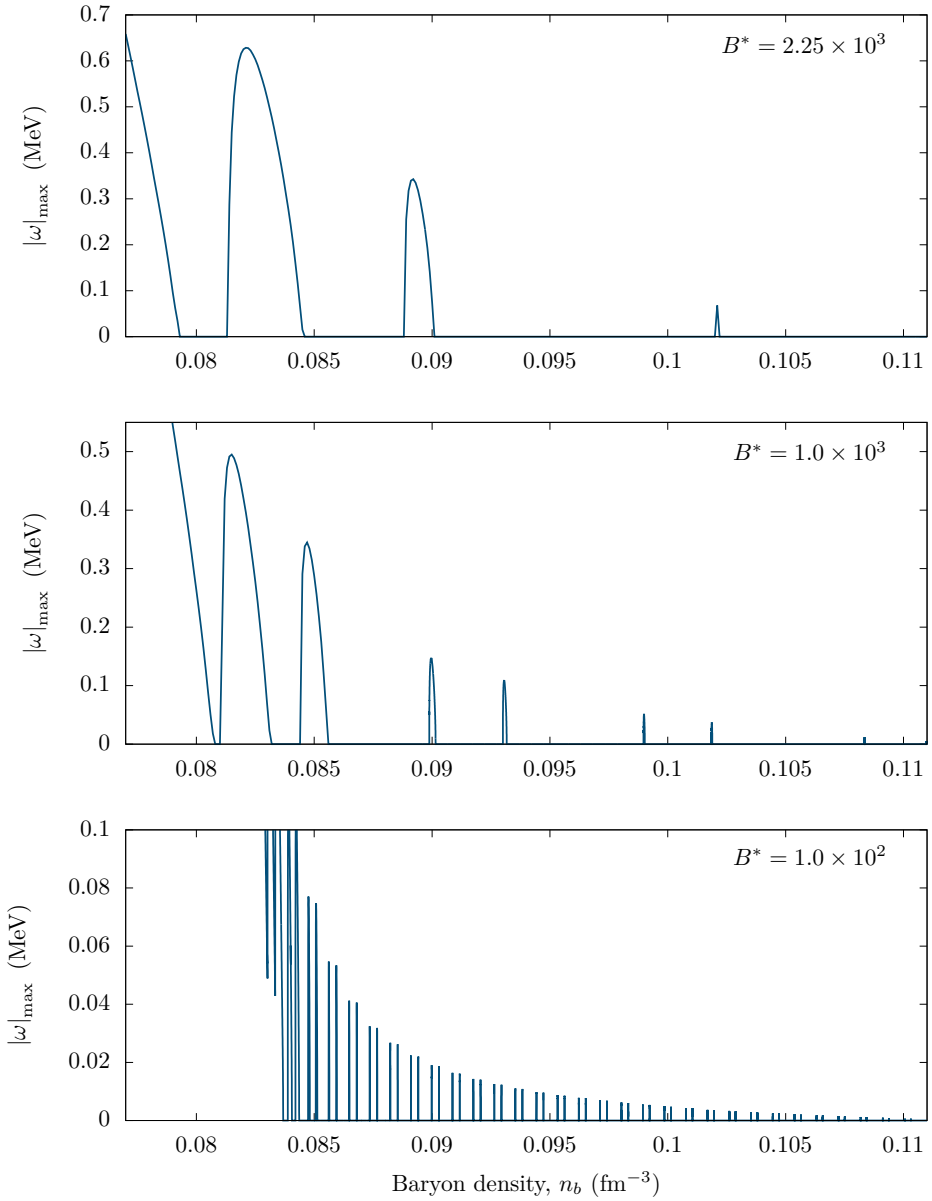

Figure 4.21: Crust-core transition zone, for the NL3$\omega\rho$ model with $L = 5$.

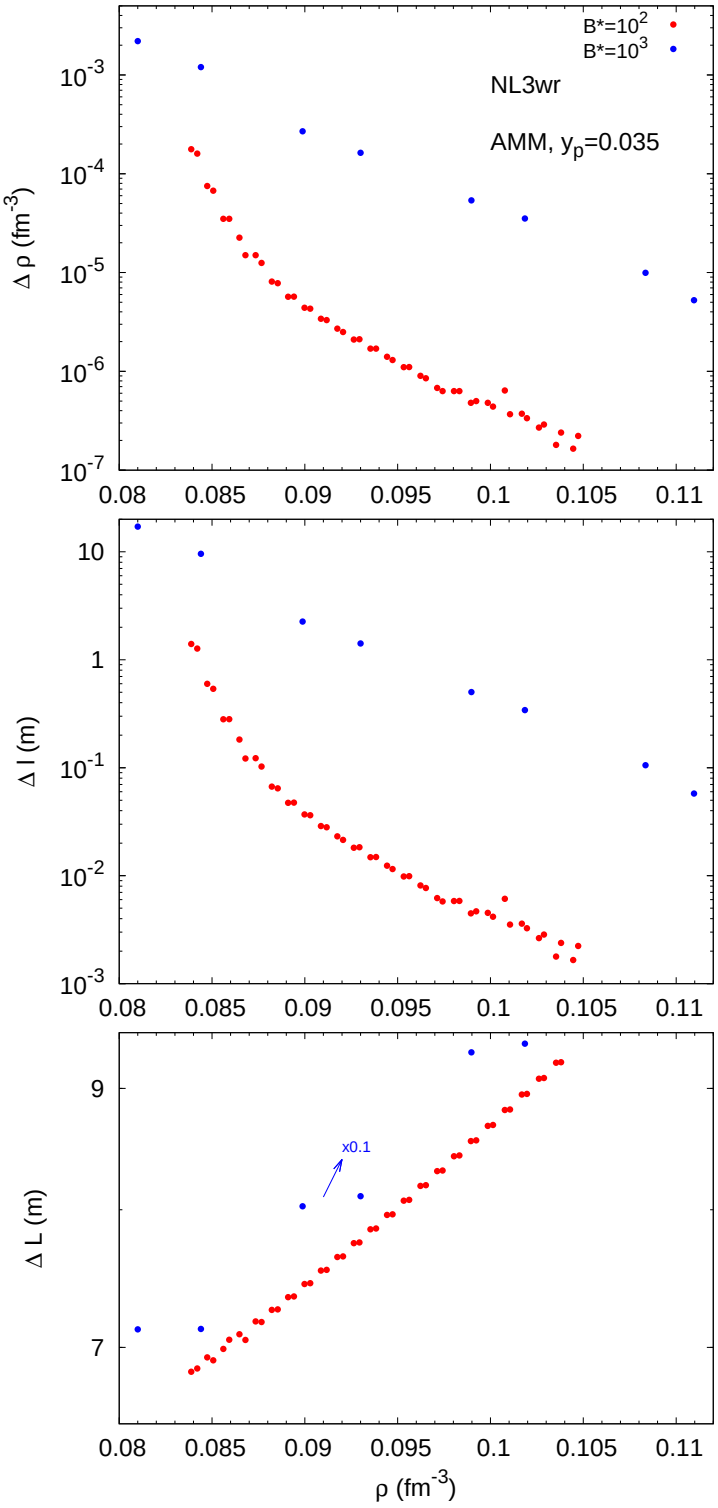

Figure 4.22: Study of cluster sizes. Top panel: width of the peaks $\Delta\rho$ in density; Middle panel: size of the clusters obtained by assuming a star of mass 1.4 $M_\odot$; Bottom panel: distance between the instabilities. NL3$\omega\rho$ model with $L = 55\,\mathrm{MeV}$, assuming a constant proton fraction of 0.035 and including the anomalous magnetic moment. [29]

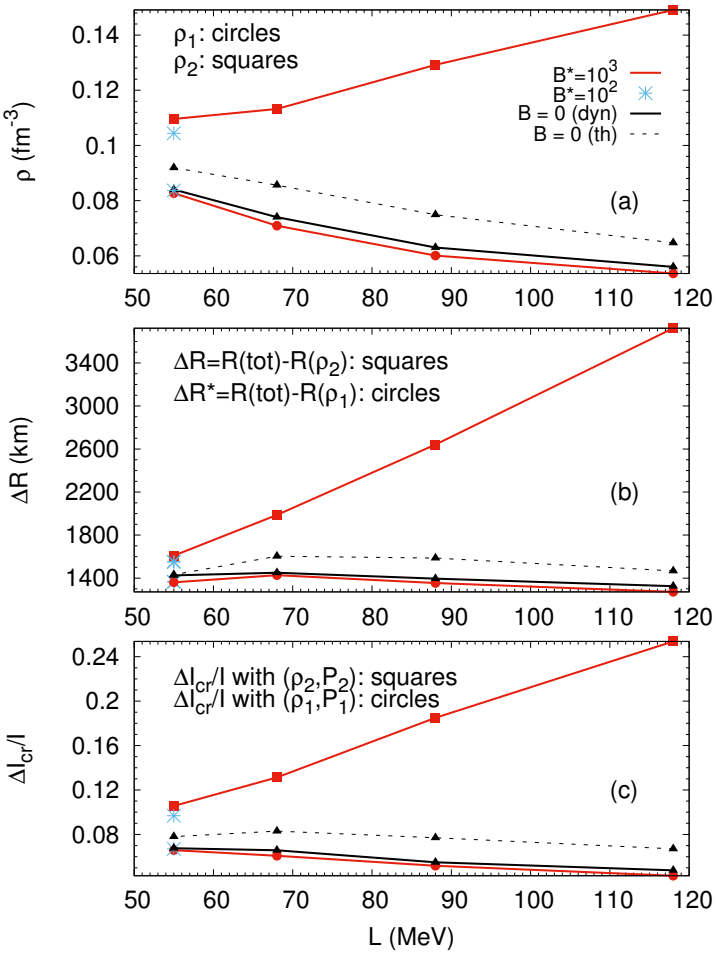

Figure 4.23: Transition densities, ρ_1 and ρ_2 (a); the crust thickness, ΔR and $\Delta R^* = R(\mathrm{tot}) - R(\rho_1)$ (b); the crust fractional momentum of inertia, calculated with (ρ_1, P_1) and with (ρ_2, P_2) (c) versus the symmetry energy slope L, obtained at $T = 0$ with $B^* = 10^3$ (red) and $B = 0$ (black solid), within the dynamical spinodal formalism including the AMM. For $L = 55\,\mathrm{MeV}$ also $B^* = 10^2$ is shown (blue stars). [30]

5. Conclusions and future work

It is hypothesized that pulsar glitches happen because fast superfluid currents inside the neutron stars suddenly transfer part of their angular momentum to the crust. There are some issues with this model, one of them being that the crust may not be able to store a large enough momentum of inertia. As such, we proposed to study two ways in which strong magnetic fields may help support this model: by increasing the size of the crust and by affecting the strength of the entrainment of superfluids inside the neutron star. These effects respectively address the issues with the storage of angular momentum and the ability for the superfluids to interact with the crust.

As we have seen, imposing a magnetic field on the star creates a complex transition region at the end of the crust, which may increase its size up to a factor of 100% in the most extreme case of $L = 118\,\mathrm{MeV}$. The effect is more modest for more realistic values of L. Also, because of this sensitivity to L, we may find ways of imposing restrictions on the density dependence of the symmetry energy by measuring quantities that depend on the size of the crust of magnetized neutron stars.

To understand the pertinence of including the magnetic field when calculating the entrainment matrix, we plot in Figure 5.1 the relative differences between the values of the entrainment matrix elements obtained with finite magnetic fields and with $B = 0$. It is immediately obvious that the magnetic field has a significant effect on the entrainment matrix, especially for the elements Y_{pp} and Y_{np}. For densities above a certain threshold, ($0.1\ \mathrm{fm}^{-3}$ for the weakest field), the corrections oscillate around 0, with an amplitude of 10%—20%, for all magnetic fields considered. However, at lower densities, the error made from not considering the magnetic field goes beyond 100%. It is then clear that it may be important for magnetohydrodynamic calculations to take the effect of the magnetic field in the equation of state into account. These conclusions apply not only to the parameterizations for which $L = 118\,\mathrm{MeV}$ but also for the more realistic value of $L = 55\,\mathrm{MeV}$. The corrections are naturally smaller for Y_{nn}, because it depends only indirectly on the magnetic field. However, for $B^* = 10^5$ the error is of the order of 10%, which is still a significant correction. For $B^* = 5 \times 10^4$ this correction drops to 5%.

The values obtained for the entrainment matrix will allow for more realistic magnetohydrodynamic simulations of neutrons stars, which will ultimately show whether this model of pulsar glitches is adequate. In the future, it will be important to include the anomalous magnetic moment of neutrons and allow for the presence of hyperons, in order to obtain a more realistic behaviour of the stellar matter.

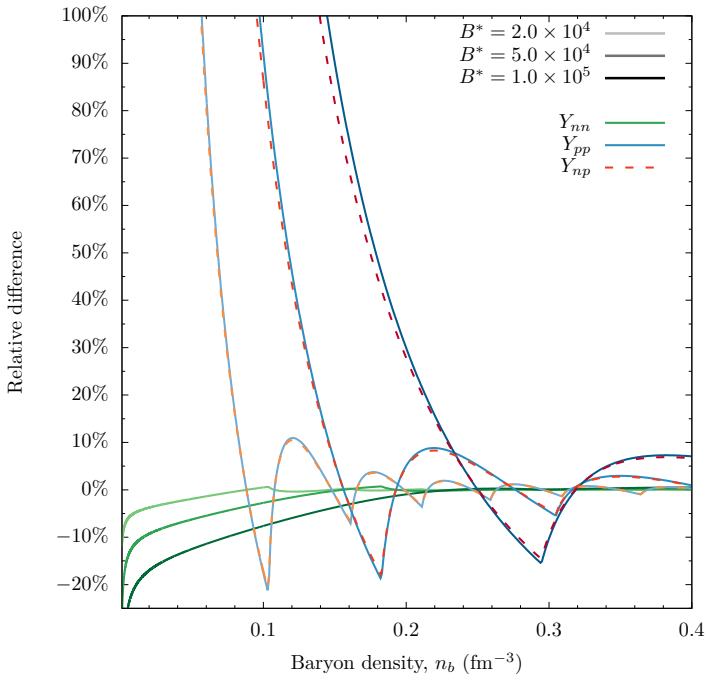

(a) $L = 118\,\mathrm{MeV}$

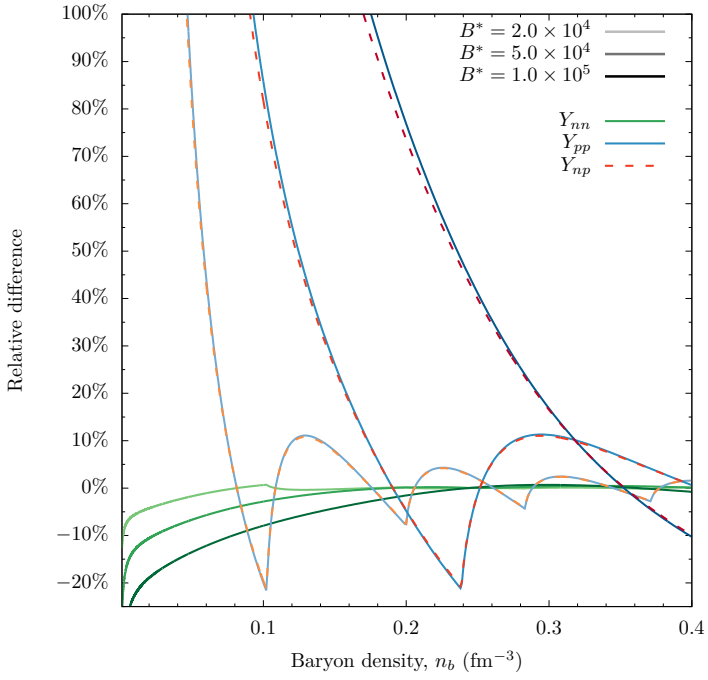

(b) $L = 55\,\mathrm{MeV}$

Figure 5.1: Relative differences of the entrainment matrix elements when compared with the $B = 0$ values.

Bibliography

[1] R. C. Duncan and C. Thompson, "Formation of very strongly magnetized neutron stars-implications for gamma-ray bursts," *The Astrophysical Journal*, vol. 392, pp. L9–L13, 1992.

[2] S. Chakrabarty, D. Bandyopadhyay, and S. Pal, "Dense nuclear matter in a strong magnetic field," *Physical Review Letters*, vol. 78, no. 15, p. 2898, 1997.

[3] A. Rabhi, C. Providência, and J. Da Providência, "Spinodal instabilities and the distillation effect in nuclear matter under strong magnetic fields," *Physical Review C*, vol. 79, no. 1, p. 015804, 2009.

[4] A. Rabhi, M. Perez-Garcia, C. Providencia, and I. Vidana, "Magnetic susceptibility and magnetization properties of asymmetric nuclear matter in a strong magnetic field," *Physical Review C*, vol. 91, no. 4, p. 045803, 2015.

[5] J. Fang, H. Pais, S. Avancini, and C. Providência, "Larger and more heterogeneous neutron star crusts: A result of strong magnetic fields," *Physical Review C*, vol. 94, no. 6, p. 062801, 2016.

[6] B. Link, R. I. Epstein, and J. M. Lattimer, "Pulsar constraints on neutron star structure and equation of state," *Physical Review Letters*, vol. 83, no. 17, p. 3362, 1999.

[7] N. Chamel, "Crustal entrainment and pulsar glitches," *Physical review letters*, vol. 110, no. 1, p. 011101, 2013.

[8] N. Andersson, K. Glampedakis, W. C. Ho, and C. M. Espinoza, "Pulsar glitches: The crust is not enough," *Physical review letters*, vol. 109, no. 24, p. 241103, 2012.

[9] R. Archibald, V. Kaspi, C.-Y. NG, K. Gourgouliatos, D. Tsang, P. Scholz, A. Beardmore, N. Gehrels, and J. Kennea, "An anti-glitch in a magnetar," *Nature*, vol. 497, no. 7451, pp. 591–593, 2013.

[10] S. S. Avancini, S. Chiacchiera, D. P. Menezes, and C. Providência, "Warm "pasta" phase in the thomas-fermi approximation," *Physical Review C*, vol. 82, no. 5, p. 055807, 2010.

[11] L. Brito, P. Chomaz, D. Menezes, and C. Providência, "Low-density expansion and isospin dependence of nuclear energy functional: Comparison

between relativistic and skyrme models," *Physical Review C*, vol. 76, no. 4, p. 044316, 2007.

[12] M. Dutra, O. Lourenço, S. Avancini, B. Carlson, A. Delfino, D. Menezes, C. Providência, S. Typel, and J. Stone, "Relativistic mean-field hadronic models under nuclear matter constraints," *Physical Review C*, vol. 90, no. 5, p. 055203, 2014.

[13] N. Chamel and P. Haensel, "Physics of neutron star crusts," *Living Reviews in Relativity*, vol. 11, no. 1, p. 10, 2008.

[14] G. Comer and R. Joynt, "Relativistic mean field model for entrainment in general relativistic superfluid neutron stars," *Physical Review D*, vol. 68, no. 2, p. 023002, 2003.

[15] M. E. Gusakov, E. M. Kantor, and P. Haensel, "Relativistic entrainment matrix of a superfluid nucleon-hyperon mixture: The zero temperature limit," *Physical Review C*, vol. 79, no. 5, p. 055806, 2009.

[16] M. Johnson and E. Teller, "Classical field theory of nuclear forces," *Physical Review*, vol. 98, no. 3, p. 783, 1955.

[17] H.-P. Duerr, "Relativistic effects in nuclear forces," *Physical Review*, vol. 103, no. 2, p. 469, 1956.

[18] J. Walecka, "A theory of highly condensed matter," *Annals of Physics*, vol. 83, no. 2, pp. 491–529, 1974.

[19] N. K. Glendenning, *Compact stars: Nuclear physics, particle physics and general relativity*. Springer Science & Business Media, 2012.

[20] C. Horowitz and J. Piekarewicz, "Neutron star structure and the neutron radius of p 208 b," *Physical Review Letters*, vol. 86, no. 25, p. 5647, 2001.

[21] C. J. Horowitz and J. Piekarewicz, "Neutron radii of 208 pb and neutron stars," *Physical Review C*, vol. 64, no. 6, p. 062802, 2001.

[22] H. Pais and C. Providência, "Vlasov formalism for extended relativistic mean field models: The crust-core transition and the stellar matter equation of state," *Physical Review C*, vol. 94, no. 1, p. 015808, 2016.

[23] S. Avancini, L. Brito, D. Menezes, and C. Providência, "Collective modes in relativistic asymmetric nuclear matter," *Physical Review C*, vol. 71, no. 4, p. 044323, 2005.

[24] C. Providência, L. Brito, S. Avancini, D. Menezes, and P. Chomaz, "Low-density instabilities in relativistic asymmetric matter of compact stars," *Physical Review C*, vol. 73, no. 2, p. 025805, 2006.

[25] S. S. Avancini, S. Chiacchiera, D. P. Menezes, and C. Providência, "Erratum: Warm "pasta" phase in the thomas-fermi approximation [phys. rev. c 82, 055807 (2010)]," *Physical Review C*, vol. 85, no. 5, p. 059904, 2012.

[26] A. Andreev and E. Bashkin, "Three-velocity hydrodynamics of superfluid solutions," *Soviet Journal of Experimental and Theoretical Physics*, vol. 42, p. 164, 1976.

[27] G. Guennebaud, B. Jacob, *et al.*, "Eigen v3." http://eigen.tuxfamily.org, 2010.

[28] R. Cavagnoli, D. P. Menezes, and C. Providência, "Neutron star properties and the symmetry energy," *Physical Review C*, vol. 84, no. 6, p. 065810, 2011.

[29] J. Fang, H. Pais, S. Pratapsi, S. Avancini, J. Li, and C. Providência, "Effect of strong magnetic fields on the crust-core transition and inner crust of neutron stars," *Physical Review C*, vol. 95, no. 4, p. 045802, 2017.

[30] J. Fang, H. Pais, S. Pratapsi, and C. Providência, "Crust-core transition of a neutron star: Effects of the symmetry energy and temperature under strong magnetic fields," *Physical Review C*, vol. 95, no. 6, p. 062801, 2017.

[31] J. M. Lattimer and M. Prakash, "Nuclear matter and its role in supernovae, neutron stars and compact object binary mergers," *Physics Reports*, vol. 333, pp. 121–146, 2000.

[32] K. Hebeler, J. Lattimer, C. J. Pethick, and A. Schwenk, "Equation of state and neutron star properties constrained by nuclear physics and observation," *The Astrophysical Journal*, vol. 773, no. 1, p. 11, 2013.

[33] S. Gandolfi, J. Carlson, and S. Reddy, "Maximum mass and radius of neutron stars, and the nuclear symmetry energy," *Physical Review C*, vol. 85, no. 3, p. 032801, 2012.

[34] M. Tsang, J. Stone, F. Camera, P. Danielewicz, S. Gandolfi, K. Hebeler, C. J. Horowitz, J. Lee, W. G. Lynch, Z. Kohley, *et al.*, "Constraints on the symmetry energy and neutron skins from experiments and theory," *Physical Review C*, vol. 86, no. 1, p. 015803, 2012.

[35] D. J. Griffiths and E. G. Harris, *Introduction to quantum mechanics*, vol. 63. American Association of Physics Teachers, 1995.

[36] C. Cohen-Tannoudji, B. Diu, and F. Laloë, *Quantum mechanics, vol. I and II*. 1977.

A. Eigenstates of the Dirac equations

A.1 Particles without magnetic field

We are going to find the energy and momentum eigenstates of a particle that does not feel the influence of a magnetic field, subject to the Dirac equation

$$[\gamma_\mu(i\partial^\mu - V^\mu) - m^*]\Psi = 0, \tag{A.1}$$

with $V^\mu = (V^0, \boldsymbol{V})$ being a constant potential, and m^* being the particle's effective mass. We are mostly interested in the case where $m^* = m_n - g_\sigma\sigma$, as this equation describes the behaviour of neutrons in the NL3$\omega\rho$ model.

Since neither V^μ nor m^* vary in spacetime, let us propose the plane wave solution

$$\Psi(x) = \Psi_0(p)e^{-ip^\mu x_\mu}, \tag{A.2}$$

for a constant vector $p^\mu = (E, \boldsymbol{p})$, which means we are choosing a state with definite energy E and momentum $\boldsymbol{p}$. Replacing in the Dirac equation yields

$$[\gamma_\mu(p^\mu - V^\mu) - m^\star]\Psi_0 = 0 \tag{A.3}$$

We define the effective momentum $\bar{p}^\mu = p^\mu - V^\mu$. If we left multiply this equation by $(\gamma_\nu\bar{p}^\nu + m^*)$, we obtain

$$[\gamma_\nu\bar{p}^\nu + m^\star][\gamma_\mu\bar{p}^\mu - m^\star]\Psi_0 = \left[\gamma_\nu\gamma_\mu\bar{p}^\nu\bar{p}^\mu - {m^*}^2\right]\Psi_0 = 0 \tag{A.4}$$

The γ matrices obey the identity $\gamma^\alpha\gamma^\beta + \gamma^\alpha\gamma^\beta = 2\eta^{\alpha\beta}$, where $\eta^{\alpha\beta}$ is the metric tensor. Notice that since ν and μ are summation indices, they can be named freely, so we can exchange them:

$$\gamma_\nu\gamma_\mu\bar{p}^\nu\bar{p}^\mu = \frac{\gamma_\nu\gamma_\mu\bar{p}^\nu\bar{p}^\mu + \gamma_\mu\gamma_\nu\bar{p}^\mu\bar{p}^\nu}{2} = \frac{\gamma_\nu\gamma_\mu + \gamma_\mu\gamma_\nu}{2}\bar{p}^\nu\bar{p}^\mu = \eta_{\nu\mu}\bar{p}^\nu\bar{p}^\mu = \bar{p}^\mu\bar{p}_\mu.$$

Therefore, the last equation becomes

$$\left[\bar{p}^\mu\bar{p}_\mu - {m^*}^2\right]\Psi_0 = 0 \Leftrightarrow \bar{p}^\mu\bar{p}_\mu - {m^*}^2 = 0. \tag{A.5}$$

Solving for $\bar{p}_0$ gives us

$$\bar{p}_0 = \sqrt{\bar{\boldsymbol{p}}^2 + {m^*}^2}. \tag{A.6}$$

Recalling that $\bar{p}^\mu = p^\mu - V^\mu$ finally gives us the energy

$$E = V^0 + \sqrt{(\boldsymbol{p} - \boldsymbol{V})^2 + {m^*}^2}. \tag{A.7}$$

A.2 Particles under magnetic fields

A.2.1 The Quantum Harmonic Oscillator

Under a constant magnetic field, charged particles such as electrons and protons behave like a quantum harmonic oscillator. We will strt by studying the oscillator, in order to obtain its energy eigenstates. We analyze both the one-dimensional case, relevant for the Landau gauge $\boldsymbol{A} = (0, By, 0)$, and the two-dimensional case, relevant for the symmetrical gauge $\boldsymbol{A} = \frac{1}{2}(-By, Bx, 0) = \frac{Br}{2}\hat{\boldsymbol{\varphi}}$. Throughout this section, we will use the position representation of the wavefunction, instead of the more general bra-ket formalism, following the analytical approach used, for example, in Griffiths [35]. A more elegant approach, based on algebraic methods, may be found in Cohen-Tannoudji et al. [36].

For both the one-dimensional and two-dimensional oscillators, the single-particle hamiltonian is

$$H = \frac{\boldsymbol{P}^2}{2m} + V(\boldsymbol{r}),$$

where m is the particle's mass, $\boldsymbol{P} = -i\hbar\boldsymbol{\nabla}$ is the momentum operator and $V(\boldsymbol{r})$ is the potential at position $\boldsymbol{r}$, given by

$$V(\boldsymbol{r}) = \begin{cases} \dfrac{m\omega^2}{2}x^2 & \text{(1D oscillator)} \\ \dfrac{m\omega^2}{2}(x^2+y^2) = \dfrac{m\omega^2}{2}\rho^2 & \text{(2D oscillator).} \end{cases}$$

Here, ω stands for the oscillator frequency and we choose ρ for the radial component of a cylindrical coordinate system. Notice that the second potential has no preferential direction in the xy plane. The time-dependent Schrödinger equation for the particle's wavefunction Ψ is then

$$i\hbar\frac{\partial\Psi}{\partial t} = H\Psi = \left[-\frac{\hbar^2}{2m}\boldsymbol{\nabla}^2 + V(\boldsymbol{r})\right]\Psi. \tag{A.8}$$

Since the hamiltonian is time-independent in both cases, we separate the time component of the wavefunction as $\Psi = e^{-iEt/\hbar}\Psi$. By substitution, we obtain

$$\left[-\frac{\hbar^2}{2m}\boldsymbol{\nabla}^2 + V(\boldsymbol{r})\right]\Psi = E\Psi.$$

We will now consider both cases separately.

The one-dimensional oscillator

Since the potential is independent of the y and z coordinates, we factor the stationary wavefunction using plane waves, as $\Psi(x,y,z) = e^{i(p_y y + p_z z)/\hbar}f(x)$. Therefore,

$$\begin{aligned} \boldsymbol{\nabla}^2\Psi &= \left[\frac{\partial^2}{\partial x^2} + \frac{\partial^2}{\partial y^2} + \frac{\partial^2}{\partial z^2}\right]\left[e^{i(p_y y + p_z z)/\hbar}f\right] \\ &= \left[\frac{\mathrm{d}^2}{\mathrm{d}x^2} - \left(\frac{p_y}{\hbar}\right)^2 - \left(\frac{p_z}{\hbar}\right)^2\right]\left[e^{i(p_y y + p_z z)/\hbar}f\right]. \end{aligned} \tag{A.9}$$

By substituting in Equation A.8 with the appropriate potential, we obtain

$$\left[-\frac{\hbar^2}{2m}\left(\frac{\mathrm{d}^2}{\mathrm{d}x^2}-\left(\frac{p_y}{\hbar}\right)^2-\left(\frac{p_z}{\hbar}\right)^2\right)+\frac{m\omega^2}{2}x^2\right]f=Ef \tag{A.10}$$

or, by rearranging,

$$\left[-\frac{\hbar^2}{2m}\frac{\mathrm{d}^2}{\mathrm{d}x^2}+\frac{m\omega^2}{2}x^2\right]f=E_x f, \tag{A.11}$$

where

$$E_x=E-\frac{p_y^2}{2m}-\frac{p_z^2}{2m} \tag{A.12}$$

is the energy of the x component of the wavefunction. To keep the notation simple, we introduce the new variable $\xi=\sqrt{\frac{m\omega}{\hbar}}x$, from which it follows that

$$\frac{\mathrm{d}}{\mathrm{d}x}=\sqrt{\frac{m\omega}{\hbar}}\frac{\mathrm{d}}{\mathrm{d}\xi} \quad \text{and} \quad \frac{\mathrm{d}^2}{\mathrm{d}x^2}=\frac{m\omega}{\hbar}\frac{\mathrm{d}^2}{\mathrm{d}\xi^2}.$$

By substitution and rearrangement, the Schrödinger equation becomes

$$\frac{\mathrm{d}^2 f}{\mathrm{d}\xi^2}-\xi^2 f+\varepsilon_x f=0 \tag{A.13}$$

where $\varepsilon_x=2E_x/\hbar\omega$ is the (unitless) energy of the x component of the particle.

The first step towards a solution is noticing that, as $\xi\to+\infty$ (or equivalently $x\to+\infty$), the term $\xi^2 f$ becomes significantly larger than $\varepsilon_x f$, and we obtain the approximate equation

$$\frac{\mathrm{d}^2 f}{\mathrm{d}\xi^2}\approx\xi^2 f. \tag{A.14}$$

This equation has the approximate solution $e^{\pm\xi^2/2}$:

$$\frac{\mathrm{d}^2}{\mathrm{d}\xi^2}\left(e^{\pm\xi^2/2}\right)=\left(\xi^2\pm1\right)e^{\pm\xi^2/2}\approx\xi^2 e^{\pm\xi^2/2}.$$

Notice, however, that the positive exponential $e^{\xi^2/2}$ grows exponentially to $+\infty$ as $\xi\to+\infty$ and, therefore, is not a normalizable solution. Therefore, we will try a solution of the form

$$f=e^{-\xi^2/2}g. \tag{A.15}$$

By replacing f, we obtain

$$\frac{\mathrm{d}^2 g}{\mathrm{d}\xi^2}-2\xi\frac{\mathrm{d}g}{\mathrm{d}\xi}+(\varepsilon_x-1)g=0. \tag{A.16}$$

To find an expression for g, we will try a power series solution of the form

$$g=\sum_{j=0}^{\infty}a_n\xi^n. \tag{A.17}$$

From this, it follows that

$$\frac{\mathrm{d}g}{\mathrm{d}\xi}=\sum_{j=0}^{\infty}j a_j\xi^{j-1} \quad \text{and}$$

$$\frac{\mathrm{d}^2 g}{\mathrm{d}\xi^2}=\sum_{j=0}^{\infty}j(j-1)a_j\xi^{j-2}=\sum_{j=0}^{\infty}a_{j+2}(j+2)(j+1)\xi^j.$$

Replacing in the last equation, and grouping the power of ξ, we obtain

$$\sum_{j=0}^{\infty}\Big(a_{j+2}(j+2)(j+1)-a_j(2j-(\varepsilon_x-1))\Big)\xi^j=0. \tag{A.18}$$

For this equation to be valid for every x, it must be the case that the coefficients of the ξ^j are zero for every j, that is,

$$a_{j+2}=\frac{2j+1-\epsilon}{(j+1)(j+2)}a_j,\quad j=0,1,2,\dots. \tag{A.19}$$

Since this relationship outputs the value of a_{j+2} by specifying a_j, all we have to do is set the values of a_0 and a_1 to obtain evey coefficient. We thus have two arbitrary constants for a solution of a second-order ordinary differential equation, which means that we have found *all* the solutions.

Notice that, as $j\to+\infty$, the relationship between a_{j+2} and a_j is approximately

$$a_{j+2}\approx\frac{2}{j}a_j.$$

If, for instance, we focus on the even coefficients we obtain the approximate relationship

$$a_{2m}\approx\frac{2}{2m}\cdot\frac{2}{2(m-1)}\cdot\frac{2}{2(m-2)}\cdots a_0=\frac{1}{m(m-1)(m-2)\cdots}\,a_0=\frac{a_0}{m!}$$

Therefore, g has the asymptotic behaviour

$$g\sim\sum_{m=0}^{\infty}\frac{a_0}{m!}\xi^{2m}=a_0\,e^{\xi^2}$$

and f will therefore be

$$f\sim a_0\,e^{\xi^2}e^{-\xi^2/2}=a_0\,e^{\xi^2/2},$$

giving us the non-normalizable solution we discarded earlier. The only way to avoid this behaviour is if, for some n, a_n is zero. If this happens, then, for every n' greater than n, $a_{n'}$ will also be zero. We should therefore impose that, for some n,

$$a_{n+2}=\frac{2n-(\varepsilon_x-1)}{(n+1)(n+2)}a_n=0\Rightarrow\varepsilon_x=2n+1. \tag{A.20}$$

By substituting the expression for the energy of the x component, we obtain

$$E_x=\hbar\omega\left(n+\frac{1}{2}\right),\quad n=0,1,2,\dots, \tag{A.21}$$

and we have thus obtained the quantization of the energy of the quantum harmonic oscillator. The full energy of the system is then

$$E=\hbar\omega\left(n+\frac{1}{2}\right)+\frac{p_y^2}{2m}+\frac{p_z^2}{2m}. \tag{A.22}$$

n	0	1	2	3	$\cdots$
$g(\xi)$	1	2ξ	$4\xi^2 - 2$	$8\xi^3 - 12\xi$	$\cdots$

The polynomials obtained with this method are called the *Hermite polynomials*. With the usual normalization for the constants a_0 and a_1, the first few polynomials are

In general, the Hermite polynomials $H_n(\xi)$ can be obtained via the Rodrigues formula:

$$H_n(\xi) = (-1)^n e^{\xi^2} \left(\frac{\mathrm{d}}{\mathrm{d}\xi}\right)^n e^{-\xi^2}. \tag{A.23}$$

The two-dimensional oscillator

As in the section before, we will factor the wavefunction with a plane wave in the z direction as $\Psi(x, y, z) = e^{ip_z z/\hbar} f(x, y)$. The Laplacian is given by

$$\begin{aligned} \boldsymbol{\nabla}^2 \Psi &= \left[\frac{\partial^2}{\partial x^2} + \frac{\partial^2}{\partial y^2} + \frac{\partial^2}{\partial z^2}\right]\left[e^{ip_z z/\hbar} f\right] \\ &= \left[\frac{\partial^2}{\partial x^2} + \frac{\partial^2}{\partial y^2} - \left(\frac{p_z}{\hbar}\right)^2\right]\left[e^{ip_z z/\hbar} f\right]. \end{aligned} \tag{A.24}$$

Therefore, the Schrödinger equation becomes

$$\left[-\frac{\hbar^2}{2m}\left(\frac{\partial^2}{\partial x^2} + \frac{\partial^2}{\partial y^2} - \left(\frac{p_z}{\hbar}\right)^2\right) + \frac{m\omega^2}{2}(x^2 + y^2)\right] f = Ef \tag{A.25}$$

which we can rearrange to obtain

$$\left[-\frac{\hbar^2}{2m}\frac{\partial^2}{\partial x^2} + \frac{m\omega^2}{2}x^2\right] f + \left[-\frac{\hbar^2}{2m}\frac{\partial^2}{\partial y^2} + \frac{m\omega^2}{2}y^2\right] f = \left(E - \frac{p_z^2}{2m}\right) f. \tag{A.26}$$

We will separate the solution as $f(x, y) = f_x(x) f_y(y)$. By renaming the energy

$$E - \frac{p_z^2}{2m} = E_{xy}$$

and dividing both sides of the equation by $f = f_x f_y$, we obtain

$$\frac{1}{f_x}\left[-\frac{\hbar^2}{2m}\frac{\mathrm{d}^2}{\mathrm{d}x^2} + \frac{m\omega^2}{2}x^2\right] f_x + \frac{1}{f_y}\left[-\frac{\hbar^2}{2m}\frac{\mathrm{d}^2}{\mathrm{d}y^2} + \frac{m\omega^2}{2}y^2\right] f_y = E_{xy}. \tag{A.27}$$

It is straightforward to see that the first term on the left-hand side of this equation is a function of x alone, while the second term is a function of y. They can therefore be varied independently. However, the right-hand side is constant, which means that these two terms must also be constant, that is, we must have

$$\frac{1}{f_x}\left[-\frac{\hbar^2}{2m}\frac{\mathrm{d}^2}{\mathrm{d}x^2} + \frac{m\omega^2}{2}x^2\right] f_x = E_x, \tag{A.28}$$

$$\frac{1}{f_y}\left[-\frac{\hbar^2}{2m}\frac{\mathrm{d}^2}{\mathrm{d}y^2} + \frac{m\omega^2}{2}y^2\right] f_y = E_y \tag{A.29}$$

and $E_x + E_y = E_{xy}$. But both these equations share the form of Equation A.11, which means that the solutions are the same, and the energies are given by

$$E_x = \left(n_x + \frac{1}{2}\right)\hbar\omega \quad \text{and} \quad E_y = \left(n_y + \frac{1}{2}\right)\hbar\omega \tag{A.30}$$

for $n_x, n_y = 0, 1, 2, \ldots$. The energy of the xy component of the wavefunction is then

$$E_{xy} = (n_x + n_y + 1)\hbar\omega = (n+1)\hbar\omega, \quad n = 0, 1, 2, \ldots \tag{A.31}$$

with each level having degeneracy $n + 1$:

n	0	1	2	$\cdots$
(n_x, n_y)	$(0,0)$	$(1,0)$	$(2,0)$	$\cdots$
		$(0,1)$	$(1,1)$	
			$(0,2)$	

The total energy of the system is

$$E = (n+1)\hbar\omega + \frac{p_z^2}{2m}. \tag{A.32}$$

The wavefunctions for the two-dimensional oscillator are products of the x and y Hermite polynomials, together with the factor

$$e^{-\xi_x^2/2} e^{-\xi_y^2/2} = \exp\left(-\frac{m\omega}{2\hbar}\left(x^2 + y^2\right)\right) = \exp\left(-\frac{m\omega}{2\hbar}\rho^2\right)$$

and the z-axis wavefunction.

A.2.2 Landau Levels

In this section, we are going to analyze the motion of a charged particle in a constant magnetic field. The particle will have charge q and we will choose the electromagnetic potential

$$A^\mu = (A^0, \boldsymbol{A}) = (0, 0, Bx, 0), \tag{A.33}$$

so that $\boldsymbol{\nabla} \times \boldsymbol{A} = B\hat{\boldsymbol{z}}$ and $\boldsymbol{\nabla} \cdot \boldsymbol{A} = 0$. Other choices, such as $A^\mu = (0, -By, 0, 0)$ or the rotationally invariant $A^\mu = (0, -By/2, Bx/2, 0)$, would be equally valid.

For the sake of generality, we are going to use the potential

$$V^\mu = V_0^\mu + qA^\mu, \tag{A.34}$$

where V_0^μ is some constant potential. This is to account for the case

$$V^\mu = g_\omega \omega^\mu + \frac{g_\rho}{2}\rho_3^\mu + eA^\mu,$$

which appears in the NL3$\omega\rho$ equation for the protons. Since V_0^μ is constant, it is still true that

$$\boldsymbol{\nabla} \times \boldsymbol{V} = qB\hat{\boldsymbol{z}} \quad \text{and} \quad \boldsymbol{\nabla} \cdot \boldsymbol{V} = 0. \tag{A.35}$$

The wavefunction Ψ of the charged, spin-1/2 particle is a 4-component spinor which obeys the Dirac equation

$$\Big[\gamma^\mu(i\partial_\mu - V_\mu) - m\Big]\Psi = 0, \tag{A.36}$$

where γ^μ are the Dirac γ matrices. In this section, we will choose the Dirac representation of the γ matrices:

$$\gamma^0 = \begin{pmatrix} \mathbb{1} & 0 \\ 0 & -\mathbb{1} \end{pmatrix} \quad \text{and} \quad \gamma^i = \begin{pmatrix} 0 & \sigma^i \\ -\sigma^i & 0 \end{pmatrix},$$

where the σ^i are also 2×2 matrices, the Pauli matrices

$$\sigma^1 = \begin{pmatrix} 0 & 1 \\ 1 & 0 \end{pmatrix} \quad \sigma^2 = \begin{pmatrix} 0 & -i \\ i & 0 \end{pmatrix} \quad \sigma^3 = \begin{pmatrix} 1 & 0 \\ 0 & -1 \end{pmatrix},$$

and $\mathbb{1}$ is the 2×2 identity matrix. It is usual practice to write a *vector* of γ matrices $\boldsymbol{\gamma} = (\gamma^1, \gamma^2, \gamma^3)$.

We begin by isolating the time and space components of the Dirac equation

$$\Big[\gamma^0(i\partial_t - V_0) - m\Big]\Psi = -\boldsymbol{\gamma} \cdot (i\boldsymbol{\nabla} + \boldsymbol{V})\Psi.$$

We separate the time component by writing

$$\Psi = e^{-iEt}\Psi_0 = e^{-iEt}\begin{pmatrix} \phi \\ \chi \end{pmatrix},$$

where ϕ and χ are 2-component spinors. By replacing Ψ and cancelling out the exponentials, the equation reads

$$\Big[\gamma^0(E - V_0) - m\Big]\Psi_0 = -\boldsymbol{\gamma} \cdot (i\boldsymbol{\nabla} + \boldsymbol{V})\Psi_0. \tag{A.37}$$

We will set $E - V_0 = \bar{E}$. Writing this equation in terms of the 2×2 components reads

$$\begin{pmatrix} \bar{E} - m & 0 \\ 0 & -(\bar{E} + m) \end{pmatrix}\begin{pmatrix} \phi \\ \chi \end{pmatrix} = \begin{pmatrix} 0 & -\boldsymbol{\sigma} \cdot (i\boldsymbol{\nabla} + \boldsymbol{V}) \\ \boldsymbol{\sigma} \cdot (i\boldsymbol{\nabla} + \boldsymbol{V}) & 0 \end{pmatrix}\begin{pmatrix} \phi \\ \chi \end{pmatrix} \tag{A.38}$$

which can be written as a set of two coupled equations

$$\begin{cases} (\bar{E} - m)\phi = -\boldsymbol{\sigma} \cdot (i\boldsymbol{\nabla} + \boldsymbol{V})\chi \\ (\bar{E} + m)\chi = -\boldsymbol{\sigma} \cdot (i\boldsymbol{\nabla} + \boldsymbol{V})\phi. \end{cases} \tag{A.39}$$

We can use the second equation to replace χ in the first, obtaining, after some rearrangement,

$$(\bar{E}^2 - m^2)\phi = [\boldsymbol{\sigma} \cdot (i\boldsymbol{\nabla} + \boldsymbol{V})]^2\phi. \tag{A.40}$$

To evaluate the square term on the right-hand side, we write it out in components:

$$\begin{aligned} \big[\boldsymbol{\sigma} \cdot (i\boldsymbol{\nabla} + \boldsymbol{V})\big]^2\phi &= \big[\sigma^i(i\partial_i + V^i)\big]\big[\sigma^j(i\partial_j + V^j)\big]\phi \\ &= \sigma^i\sigma^j\big(i\partial_i + V^i\big)\big(i\partial_j + V^j\big)\phi. \end{aligned}$$

The product of two Pauli matrices is given by $\sigma^i\sigma^j = \mathbb{1}\delta_{ij} + i\epsilon_{ijk}\sigma^k$, where ϵ_{ijk} is the Levi-Civita symbol. Expanding the products on the right-hand side gives

$$\begin{aligned}\big[\boldsymbol{\sigma}\cdot(i\boldsymbol{\nabla}+\boldsymbol{V})\big]^2\phi = \\ = \big(\mathbb{1}\delta_{ij} + i\epsilon_{ijk}\sigma^k\big)\big(-\partial_{ij}\phi + i\big(\partial_i V^j\big)\phi + i(V^j\partial_i + V^i\partial_j)\phi + V^iV^j\phi\big)\end{aligned} \tag{A.41}$$

Notice that the terms $(-\partial_{ij}\phi)$, $i(V^j\partial_i + V^i\partial_j)\phi$ and $V^iV^j\phi$ are symmetric under the exchange of i and j. Therefore, they vanish when multiplied by the Levi-Civita symbol and perform the implied sum. The surviving terms are

$$\begin{aligned}\big[\boldsymbol{\sigma}\cdot(i\boldsymbol{\nabla}+\boldsymbol{V})\big]^2\phi &= -\partial_{ii}\phi + i\partial_i V^i\phi + 2iV^i\partial_i\phi + V^iV^i\phi - \epsilon_{ijk}\partial_i V^j\sigma^k\phi \\ &= \big[-\nabla^2 + i(\boldsymbol{\nabla}\cdot\boldsymbol{V}) + 2i\boldsymbol{V}\cdot\boldsymbol{\nabla} + V^2 - (\boldsymbol{\nabla}\times\boldsymbol{V})\cdot\boldsymbol{\sigma}\big]\phi\end{aligned} \tag{A.42}$$

Given that $\boldsymbol{\nabla}\cdot\boldsymbol{V} = 0$ and $\boldsymbol{\nabla}\times\boldsymbol{V} = qB\hat{\boldsymbol{z}}$, the equation we are trying to solve finally simplifies to

$$\big(\bar{E}^2 - m^2\big)\phi = \big[-\nabla^2 + 2i\boldsymbol{V}\cdot\boldsymbol{\nabla} + V^2 - qB\sigma^3\big]\phi. \tag{A.43}$$

To proceed, we factor out the dependence on the y and z coordinates:

$$\phi = e^{i(p_y y + p_z z)}f(x) = e^{i\boldsymbol{p}\cdot\boldsymbol{r}}f(x), \tag{A.44}$$

where $\boldsymbol{p} = (0, p_y, p_z)$ and $\boldsymbol{r} = (x, y, z)$ is the position vector. Therefore,

$$\begin{cases}\nabla^2\phi = \boldsymbol{\nabla}\cdot\big[\boldsymbol{\nabla}\big(e^{i\boldsymbol{p}\cdot\boldsymbol{r}}f\big)\big] = \boldsymbol{\nabla}\big[i\boldsymbol{p}e^{i\boldsymbol{p}\cdot\boldsymbol{r}}f + e^{i\boldsymbol{p}\cdot\boldsymbol{r}}\boldsymbol{\nabla}f\big]\phi \\ \qquad = e^{i\boldsymbol{p}\cdot\boldsymbol{r}}\big[-p^2 f + 2i\boldsymbol{p}\cdot\boldsymbol{\nabla}f + \nabla^2 f\big] \\ \boldsymbol{V}\cdot\boldsymbol{\nabla}\phi = \boldsymbol{V}\cdot(i\boldsymbol{p}e^{i\boldsymbol{p}\cdot\boldsymbol{r}}f + e^{i\boldsymbol{p}\cdot\boldsymbol{r}}\boldsymbol{\nabla}f)\end{cases}$$

Since f depends only on the x coordinate, it is clear that $\boldsymbol{\nabla}f = \frac{\mathrm{d}f}{\mathrm{d}x}\hat{\boldsymbol{x}}$. Therefore, $\boldsymbol{p}\cdot\boldsymbol{\nabla}f = 0$. The Dirac equation then becomes, after replacing ϕ and cancelling out the exponentials,

$$(\bar{E} - m^2)f = \left[p^2 - \frac{\mathrm{d}^2}{\mathrm{d}x^2} - 2\boldsymbol{V}\cdot\boldsymbol{p} + 2i\boldsymbol{V}\cdot\hat{\boldsymbol{x}}\frac{\mathrm{d}}{\mathrm{d}x} + V^2 - qB\sigma^3\right]f. \tag{A.45}$$

We now have to expand the dot products $\boldsymbol{V}\cdot\boldsymbol{p}$ and $\boldsymbol{V}\cdot\hat{\boldsymbol{x}}$, and also the term V^2. We omit these steps to give the rearranged result

$$-\left(i\frac{\mathrm{d}f}{\mathrm{d}x} + V_0^x\right)^2 - (qBx - \bar{p}_y)^2 f + \big(\bar{E}^2 - m^2 - \bar{p}_z^2 + qB\sigma^3\big)f = 0$$

where

$$\bar{p}_y = p_y - V_0^y \quad \text{and} \quad \bar{p}_z = p_z - V_0^z. \tag{A.46}$$

We can make the constant V_0^x vanish by defining

$$f(x) = e^{iV_0^x x}g(x), \tag{A.47}$$

giving us the equation

$$\frac{\mathrm{d}^2 g}{\mathrm{d}x^2} - (qBx - \bar{p}_y)^2 g + \big(\bar{E}^2 - m^2 - \bar{p}_z^2 + qB\sigma^3\big)g = 0 \tag{A.48}$$

Notice that this equation still has two components, given that σ^3 is a 2×2 matrix. But we can write g as

$$g(x) = \begin{pmatrix} g_+(x) \\ g_-(x) \end{pmatrix}, \tag{A.49}$$

and the action of σ^3 is

$$\sigma^3 g = \begin{pmatrix} 1 & 0 \\ 0 & -1 \end{pmatrix} \begin{pmatrix} g_+(x) \\ g_-(x) \end{pmatrix} = \begin{pmatrix} +g_+(x) \\ -g_-(x) \end{pmatrix}$$

Therefore, the Dirac equation in terms of $g_\pm$ is

$$\frac{\mathrm{d}^2 g_\pm}{\mathrm{d}x^2} - (qBx - \bar{p}_y)^2 g_\pm + \big(\bar{E}^2 - m^2 - \bar{p}_z^2 \pm qB\big) g_\pm = 0. \tag{A.50}$$

We use the notation g_s by letting $s = \pm 1$; the term $\pm eB$ becomes qBs.

We can simplify this equation by changing variables:

$$\xi = \frac{qBx - \bar{p}_y}{\sqrt{qB}} \tag{A.51}$$

and naming the factor

$$a_s = \frac{\big(\bar{E}^2 - m^2 - \bar{p}_z^2 + qBs\big)}{qB}, \tag{A.52}$$

which yields

$$\frac{\mathrm{d}^2 g_s}{\mathrm{d}\xi^2} - \xi^2 g_s + a_s g_s = 0. \tag{A.53}$$

But notice that this is the reduced form of the harmonic oscillator equation, Equation A.13 of the previous section. Therefore, the solutions are the same, and we obtain the quantization condition $a_s = 2n + 1$ for $n = 0, 1, 2, \ldots$, analogous to A.20. Here, we read

$$\bar{E}^2 - m^2 - \bar{p}_z^2 + qBs = (2n + 1)qB, \quad n = 0, 1, 2, \ldots$$

which, solving for $\bar{E}$, yields:

$$\bar{E} = \sqrt{\bar{p}_z^2 + m^2 + 2qB\left(n + \frac{1 - s}{2}\right)}. \tag{A.54}$$

Since $\frac{1-s}{2}$ is either 0 for $s = 1$ or 1 for $s = -1$, it is common to write the energy as

$$\bar{E} = \sqrt{\bar{p}_z^2 + m^2 + 2\nu qB} \tag{A.55}$$

with $\nu = n + \delta_{s,-1}$, for $n = 0, 1, 2, \ldots$. All the energy levels are therefore doubly degenerate, except for the case $\nu = 0$, which appears only when $s = 1$.

Finally, we can write the energy in terms of E as

$$E = V_0 + \sqrt{(p_z - V_z)^2 + m^2 + 2\nu qB}. \tag{A.56}$$